UNIVERSITÀ DI SIENA 1240

Department of Medical Biotechnology

Doctorate in Genetics, Oncology and Clinical Medicine

GenOMeC

XXXV Cycle (2019-2022)

Coordinator: Prof. Francesca Ariani

Identification of the molecular mechanisms by which pigmentation limits Vemurafenib activity in melanoma cells

Scientific disciplinary sector: BIO/11 - Molecular Biology

PhD Candidate:

Dr. Caterina Baldanzi

CNR IFC Pisa

Tutor:

Dr. Laura Poliseno

CNR IFC Pisa

2022/2023

Table of contents

Abstract

Melanoma is the most aggressive type of skin cancer and remains a therapeutic challenge. BRAFV600E is the most common mutation in melanoma and causes the hyperactivation of the MAPK pathway. BRAF and MEK inhibitors have substantial therapeutic efficacy in patients with BRAF mutant melanoma. However, they still have significant limitations, including short-lasting efficacy, hence short-lived responses, due to early onset of acquired resistance.

An early phase exists, in which cells are in a drug tolerant state that can be used in our favor before genetic resistance occurs. We showed that one of the mechanisms that cells implement to find a strategy of survival from targeted therapy is an increase in pigmentation upon vemurafenib treatment, which confers to pigmentable melanoma cells higher resistance to BRAF inhibitors compared to non-pigmentable cells. Here we build on our previous data to confirm that melanin induction negatively affects therapy outcome *in vitro*, *in vivo* and in patients. We also demonstrate that intracellular melanosomes are the source of resistance to MAPKi in pigmentable cells. Crucially, we show that melanin acts as scavenger of ROS induced by MAPK inhibitors (MAPKi). Pigmentable cells present lower levels of ROS, as well as DNA damage, compared to non-pigmentable cells and by chemically or genetically removing melanin, we obtain an increase in ROS levels and a rescue in the efficacy of MAPKi treatment. Conversely, when we turn non-pigmentable into pigmentable cells, by adding melanin nanoparticles, we obtain opposite results. In addition, we demonstrate that melanosomes-mitochondria physical contacts favor the melanin-mediated scavenging of vem-induced ROS and we propose RAB27A as a possible candidate that can mediate the connections among the two organelles.

Finally, we expand on our previous findings that the efficacy of vem plus pigmentation inhibitors on pigmentable cells is further increased by blocking a second adaptive response, i.e. vem-induced shift toward oxidative phosphorylation. In conclusion, we affirm that pigmentation is an adaptive cellular response that limits the efficacy of MAPKi. We also propose the combination of MAPKi with pigmentation inhibitors as a way to tame the resistance of pigmentable melanoma cells. Finally, we emphasize the necessity to stratify metastatic melanoma tumors according to their pigmentation status.

1 Introduction

1.1 Skin cancer

Ultraviolet radiation (UVR) can neither be seen nor felt. While some people are exposed to artificial UVR sources (e.g. in medicine, industry and for disinfection and cosmetic purposes), everyone is exposed to solar UVR. Small amounts of UVR are beneficial to health and play an essential role in the production of vitamin D. However, excessive exposure to UVR is associated with negative health consequences as UVR is carcinogenic to humans. Acute effects of UVR include DNA damage, sunburn, phototoxic and photoallergic reactions, and suppression of the immune system. Immunosuppression can be considered as a risk factor for cancer and can cause reactivation of viruses (e.g. cold sores in the lip).

Skin cancers are the most common groups of cancers diagnosed worldwide, with more than 1.5 million new cases estimated in 2020. Excessive exposure to UVR caused around 1.2 million new cases of non-melanoma skin cancers (SCC and BCC) and 325.000 melanomas of the skin, and 64.000 premature deaths from non-melanoma and 57.000 melanomas of the skin in the year 2020. (WHO, Fact Sheets, Ultraviolet radiation, 21 June 2022).

Skin cancer is divided into two major groups: cutaneous melanoma (CM) (from melanocyte dysfunction) and non-melanoma skin cancer (NMSC) (from epidermal-derived cells). CM represents 1% of all malignant skin tumors, but is the most aggressive, with only 15-20% of 5 year survival rate. NMSC constitutes 95% of skin cancers and are principally grouped into squamous cell carcinoma (SCC), basal cell carcinoma (BCC),

and Merkel cell carcinoma (MCC). Since 1960, the incidence rate has increased, and it is 18-20 time higher than that of melanoma. The pathogenesis of BCC, SCC and MCC is multifactorial, but malignant transformation of progenitor cells due to UV radiation and so of skin exposure is the prevalent risk factor. Other risk factors are: concomitant diseases and dedicated therapies, targeted therapy for melanoma, chronic exposure to the human papilloma virus and suppression of the immune system induced by drugs in transplant patients.

1.1.1 Non Melanoma Skin Cancer

BCC arises from basal membrane of epidermis. In the 80% of the patients it develops in the head/neck region. BCC rarely metastasizes, but shows high morbidity due to frequent local invasion and tissue destruction. Mortality is low and often affected by concurrent diseases, age and clinical complications. The clinical manifestations of BCC are extremely heterogeneous and the variants can be subdivided into nodular, superficial, dibroepithelial and morpheaform. Genetic mutations in the Sonic Hedgehog (HH) ligand, Smoothened (SMO) or Pathed1 (PTCH1) receptor can inhibit the signal progression of the Hedgehog pathway and promote BCC development. The presence of high levels of lead, mercury and copper in illegal comestic brands and tattoos is among the extrinsic factors.

SCC originates from the epidermal keratinocytes. Dysplasia begins with these cells and then spreads into the epidermis, derma, and other surrounding stromal tissues. SCC is the second most common skin cancer and presents higher aggressiveness and ability to metastasize than BCC. Clinical evidence is highly heterogeneous in relation to site, size, thickness and pigmentation. There are many different subtypes, but the most common is

the superficial type, which often arises from an actinic keratosis (AK) or Bowen disease. Among the risk factors for the onset of SCC are exposure to UV (95% of SCC carry mutations in TP53), chronic inflammatory dermatological conditions and human viral infections (HPV and HIV). Metastasis, older age, male gender, site and thickness, transplantation, HIV infection or chronic lymphatic leukemia and treatment with BRAF inhibitors contribute to higher mortality

MCC, also known as primary cutaneous neuroendocrine carcinoma, is a rare, aggressive and poorly differentiated tumor that lacks a recognized benign or dysplastic precursor. Historically thought to arise from Merkel cells, MCC instead derives from a yet to be defined cellular population which is subjected to neuroendocrine differentiation before or during malignant transformation. The cancer mainly affects white people and a higher frequency is associated to UV exposure. An increased risk of developing MCC concerns transplanted patients and patients with B cell malignancies. Among risk factors are those viral, as Merkel cell polyomavirus, and those non-viral, as inactivating mutations of TP53, RB1and other genes involved in the Notch signalling. MCC typically presents as a solitary, painless, red or violaceous intracutaneous. Metastasis occur in skin, lungs, adrenals, liver, brain and skeleton. However, in up to 15% of patients, lymph-node implication is detected in the absence of a recognizable cutaneous tumor, on account of the spontaneous regression of the primary tumor [1,2].

1.1.2 Cutaneous melanoma

Among skin cancers, melanoma is the most aggressive and lethal and principally affects young and middle-aged people. There are large geographical variations in incidence rates across countries and world regions. Melanoma occurs more frequently in men than in

women in most regions of the world. The highest incidence rates per 100.000 were observed in Australia and New Zealand (42 in men and 31 in women), followed by Western Europe (19 in both men and women), Northern America (18 in men and 14 in women) and Northern Europe (17 in men and 18 in women). Melanoma continues to be rare in most countries in Africa and Asia, where incidence rates are commonly below 1 per 100.000. On the basis of global population changes, the scientists estimated that more than 500.000 new cases of melanoma per year and almost 100.000 deaths from melanoma should be expected worldwide by 2040 [3].

Fortunately, during the last two decades, great strides have been made in targeted and immune therapy, resulting in greater survival for patients with unresectable stage III and IV melanoma, compared to chemotherapy.

1.1.2.1 Melanoma progression and histological classification

The initial classification of melanoma was performed on the basis of its presumed origin (existing nevus, acquired melanocytic lesion, blemish free skin). From 1960s, melanoma is recognized as a heterogeneous disease, whose variants behave differently, have different prognoses and should not be treated in the same way [4]. According to Clark scale, skin is divided into histopathological anatomic compartments according to the depth of invasion of melanoma cells:

Level 1: melanoma cells are confined to the epidermis (melanoma in situ)

Level 2: invasion of single cells or very small nests of melanoma into the papillary dermis

Level 3: melanoma cells "fill and expand" the papillary dermis

Level 4: invasion into the reticular dermis

Level 5: invasion into the subcutaneous fat.

A second classification, Breslow's depth, is based on the depth of invasion in millimeters rather than the depth by anatomic compartments.

Stage I: less than or equal to 0.75 mm

Stage II: 0.76−1.5 mm

Stage III: 1.51–2.25 mm

Stage IV: 2.26–3.0 mm

Stage V: greater than 3.0 mm.

Melanoma evolves through two major stages of tumor progression, the radial growth phase (RGP) and the vertical growth phase (VGP). In the first stage, lesions appear as pigmented patches or plaques, which expand more or less along the orizontal axis within the skin; in the second stage of progression, a nodule is formed, whose direction of growth includes the vertical axis, because the tumor may infiltrate the dermis or elevate the epidermis. Based on the presence or absence of the RGP, cutaneous melanoma is classified in nodular melanoma (NM), superficial spreading melanoma (SSM) and lentigo maligna melanoma (LMM). Acral melanoma and mucosal melanoma arise via pathways in which solar damage does not appear to play a role [5].
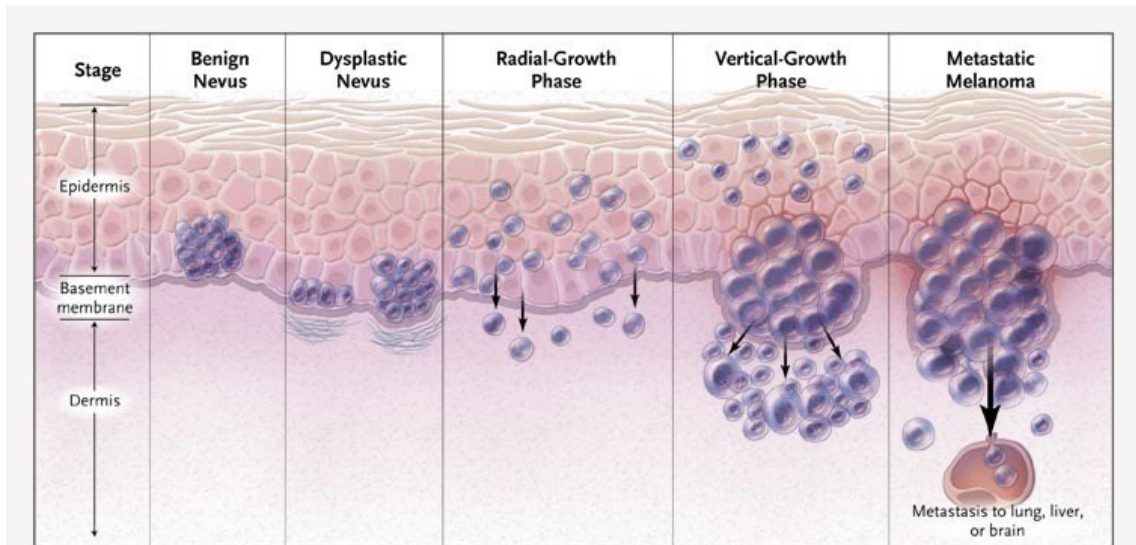
Figure 1. Melanoma progression. Schematic representation of cutaneous melanoma development from healthy melanocyte to metastatic disease. (Adapted from Miller and Mihm, 2006).

In 2018, the WHO proposed a new multidimensional classification of melanoma based on histologic, clinical, epidemiologic and genetic characteristics. There are nine categories, each defined by a specific genetic driver, clustered in three main group according to the degree of Cumulative Sun Damage (CSD).

Melanomas arising in CSD skin (low and high UV): pathways I-III	Melanomas not consistently associated with CSD (low or no UV): pathways IV-IX	Melanomas arising in any pathway (no or variable UV)
Pathway I: low-CSD melanoma	Pathway IV: Spitz melanoma	Nodular melanoma
Pathway II: high-CSD melanoma	Pathway V: acral melanoma	Nevoid melanoma
Pathway III: desmoplastic melanoma	Pathway VI: mucosal melanoma	
	Pathway VII: melanoma in congenital nevus	
	Pathway VIII: melanoma in Blue nevus	
	Pathway IX: uveal melanoma	
CSD: cumulative sun damage; UV: ultraviolet radiation		

Table 1. Classification of melanoma (modified from 2018 WHO Classification). (Adapted from Bobos 2021).

Low-CSD melanoma/superficial spreading melanoma (LCSD/SSM) is the most common form of melanoma. Sun exposure, especially during childhood, and continuing intermittent exposure in adulthood are associated with an increased risk of developing

this type. It is commonly present in adults and the most frequent sites are the back and shoulders in men and the legs in women[5]. The most frequent genetic alteration is BRAFV600E mutation; then TERT promoter and CDKN2A mutations. In advanced tumors, TP53 and PTEN mutations are common. High-CSD (HCSD) includes lentigo maligna melanoma (LMM) and desmoplastic melanoma (DM). They occur on heavily sun-damaged skin, such as the face or hands, and concern older people. They have a higher mutation burden and may harbor NRAS, BRAF non-V600E or NF1 mutations. TERT promoter and CDKN2A mutations are also frequently found, while KIT mutations are found in a subset of cases[6]. The group of low to non-UV exposure/CSD melanomas includes Spitz melanomas, acral melanomas, mucosal melanomas, melanomas developed from congenital nevi and blue nevi and uveal melanomas. These melanomas rarely show BRAF, NRAS or NF1 mutations (triple wild-type). Among a subset of acral and mucosal melanomas KIT and CDKN2A mutations and CCN1 amplification are found, in addition the former presents NRTK3 rearrangement, while the second mutations in SF3B1 gene. Spitz melanomas show a particular oncogenic signalling pathway involving tyrosine kinase or serine-threonine kinase fusions (ALK, NRTK1 and NRKT3). Congenital melanocytic nevi have frequently somatic mutations in NRAS codon Q6, whereas BRAF mutation or fusion is uncommon. Melanomas in blue nevus and uveal melanomas are characterized by GNA11 or GNAQ mutations [5,6]. In any pathway category (UV or no UV) nodular melanoma (NM) and nevoid melanoma are found [5].

Arising from Skin High CSD	Arising from Skin Low CSD	Arising from Acral Surfaces	Arising from Mucosal Surfaces	Uveal Melanoma
BRAF non V600Emut.	APC mut.	ALK rearr.	BRAF mut.	BAP1 mut.
EGFR mut.	BAP1 mut.	BRAF mut.	CCND1 amp.	CYSLTR2 mut.
ERBB2 mut.	BRAFV600E mut.	CCND1 amp.	CDK4 amp.	EIF1AX mut.
KIT mut.	CDKN2A mut.	GAB2 amp.	CDKN2A mut.	GNA11 mut.
MAP2K1 mut.	CTNNB1 mut.	HRAS mut.	KIT mut.	GNAQ mut.
MAP3K1 mut.	MAP2K1 mut.	KIT mut.	KRAS mut.	PLCB4 mut.
MET mut.	NRAS mut.	KRAS mut.	MDM2 amp.	SF3B1 mut.
NF1 mut.	PRKAR1A mut.	NF1 mut.	NF1 mut.	
NFKBIE mut.	PRKCA mut.	NRAS mut.	NRAS mut.	
NRAS mut.	PTEN mut.	NTRK3 rearr.	SF3B1 mut.	
PIK3CA mut.	TERT mut.	TERT mut.		
PTEN mut.	TP53 mut.			
PTPN11 mut.				
RAC1 mut.				
TERT mut.				
TP53 mut.				

UV signature
High TMB

Lack UV signature
Low TMB

Figure 2. Genomic alterations of melanoma subtypes defined by UV exposure. Abbreviations: amp, amplification; CSD, cumulative sun damage; rearr, rearrangement; TMB, tumor mutational burden; UV, ultraviolet. (Adapted from Teixido 2021).

Recent recommendations indicate that pathology laboratories should perform basic IHC tests, such as: HMB-45; SOX10; MITF, tyrosinase, MART-1; P16; Ki-67/MIB1; BAP1 (BRCA1-associated protein 1); β-catenin; PRAME; and at least one molecular method to detect BRAF codon 600 and NRAS mutations [6].

1.1.2.2 Genomic classification of cutaneous melanoma

Cutaneous melanoma derives from the tumoral transformation of melanocytes. The main risk factor is excessive exposure to UV radiation, intense and intermittent, as well as exhibition to artificial sources. The number of nevi, family history of melanoma and genetic susceptibility are among the most significant host risk factors for melanomagenesis.

Around 5-12% of melanomas are hereditary and show different mutation profiles than non-hereditary melanomas. Up to 40% contain CDKN2A mutations and as less common but more aggressive are mutations in NER pathways [4,6].

Non-hereditary melanomas occur from somatic mutations acquired later in life. The major signalling pathways involved are: regulation of proliferation (BRAF, NRAS and NF1), growth and metabolism (PTEN and KIT), resistance to apoptosis (TP53), replicative lifespan (TERT), cell identity (ARID2) and cell cycle control (CDKN2A) [4].

According to the analysis from Cancer Genome Atlas Network, carried out in 333 cutaneous primary and/or metastatic melanoma, cutaneous melanoma can be divided into four genomic subtypes: BRAF, RAS (N/H/K), NF1 and Triple-Wild Type.

The first group is the most representative and is defined by the presence of BRAF hotspot mutations, among which the most frequent is BRAFV600 and the second one is the K601 residue. Patients with BRAF subtype are young and 90.7% of tumors harbor a UV signature. Frequently focal amplifications of BRAF, MITF and PD-L1 are present. 75% of tumors present TERT promoter mutations and show also mutations and deletions for PTEN.

The second major subtype is defined by the presence of RAS hotspot mutations in all three RAS family members – N, K and H. This subtype also shows the UV signature, mutations in TERT promoter and a significant amplification and mRNA overexpression of AKT3.

NF1 subtype contains more than half loss-of-function predicted mutations, that represent an alternative way to activate MAPK signalling pathway. Patients with this subtype are significantly older than those with the BRAF one. NF1 subtype correlates with the UV

signature, shows mutations in TERT promoter and in RB1 gene. Notably, these tumors have the highest median level of CRAF expression, underling its differential mode for MAPK pathway activation.

The triple wild-type subtype is characterized by a lack of hotspot BRAF, N/H/K-RAS or NF1 mutations. Only 30% of these tumors harbor a UV signature but have more copy-number changes and complex structural arrangements compared to the other groups. Indeed, this subtype contains focal amplification of the oncogene KIT, frequently together with PDGFRA and KDR. It shows high levels of focal CNAs containing the oncogenes CDK4 and CCND1. Moreover, it includes a higher median level of BCL-2 and amplification of MDM2 than the other subtypes [7].
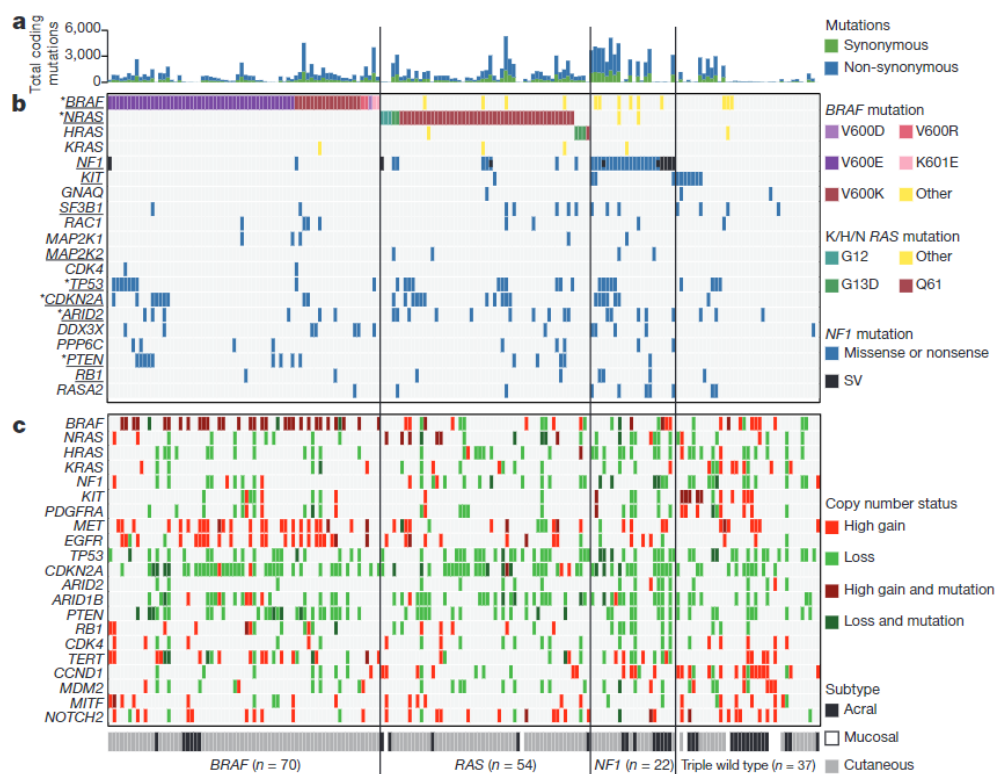
Figure 3. Mutations and copy number changes in melanoma driver genes. a. Somatic coding mutation rate. b. Mutations in significantly mutated genes (underlined); BRAF, RAS and NF1 aberrations coloured by mutation type. c. Copy number changes in melanoma-associated genes: loss (green), high gain (at least six copies, red). Melanoma subtype shown below. (Hayward et al. 2017).

1.1.2.3 MAPK pathway

The mitogen-activated protein kinase (MAPK) cascade is an intracellular signal transduction pathway, evolutionary conserved, that reacts to different extracellular stimuli and controls a variety of fundamental cellular processes, such as proliferation, differentiation, development, motility, stress response, survival, apoptosis and transformation, and is the most significant pathway involved in melanomagenesis [6,8]. MAPK cascade transmits signals through sequential activation of three to five layers of protein kinases known as MAPK kinase kinase kinase (MAP4K), MAPK kinase kinase (MAP3K), MAPK kinase (MAPKK), MAPK and MAPK-activated protein kinases (MAPKAPK)[9]. MAP3K, MAPKK and MAPK constitute the core kinase, while MAP4K acts as upstream and MAPKAPK as downstream components, and they occur in some cascades and can be different according to the cell type and stimuli. [9]. Fourteen different mammalian MAPKs have been described and have been distributed into three main groups: extracellular signal-regulated kinase (ERK), c-Jun N-terminal kinase (JNK) and p38 [6].

The MAPK/ERK pathway is activated by the binding of a growth factor (GF) or hormone or cytokine to a membrane receptor with a tyrosin kinase activity (RTK). This leads to its dimerization and autophosphorylation of Tyr residues on its intracellular domains. This modification allows the binding of proteins containing Src homology 2 or phosphotyrosine-binding domains. In return, adapter protein, such as Growth factor Receptor bound protein 2 (GRB2), are recruited to the receptor. After that, the guanine nucleotide exchange factor (GEF) son of seven-less (SOS) binds to GRB2 and accelerates the activation of RAS (Rat Sarcoma), by switching the inactive guanosine-5-diphosphate (GDP-RAS) to active guanosine-5-triphosphate (GTP-RAS). Ras activation is

subsequently attenuated by the GTPase-activating protein (GAP) neurofibromin 1 (NF1). This nucleotide exchange enables the direct interaction of RAS (Rat Sarcoma) with a RAF (Rapidly Accelerated Fibrosarcoma) family protein (ARAF, BRAF and CRAF rapidly accelerated fibrosarcoma proteins), which successively phosphorylates and activates MEK (mitogen-activated protein kinase kinases MEK1 and MEK2, also known as MAP2K1 and 2 or MAPKK1 and 2). Finally, MEK phosphorylates and activates mitogen-activated protein kinase (MAPK/ERK), which translocates to the nucleus and activates more than fifty transcription factors [10,11].
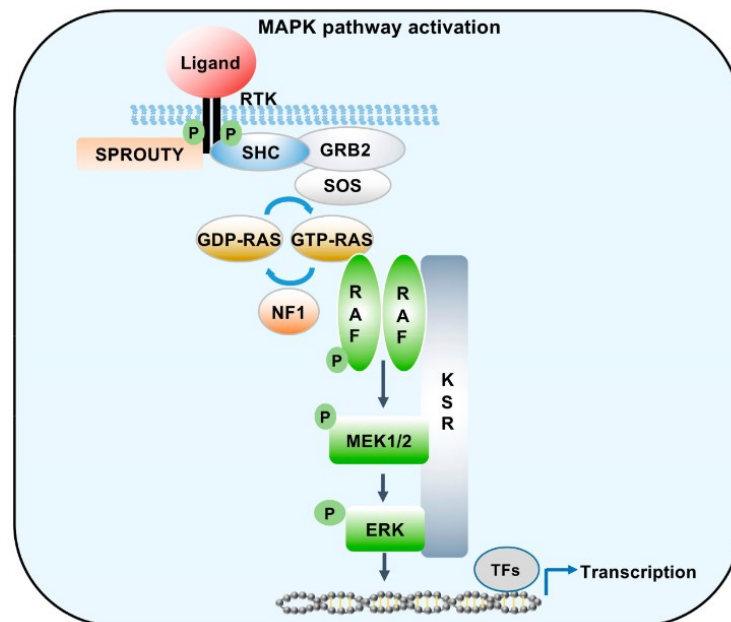
Figure 4. Schematic of MAPK signalling in the context of wild type BRAF. (Saei et al. 2019).

1.1.2.4 Dysregulation of MAPK pathway

Dysregulation of MAPK pathway is found in 98% of melanomas and can lead to hyperactivation of the cascade [10]. Approximately 15-20% of melanomas have NRAS mutations. KRASQ61 is the most frequent mutation of KRAS in melanoma, which implies a decrease in its intrinsic hydrolytic activity and a sustained active state of KRAS. When NF1 loss of function mutation is found, RAS is not more inactivated and is free to

act downstream [6]. In about 50-60% of metastatic melanomas BRAF mutations were found and can be grouped into three groups (classes 1-3). Class 1 refers to a transversion point mutation in the activation segment of the kinase domain at codon 600, resulting in the replacement of the wild-type amino acid, valine, with, most commonly (80-90%), glutamic acid. Other rarer substitutions include about 7.7% V600K (lysine substitution), 1% V600R (arginine substitution) and leucine and aspartic acid substitutions with a frequency of 0.3% and 0.1%, respectively. There are also substitutions in other BRAF sites but represent only 1% [10]. The mutated BRAFV600E gene generates a constitutively active oncoprotein, which behaves as a monomer irrespective of upstream signals (i.e., RAS), thereby causing the hyperactivation of the MEK-ERK cascade. Class 2 involves activating BRAF mutations that are RAS-independent, but function as dimers, resulting in intermediate kinase activity. In this category non-V600 mutations have been found in the activation segment (K601E, L597Q), the DFG motif (F595L) as well as the P-loop (G469A) of the BRAF kinase. In class 3 BRAF mutations (also non-V600) are RAS-dependent and work as dimers, with mutations in either the P-loop (G466), catalytic loop (N581) or the DFG motif (D594). These mutants homodimerize with either wild-type BRAF or heterodimerize with CRAF to signal and have lower kinase activity than their wild-type counterparts [12].
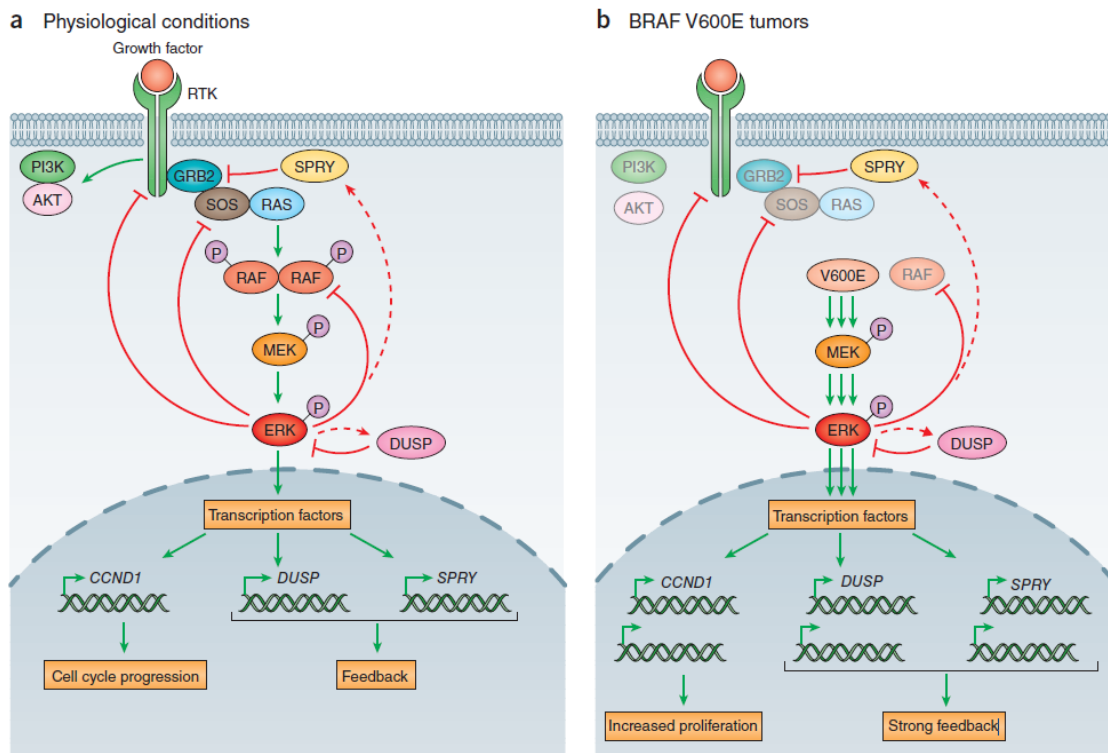
Figure 5. ERK signalling under physiologic conditions and in tumors harboring BRAF V600E mutations. (Lito et al. 2013).

1.1.2.5 Melanoma treatment

Great progress has been made in the therapeutic field, which has allowed a huge improvement in the survival and quality of life of patients with advanced melanoma.

1.1.2.5.1   Surgical resection

For localized melanoma, surgical resection of the tumor and surrounding healthy tissue is the first option. Indeed, it is the standard of care for early-stage melanoma, with a very good long-term prognosis [13]. Sentinel lymph node biopsy is performed when tumors are greater than 0.8 mm thick or are thinner than this but ulcerated (stage pT1b or greater), and when tumor cells are found, lymph nodes are removed. Sometimes, metastatic

melanoma can be surgically removed; this is the case for metastasis to the gastrointestinal tract, which has the greatest survival rate compared to the liver, spleen and pancreas. Still, surgery combined to systemic treatment reaches a major benefit [4,14].

1.1.2.5.2 Chemotherapy

The first chemotherapeutic drug approved by FDA was Dacarbazine in 1975. Then, in 2000, Temozolomide was accepted as an oral agent and it was used mainly for brain metastases, thanks to its property of crossing the blood-brain barrier. Finally, Fotemustine, a chloroethyl nitrosourea drug, showed a better response rate than Dacarbazine. However, these chemotherapeutic agents induce very mild long-term effects and do not show survival benefit for patients [4,14].

1.1.2.5.3 Radiation

Radiotherapy is indicated for palliation of non-CNS metastases and symptomatic patients. For brain metastasis a gamma knife radiosurgery is applied. Moreover, through the abscopal effect, radiotherapy can reduce tumor growth outside the direct irradiated region, because the electromagnetic waves activate inflammatory pathways that start the dendritic cell activation of tumor-specific T cells.

1.1.2.5.4 Immune response and immunotherapies

Interleukin-2 (IL2) was approved in 1992 as one of the first immune therapies for metastatic melanoma. It is a pro-proliferative cytokine that stimulates the proliferation and activation of tumor-infiltrating T cells. As systemic drug is used as first-line treatment for unresectable stage IV melanoma patients with "good performance status", indipendently of BRAF mutation status. However, intralesional IL2 is preferred because

of toxicity reduction [4,14]. The first immune checkpoint inhibitor (ICI) was approved in 2011 and since then treatment and prognosis of metastatic melanoma change a lot, using antibodies against CTLA-4 and PD1. CTLA-4 is an immune checkpoint receptor, constitutively expressed by naive T cells, that recognizes and binds the costimulatory protein B7 receptor on APCs in the lymph node. When the binding is precluded by CD28, an immune response is activated, which is downregulated when CTLA-4 binds protein B7. Ipilimumab is a fully human IgG1 monoclonal antibody directed against CTLA-4, which counteracts its inhibitory effect, allowing for T-cell activation and tumor lysis. It can be used in combination with chemotherapy. The PD-1 immune checkpoint is expressed by CD8+ T cells and usually regulates the induction of apoptosis of maturing T-cells that recognize self-antigens in the lymph nodes. At the same time, it prevents apoptosis of regulatory T-cells, which repress the immune response to self-cells. The PD-1 ligand is expressed by tumor cells; when PD-1 receptor binds its ligand, an adaptive immune resistance starts: T-cells are less effective in immune response and cancer cells are protected from immune-mediated cell death. From 2014, Pembrolizumab and Nivolumab are approved as anti-PD1 (CD279) directed monoclonal antibodies for advanced or metastatic melanoma. Moreover, the combination therapy with ipilimumab and nivolumab exceeds to either anti-CTLA-4 monotherapy or anti-PD1 monotherapy [4,6,14].
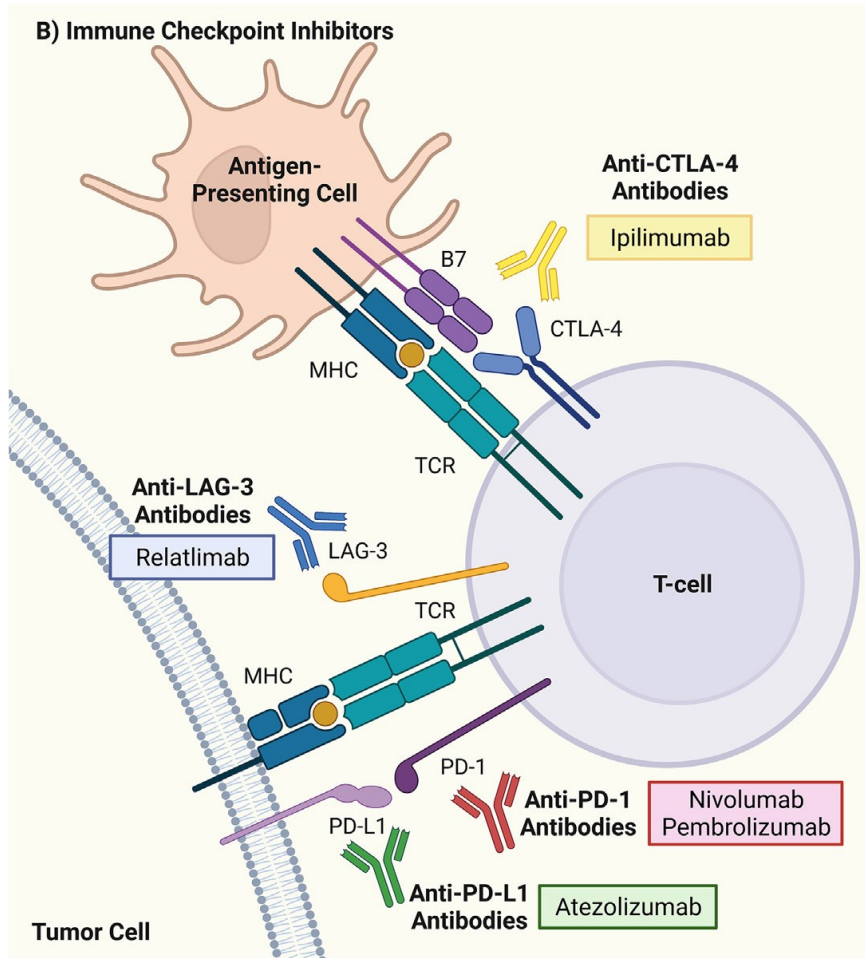
Figure 6. The mechanism of action of ICI approved for stage IV metastatic CM. (Caksa et al. 2022).

The combination of ICI and BRAF/MEK inhibitors seems promising given the durable response observed with the former and rapid and deep response of the latter. The IMspire 150 trial (atezolizumab, an anti-PD-L1 monoclonal antibody plus vemurafenib and cobimetinib) showed the addition of atezolizumab to targeted therapy was tolerable and significantly increased PFS in patients with BRAFV600-mutant metastatic melanoma. On the other hand, COMBI-I trial phase III (spartalizumab, a new monoclonal antibody anti-PD1 plus dabrafenib and trametinib) did not meet its primary endpoint of investigator-assessed PFS for patients treated with the triplet therapy [6].

Other strategies are adoptive T cell therapies (ACT) which involve the injection of selected *in vitro* lymphocyte cells against tumor cells. There are mainly three approaches: tumor-infiltrating lymphocytes (TILs), T cell receptor-engineered T cells (TCR-T), and chimeric antigen receptor T cells (CAR-T).

Melanoma vaccines activate the systemic host immune response against tumor cells. They can be divided according to their composition: whole-cell, dendritic-cell, ganglioside, DNA and peptide vaccines. gp100 and MAGE-3 peptide vaccines are the most successful because of their 11-16% response rate when combined with immunotherapy [6,14].

1.1.2.5.5 Targeted therapy

Initially, to target irregular MAPK pathway signalling, patients with melanoma were treated with Sorafenib (Nexavar), that belongs to the first-generation ATP-competitive RAF inhibitor, which inhibits CRAF, wild-type and mutant BRAF and RTK implicated in cancer angiogenesis and progression. However, the treatment was not so effective because of the weak affinity of the drug for mutant BRAF at clinically achievable concentrations. To get over this limitation, the second-generation ATP-competitive inhibitors that target class 1 BRAF mutations have been developed, such as Vemurafenib (Zelboraf; PLX4032), Dabrafenib (Tafinlar; GSK2118436) and Encorafenib (Braftovi; LGX818). These drugs bind specifically to the ATP-binding pocket of the active form of the protein target [13].

Vemurafenib was the first specific inhibitor that acts on the BRAF/MEK pathway and was approved in 2011. Encorafenib shows a ten-fold longer dissociation half-life (>30 h), which results in extended inhibition of the MAPK signalling pathway and a more potent anti-cancer activity. However, these drugs are not effective against tumors with class 2 or

3 BRAF mutations, where BRAF signals as a dimer. Then, "dimer inhibitors" have also been developed, such as LXH254 and LY3009120, that are able to inhibit both mutant BRAF monomers and dimers at similar doses, as they do not induce negative cooperativity at the second site of BRAF dimer. Furthermore, "paradox breakers" such as PLX8394 are small molecules that disrupt BRAF-containing dimers, including BRAF homodimers and BRAF-CRAF heterodimers, but not CRAF homodimers or ARAF-containing dimers [12].

Subsequently, the MEK inhibitors (MEKi) Cobimetinib (Cotellic), Trametinib (Mekinist) and Binimetinib (Mektovi) were registered. All three compounds are allosteric inhibitors that bind to the MEK kinase and induce conformational changes that subsequently block its kinase activity. They inhibit ERK signalling in both BRAF-mutant and BRAF-wild type cells [10,12].

Among BRAFi side effects are photosensitivity, which can limit the treatment, and the rapid development of cutaneous squamous cell carcinoma (CSCC) or other keratinocytic secondary neoplasias, probably due to the paradoxical activation of the MAPK pathway. Preclinical data showed that BRAFi-resistant cells recovery very fast the MAPK pathway signalling, suggesting the necessity to blockade completely the cascade. Thus, the combination of BRAF and MEK inhibitors (BRAFi plus MEKi) was predicted to decrease this side effect and indeed to improve PFS and OS compared to BRAFi monotherapy [6,13].

At present, three combinations of BRAFi and MEKi have been approved for clinical treatment:

Dabrafenib plus Trametinib: was the first approved since 2014 for metastastic and unresectable melanoma. Apart from pyrexia, photosensitivity reactions and cutaneous adverse events are less. From 2018 the combination is used as adjuvant therapy in patients with III stage melanoma.

Vemurafenib plus Cobimetinib: its clinical development paralleled that of the first combination. From 2015 is approved for metastatic melanoma. The toxicity profile is higher caused by Vemurafenib, including serious retinopathy, decreased left ventricular ejection fraction (LVEF) and increased creatine phosphokinase level.

Encorafenib plus Binimetinib: it was approved from 2018. Encorafenib has a higher potency for wild-type BRAF and CRAF and could attenuates some resistance mechanisms and/or reduces the paradoxical activation. Relevant adverse effects are increased glutamyltransferase, increased creatine phosphokinase and hypertension [13].
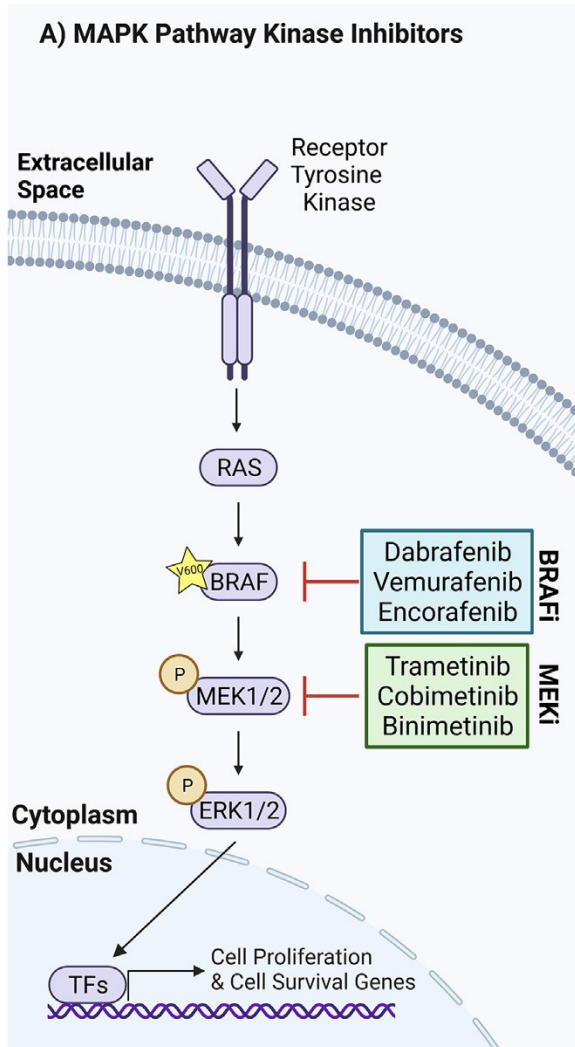
Figure 7. The mechanism of action of MAPKi approved for stage IV metastatic CM. (Caksa et al. 2022).

1.1.2.5.5.1 Mechanisms of resistance

In most patients, the appearance of resistance to treatment is an unescapable event. Indeed, at first patients show response to BRAF and MEK inhibitors, but within 6-7 months approximately half of them develop tumor relapse [6,13,15]. The mechanisms of resistance are various and can be grouped into: intrinsic, adaptive and acquired.
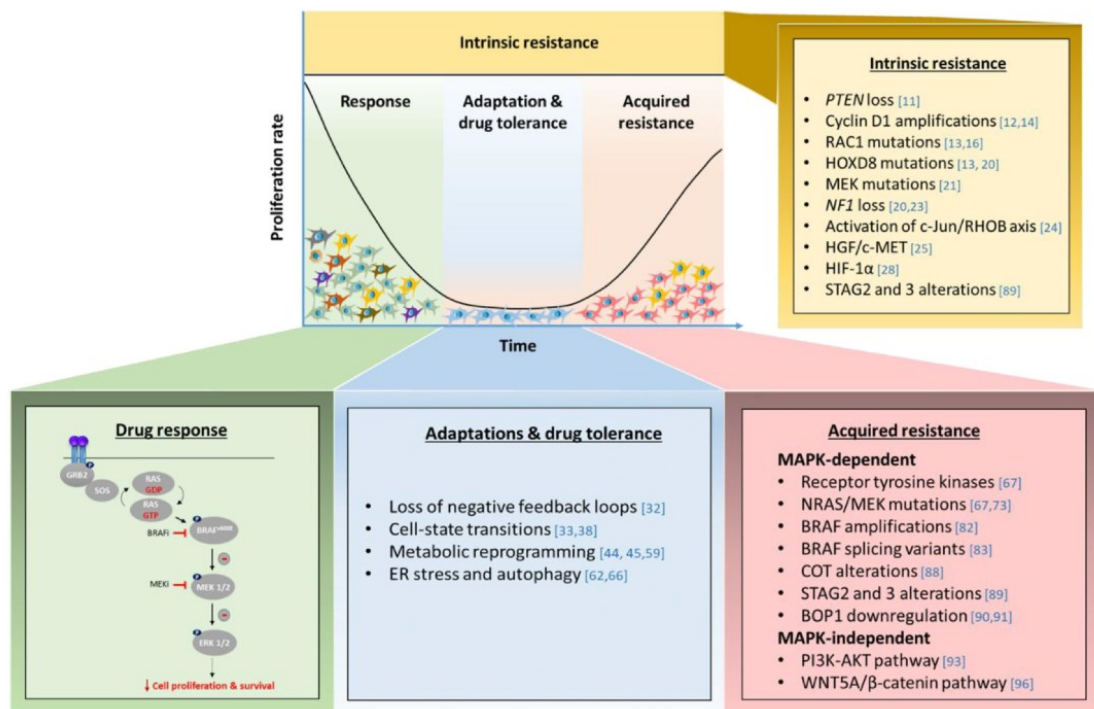
Figure 8. Mechanisms conferring intrinsic, adaptive and acquired resistance in BRAF-mutant melanomas. (Tangella et al. 2021).

1.1.2.5.5.1.1 Intrinsic

Intrinsic resistance is due to pre-existing genetic alterations, of which many were not accounted as validated mutations but appear as transcriptomic alterations (Cancer Genome Atlas Network, 2015), and to factors secreted from stromal and tumor cells. PTEN loss occurs in 10–35% of melanomas, is incompatible with NRAS mutations but coexists with BRAF mutations. It activates MAPK and PI3K/AKT pathways and suppresses the BIM-mediated apoptosis. Moreover, the activation of the pathways mentioned above leads to the dysregulation of the RB pathway, that includes inactivation mutations and epigenetic silencing of CDKN2A and amplification of CCND1 gene (found in about 20% of BRAF mutated melanomas). Other genes that present mutations are: MEK1/2, ERK, RAC1, HOXD8 and NF1 loss. Among the endogenous secreted

factors are HIF1alpha and HGF/c-MET, that are able to activate tumor cell growth in a paracrine form upregulating PI3K.

1.1.2.5.5.1.2 Adaptive

Adaptive response and drug tolerance are attributable to a fraction of the tumor population that develops a pro-survival capacity, which is temporary and reversible and cannot be passed to progenies. Some of the adaptive mechanisms are: loss of kinase-dependent negative feedback loop, phenotypic switching or cell-state transition, metabolic reprogramming and ER stress and autophagy [16,17].

The reactivation of the MAPK pathway, following BRAFi treatment, can arise through loss of negative feedback loop. Indeed, all of the core components of the canonical MAPK pathway are regulated through feedback inhibition. ERK phosphorylates EGFR at T669 residue, attenuating receptor activation. ERK, by phosphorylating SOS, allows the dissociation of the GRB2-SOS complex and the inhibition of RAS activation. RAS activation is further inhibited through the upregulation of NF1 GAP activity. Finally, SPROUTY phosphorylation creates a docking site for GRB2 inhibiting GRB2 function and downstream RAS activation. Moreover, to limit continuous RAF activation, ERK phosphorylates RAF at a number of different serine/threonine residues (S151, T401, S750, T753). Finally, ERK phosphorylates MEK1 at T292 residue, decreasing its dimerization and inhibiting further ERK activation [11]. The inhibition of MAPK pathway relieves these regulation feedback loop.
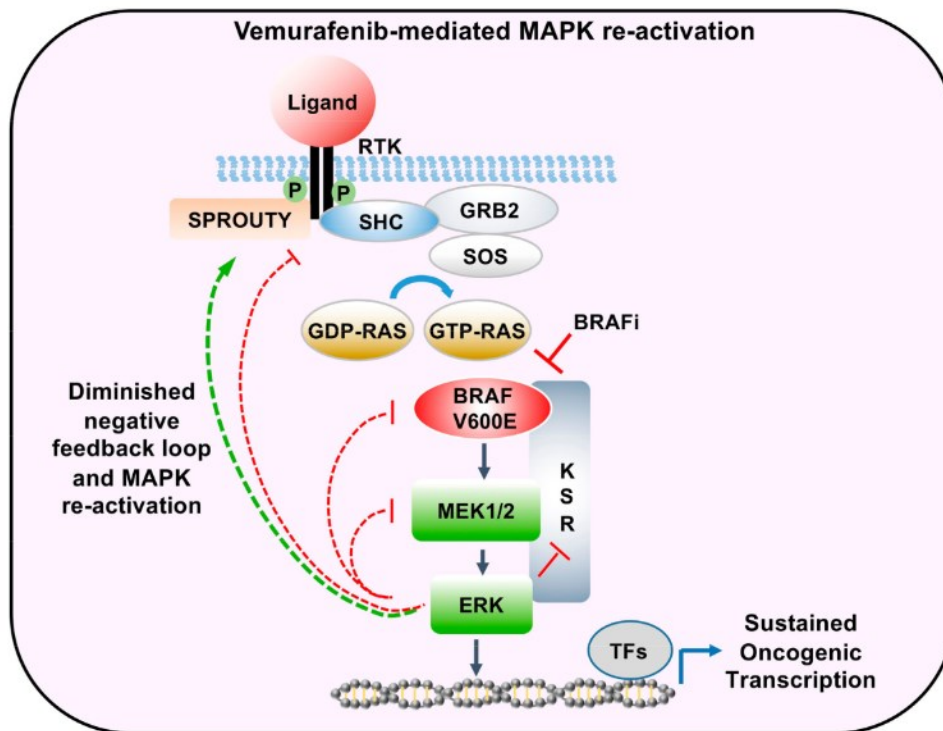
Figure 9. Negative feedback regulation of activated ERK on EGFR, RAF and MEK, resulting in the downregulation of MAPK signalling. (Saei et al. 2019).

Within the same tumor, two subpopulations with high and low levels of MITF expression are often identifiable, highlighting the importance of the MITF-rheostat model. MITF is a melanocytic-lineage transcriptional factor fundamental for early melanogenesis and differentiation in melanocytes, but is also involved in numerous biological processes in melanoma cells. Indeed, acquisition of MITF-low signature correlates with invasiveness, as well as with the high expression of genes such as the WNT ligand WNT5A, receptor tyrosine kinase AXL, TGFβ, TNFα/NF-κβ activation, JUN, and TEAD. MITF-high signature population results in increased pigmentation, thanks to the high levels of MITF downstream targets, such as MLANA, PMEL, TYRP-1 and TYRP-2 genes, and enhanced oxidative phosphorylation and with a higher rate of proliferation. Among other phenotypes switching and global alterations in gene expression programs are the acquisition of a stress signature [18], a neural crest-like state by NGFR and markers of

the neural crest, a melanocyte precursor [12,18–21] and an undifferentiated state characterized by low levels of the transcription factor SOX10 and high expression of receptor tyrosine kinases such as AXL and EGFR [12].

Usually, BRAF mutant melanoma cells display high glycolytic activity by increasing the production of HIF-1 alpha and MYC and decreasing the activity of MITF as a regulator of oxidative phosphorylation. However, treatment with BRAFi and MEKi leads to an increase in the axis MITF/PGC1alpha, activating the OXPHOS pathway. Moreover, cells that overexpress PGC1alpha and JARIDB1 exhibit slow cycling and are more resistant to oxidative stress. In addition, short-term treatment with MAPKi alters the fatty acid oxidation (FAO) through upregulation of fatty acid transporter CD36 and of CPT1A.

The inhibition of MAPK pathway increases also the transcription of autophagy-associated genes, including the autophagy marker, LCS. Moreover, BRAFi triggers autophagy-lysosomal activation through TFEB, by inhibiting its binding to ERK and permitting nuclear localization and upregulation of TFEB target genes. Finally, ERK inhibition improves phosphorylated AMPK and Beclin1, facilitating the initiation of autophagy and localization of autophagic proteins to phagophore [11,16].

1.1.2.5.5.1.3 Acquired

Acquired resistance often arises from MAPK dependent or MAPK independent mechanisms. Regarding MAPK re-activation, overexpression of multiple receptor tyrosine kinases (RTKs) as EGFR, PDGFRβ, MET, ERBB3, IGFR1, FGFR has been reported. Upstream activating mutations are included, as for NRAS and KRAS. BRAF amplification is a copy gain of the mutant allele of BRAF, resulting in overexpression and leading to reactivation of ERK independently of RAS. Alternative splicing variants

lack the RAS binding domain encoded by exons 3-5, but are still able to dimerize in presence of low levels of RAS. Downstream MAPK pathway alterations include MEK1/2 mutations, ERK mutations or CDKN2A loss. Other alterations are: overexpression of COT1, loss-of-function of STAG2 and decreased expression of STAG2 and STAG3. In MAPK independent mechanisms encompass the activation of parallel signalling pathways as PI3K-AKT and WNT5A/beta-catenin [13,16,17].

1.1.2.6 Melanotic and amelanotic melanoma

Melanomas can also be classified as either melanotic or amelanotic, according to the presence of pigmented lesions. Amelanotic melanoma (AM) is rare and is characterized by little to no pigment and can present as red-to-pink macules, papules, or plaques [22]. Because it is often overlooked or confused with other benign skin lesions, amelanotic melanoma may be diagnosed at a later stage compared with brown, black, or blue melanomas. Approximately 5% of melanomas overall are amelanotic (Memorial Sloan Kettering Cancer Center).

At metastatic level, melanotic melanomas display higher resistance to therapy in general.

Radiotherapy. Melanin exhibits radioprotective and scavenging properties. The evaluation of survival time of patients treated with radiotherapy shows higher rate for those with amelanotic melanomas [23].

Phototherapy. Several mechanisms are involved in melanoma resistance against photodynamic therapy (PDT) as: presence of melanin, especially in hyper pigmented melanomas, quenching activity of melanosomes and defects in the apoptotic pathways [24]. Indeed, Sharma et al. demonstrated that the removal of melanin with Kojic acid (KA), a tyrosinase-specific inhibitor, increases the susceptibility of cells to PDT [25].

More recently, photobiomodulation therapy occurs harmless for amelanotic melanoma but triggers different responses in melanotic pigmented cells depending on light parameters [26]. So, one of the main issues in PDT is to find improved tumor targeted photosensitizers, mainly NIR absorbing, to avoid melanin protection, with high selective tumor accumulation, possibly with the help of nano carriers, capable of inducing high amounts of different ROS inside tumor and vasculature cells [24,27].

Chemotherapy. Pigmented melanoma cells are less sensitive to cyclophosphoamide and to killing action of lymphocytes, indeed melanin alters the cytotoxic effect of the drug and shows potent immunosuppressive properties. But when it is inhibited through blocking catalytic tyrosinase activity or chelating copper ions, the cells response well to the treatment [28]. Coriolus versicolor fungus-derived protein-bound polysaccharides (PBPs) in melanoma cells induces an alternative programmed cell death, accompanied by increased ROS production, in a melanin content dependent way, thus only amelanotic but not melanotic cells die [29]. In MNT-1 cells the depletion of VPS33A (vacuolar protein sorting 33A protein) or of CNO (cappuccino protein which is a subunit of the heteromeric biogenesis of lysosome-related organelle complex-1 (BLOC-1)), two important proteins involved in protein trafficking and melanosomes maturation, results in increased cells chemosensitivity to cDDP, carboplatin, DTIC and the combination of TMZ/veliparib. This increased sensitivity correlates with a decreased proportion of mature eumelanosomes being formed [30]. HeLa cancer cells, that do not contain melanosomes, are more sensitive to cDDP compared with MNT-1 melanoma cells with mature melanosomes, and SK-Mel-24 melanoma cells with immature melanosomes show increased sensitivity to cDDP compared with MNT-1. Furthermore, independent mutations in three separate genes that regulate protein trafficking to melanosomes,

Dtnbp1, Pldn, and Vps33a, or in tyrosinase, or the absence of gp100/Pmel17, result in perturbation of melanosome biogenesis and concurrent increased drug sensitivity. The data clearly establish that sensitivity to the chemotherapeutic agents cDDP, vinblastine and etoposide is improved when regulators of melanosomes biogenesis are stopped [31]. Chen et al. provide evidences that one of the mechanisms of melanoma drug resistance is due to melanosomes that sequester cytotoxic drugs, as CDDP, and facilitate their export from the cells [32]. Sanchez del Campo et al. in 2009 confirm this melanosome property also for methotrexate (MTX), which is sequestered through a particular FRa-induced endocytic transport [33] .

Worse prognosis. Interestingly, clinicopathological analyses on advanced melanomas have shown negative correlation between tumor pigmentation and diseases outcome as defined by overall survival and disease-free time. In patients with metastatic melanoma, those with melanotic tumors showed significantly shorter DFS and OS than those with amelanotic lesions, as well as for melanin-producing lymph node [34,35]. Damsky et al. have showed that beta-catenin accelerates melanomagenesis in a BRAF/PTEN mouse model; in particular, metastasis in Pten/Braf/Bcat-STA melanomas is accompanied by an increase in melanocytic differentiation markers [36]. In 2017, Kim et al. observed that, in a zebrafish model, microenvironment-derived factors, such as EDN3, support metastasis diffusion through a phenotype switching versus MITF high/differentiated/proliferative state [37]. Notably, there is a link between TYRP1 levels and the survival of patients with metastatic melanoma, that is enforced by the fact that TYRP1 sequesters miR-16 and reduces its tumor-suppressor activity [38]. In a study conducted in 57 patients with IV stage of melanoma, a hierarchical clustering of global gene expression identified four different subtypes: immune response, pigmentation differentiation and proliferation. It

showed that tumors with a proliferative or pigmentation phenotype were genetically more unstable with a higher fraction of altered genome. In particular, these two subtypes were characterized by frequent hemizygous chromosome 9p and 10 deletions, suggesting targeted deletions of the known melanoma suppressor genes CDKN2A and PTEN [39]. In 2015, the same research group, by perfoming expression profiling on 214 cutaneous melanoma tumors, found an increased risk of developing distant metastases in the pigmentation (HR, 1.9; 95% CI, 1.05-3.28; P=0.03) and proliferative (HR, 2.8;95% CI, 1.43-5.57; P=0.003) groups as compared to the high-immune response group [40]. TYRP1 mRNA expression is a prognostic marker for clinical outcomes in metastatic melanoma. Indeed, it has been showed to be significantly correlated with distant metastasis-free survival (DMFS), overall survival (OS) and Breslow thickness [41]. In 2017, we found that metastatic melanoma patients with high TRPM1/EDEM1 ratio are characterized by lower overall survival compared to those with low TRPM1/EDEM1 ratio. We also noticed that melanotic cell lines display higher IC50 to vemurafenib and trametinib compared to amelanotic cell lines. Finally, metastatic melanoma patients with melanotic tumors respond poorly to BRAFi/MEKi treatment [42].

Targeted therapy: In 2017, we demonstrated that miR-211, a known transcriptional target of MITF, is induced in melanotic melanoma cells when treated with vemurafenib and mediates its pro-pigmentation activity; miR-211 targets EDEM1 and as a consequence impairs the degradation of tyrosinase through the ER-associated degradation (ERAD) pathway. We showed also that pigmentation impairs the activity of BRAFi and MEKi [42]. In 2019, Sahoo et al. displayed that miR-211 is upregulated by vemurafenib in melanoma cell lines, while its loss makes them more sensitive and reduce their growth and invasion *in vitro* and *in vivo* [43]. In 2020, it has been observed that miR-211

promotes proliferation through post transcriptional activation of ERK5 signalling and modulates melanoma resistance to vemurafenib and cobimetinib [44].

1.2   Reactive oxygen species

Reactive oxygen species are partially reduced or excited forms of atmospheric oxygen. In cells, they function as signalling molecules, but are also considered as toxic by-products of aerobic metabolism. To prevent oxidation of DNA, RNA, protein and membrane, as referred in general to oxidative stress, these species are constantly removed by anti-oxidant mechanisms. Overall, maintaining a basal level of ROS in cells is essential for their survival, and oxidative stress is simply an activation of physiological cell death pathway [45].

These reactive molecules can be divided in radical and non-radical species. Radicals are free-electrons that include: superoxide anion ($O_2\bullet^-$), its conjugated hydroperoxyl radical ($HO_2\bullet^-$), hydroxyl ($\bullet OH$), carbonate ($CO_3\bullet^-$), peroxyl ($RO_2\bullet$) and the alkoxyl radical ($RO\bullet$). Non-radicals can be reduced into free electron-containing species and are: hydrogen chloride (HCl), hydrogen peroxide (H_2O_2), reactive aldehydes, fatty acid hydroperoxides (FaOOH) and singlet oxygen. ROS are highly versatile thanks to their different levels of reactivity, sites of production and diffusion capabilities to cross biological membranes [46]. Also called as free radicals, ROS share a short life and a generation of chain reactions that can lead to cell damage [47].
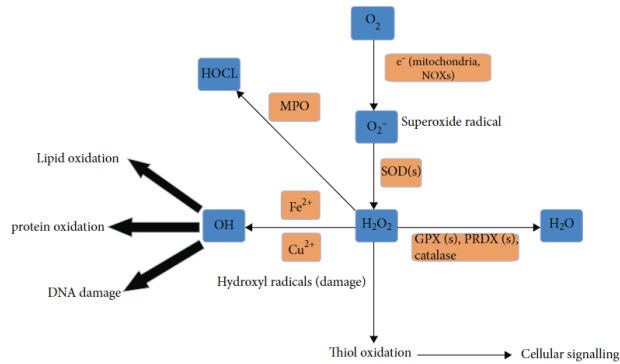
Figure 10. ROS types and generation. Abbreviations: GPXs: glutathione peroxidases; PRDXs: peroxiredoxins; SODs: superoxide dismutases. (Sagwal et al. 2021).

Mitochondria and NAPDH oxidases are two major providers to endogenous ROS levels. Other cellular compartments are peroxisomes and melanosomes. The highest quantity of ROS is generated at the mitochondria electron chain; indeed, during the tricarboxylic acid cycle, one electron is removed from metabolites, such as amino acids, glucose and lipids, and transferred to the electron transport, resulting in the reduction of O2 to $O_2\bullet^-$ (resulted in 1% of all consumed O2 in the mitochondria)[48]. Chain formation of $O_2\bullet^-$ is produced by complex I, which releases it into mitochondrial matrix via electron leaks, and by complex III, which releases $O_2\bullet^-$ both into inner mitochondrial space and matrix. Most of the $O_2\bullet$- generated at the mitochondria are dismutated to H2O2 by manganese superoxide dismutase (MnSOD) in the mitochondrial matrix. H2O2 is highly diffusible, can cross the mitochondrial membrane through aquaporins and can acts as second messenger. Enzymes like NADPH oxidases contribute to the production of cytosolic ROS. NAPDH oxidases is a family composed of 7 members (5 Nox isoforms, Nox1-5 and two dual oxidases, Duox1 and Duox2) and controls the production of $O_2\bullet^-$ via coupling NADPH-derived electrons to oxygen, which is quickly converted into H2O2 [46]. Nox proteins have similar structures, but differ according to the activation and

regulation mechanisms [48]. Among other sources of ROS are cyclooxygenases (COXs), lipooxygenases, xanthine oxidases, nitric oxide synthases and cytochrome p450 enzymes.
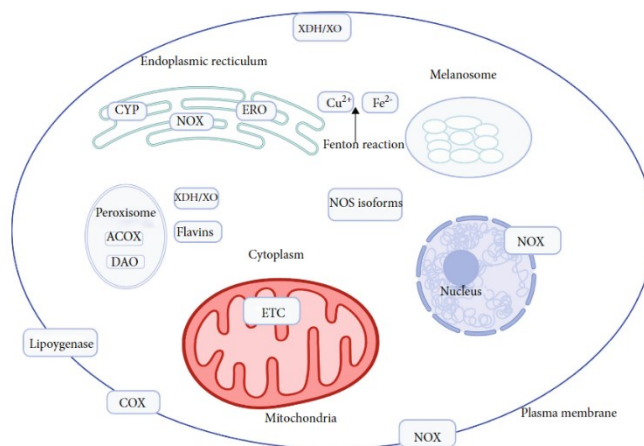
Figure 11. Sources of cellular ROS production. (Sagwal et al. 2021).

1.2.1 Regulation of ROS

ROS homeostasis is fundamental for cell survival and for the prevention of cell damage. Cells have evolved two kinds of ROS scavenging systems: enzymatic and non-enzymatic, that are very modulated and respond in a rapid and accurate way.

Non-enzymatic pathway includes vitamins or its analogs (vitamins A, C, and E; coenzyme Q10; and flavonoids), minerals (selenium and zinc) and metabolites (bilirubin and melatonin). Vitamin A (retinol) results from the breakdown of β-carotene and is synthesized in the liver. It can react with peroxyl radicals forming free carbon-centered radical adducts and scavenge them before they spread peroxidation to lipids. Vitamin C (ascorbic acid) can scavenge a variety of oxygen free radicals. Vitamin E (a-tocopherol) is a fat-soluble antioxidant that can preserve the polyunsaturated fatty acids in the membrane from oxidation. Coenzyme Q10 (CoQ10) is essential for electron transport during mitochondrial respiration, can enhance mitochondrial biogenesis and can inhibit oxidative damage of lipid peroxyl radicals. Flavonoids impede the action of the enzymes

responsible for superoxide production as well as NADH oxidase. Zinc is a component of SOD and contributes in the stabilization of membranes by suppressing NADPH-oxidase and inducing the synthesis of metallothioneins. Selenium works as a structural and catalytic cofactor for numerous proteins such as GPxs and thioredoxin reductase (TrxR). Many metabolites such as bilirubin and melatonin have an antioxidative function.

Enzymatic pathway comprises catalase (CAT), superoxide dismutase (SOD), superoxide reductase, glutathione peroxidase (GPX), glutathione reductase, peroxiredoxin (PRX), glutaredoxins (Grx) and thioredoxin (TRX). Catalase is mostly situated in the cytosol and in peroxisomes and transforms H_2O_2 in H_2O and O_2. It can restore mitochondrial structure by enhancing the mitochondrial membrane potential. SODs are defined metalloenzymes because utilise metal ions, such as copper (Cu^{2+}), iron (Fe^{2+}) manganese (Mn^{2+}) and zinc (Zn^{2+}) as cofactors. They are located in many cellular compartments and rapidly convert $O_2^{\bullet-}$ to H_2O_2. SOD1 (Cu/ZnSOD) is found in the cytosol, SOD2 (MnSOD) is located in the mitochondria and SOD3 (Cu/ZnSOD) is extracellular. The glutathione system is composed of glutathione (GSH), glutathione reductase, glutathione peroxidase (GPX) and glutathione-s-transferase (GST). The glutathione functions by reducing the disulphide bonds of cytoplasmic proteins to cysteines. There are eight GPXs, are located in the cytosol and mitochondria, exhibiting different tissue-specific expression patterns and scavenge H_2O_2 at high levels during persistent oxidative stress. GPxs detoxify other toxic organic hydroperoxides by catalyzing the reduction of H_2O_2 and hydroperoxides to water or alcohols. glutathione peroxidase, peroxiredoxin and thioredoxin turn intracellular H_2O_2 in H_2O. PRXs and TRXs possess an active site reactive cysteine that make easier the reduction of peroxynitrites and hydroperoxides to H_2O. PRXs are a family of six members, are highly

abundant and are located in many cellular compartments, defined as ideal scavengers of H_2O_2. The thioredoxin (Trx) antioxidant system is composed of NADPH, thioredoxin reductase (TrxR) and Trx. Trx and TrxR stimulate the NADPH-dependent reduction of the active-site disulfide in oxidized Trx to provide a dithiol in reduced Trx. [47–49].
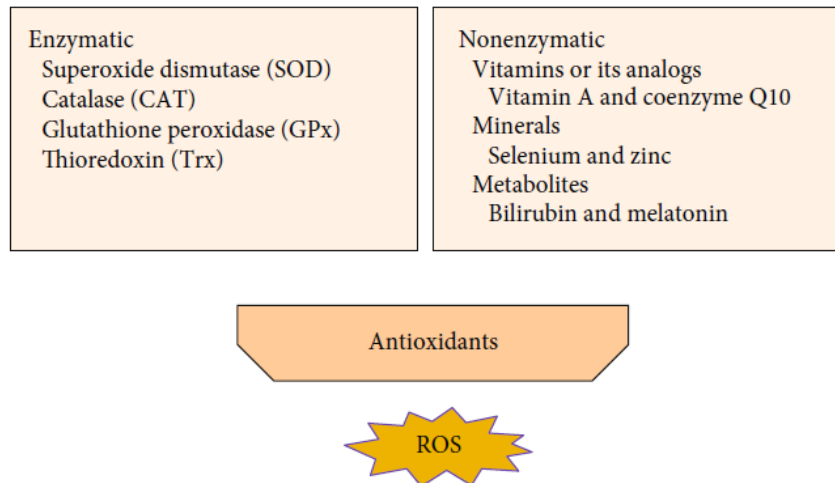
Figure 12. Antioxidant systems. (Su et al 2019).

1.2.2   ROS effects

In aerobic cells a basal level of intrinsic ROS is a mandate, indeed it is produced in the mitochondria during oxidative phosphorylation from the electron transport chain as a by-product. At low levels, ROS enable cell survival and are implicated in important signal transduction such as activation of p53, Mitogen activated protein kinase (MAPK) and Nuclear Factor-κB (NF-κB) pathways. Even so, excessive production of ROS can result in induction of oxidative stress, and generally, its harmful effects include damage on DNA or RNA, lipid peroxidation of polyunsaturated fatty acids (such as membrane phospholipids) and oxidation of proteins, which ultimately lead to apoptosis, autophagy and necrosis [50].
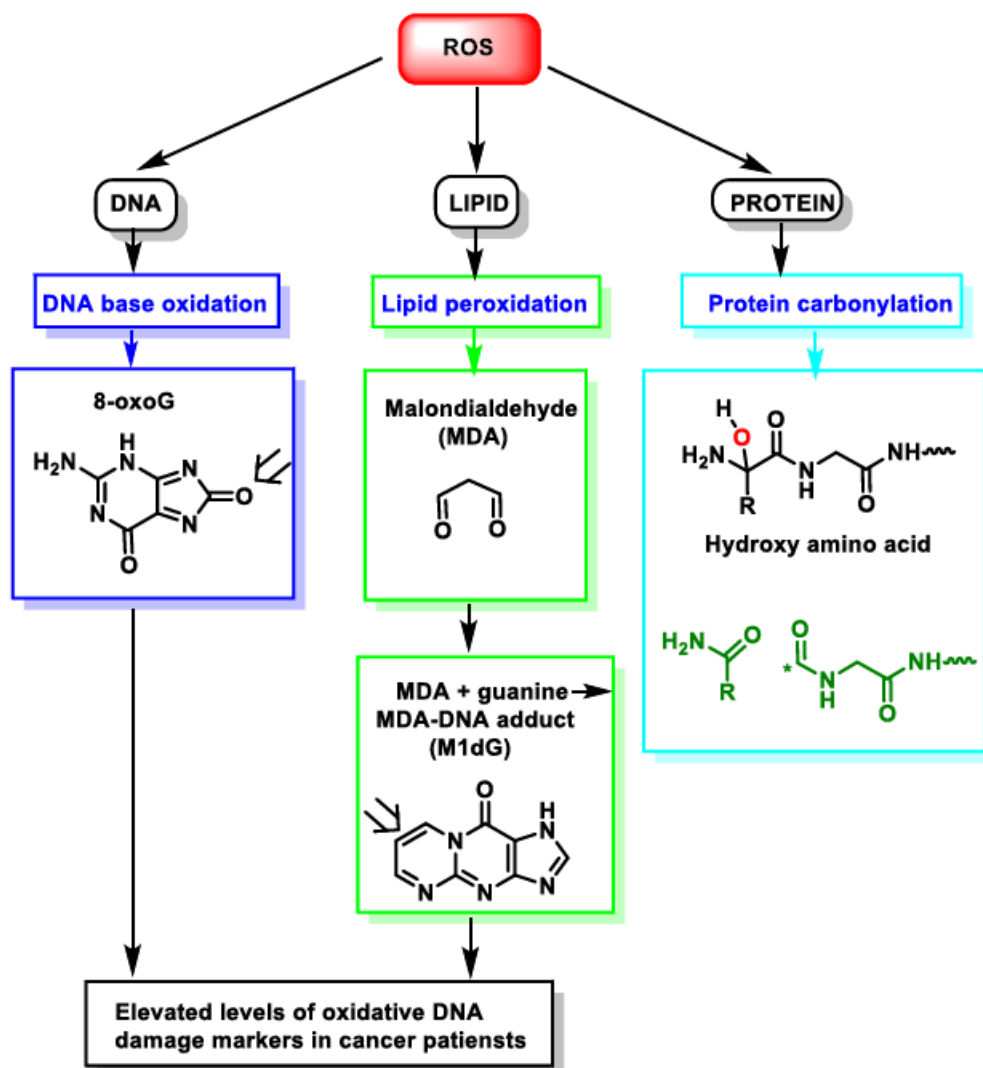
Figure 13. ROS action on DNA, lipids and proteins lead to DNA base oxidation, lipid peroxidation and protein carbonylation, respectively. (Juan et al. 2021).

1.2.3 Oxidative stress

Excessive ROS disrupt the redox homeostasis and induce improper cell signalling and oxidation of the main cellular molecules. Metabolic changes from oxidative stress include: reduction of ATP concentration due to damaged mitochondria, deactivation of glyceraldehyde-3-phosphate dehydrogenase, which causes glycolysis inhibition, increase of catabolism of adenine nucleotides, enhanced ATP consumption due to the active

transport of oxidized glutathione, increase of cytoplasmic calcium concentration from deactivated calcium pumps, cell membrane depolarization, possibly due to deactivation of K, Ca, and Na channels, resulting in increased cell membrane permeability, and decrease of glutathione level and ratio between reduced and oxidized glutathione. As a matter of fact, too much ROS impairment structures of macromolecules, membranes and organelles that are eliminated from the cells through autophagy system. Indeed, oxidative stress serves as a stimulus for autophagy and excessive ROS can activate this process (for example Atg4 is under redox control)[47].
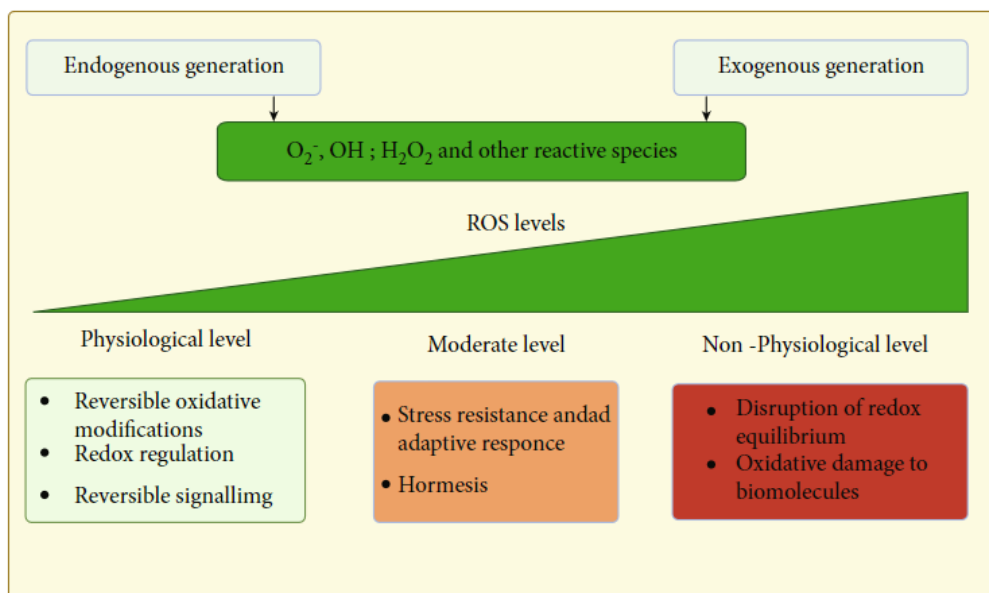
Figure 14. Cellular responses to endogenous and exogenous ROS. (Sagwal et al. 2021).

1.2.4 ROS in cancer

Elevated levels of ROS stimulate several pathways which cumulatively result in activation of oncogenes, inhibition of tumor suppressor genes and inflammation triggering, that can promote cancer development and metastasis. Alternatively, in certain cancers, high ROS levels may activate certain preventive and tumor suppressive mechanisms, such as DNA damage repair, which in turn inhibit the cancer growth and proliferation.
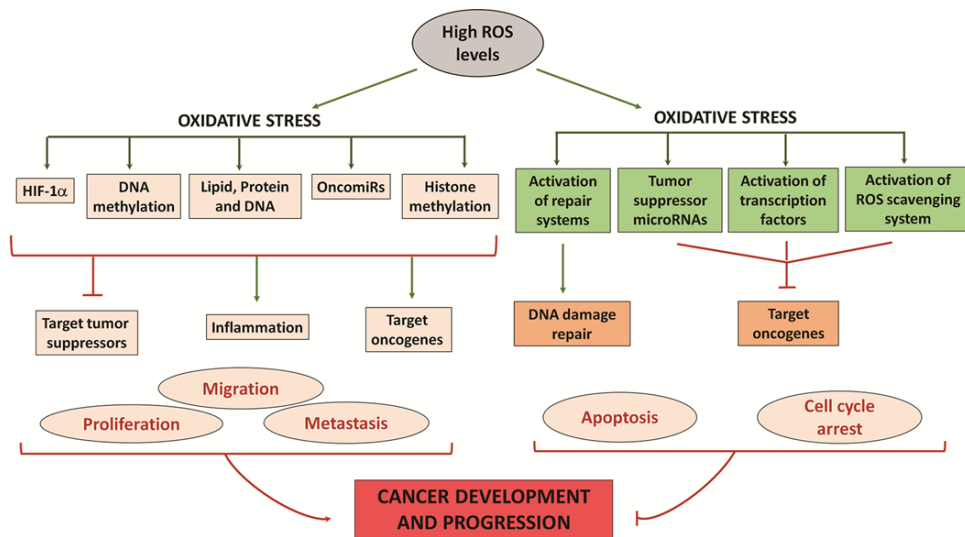
Figure 15. Context dependent effects of oxidative stress in cancer. (Bhat et al. 2017).

1.2.5 Pleiotropic roles of ROS in melanoma

ROS are involved in different stages of melanomagenesis, from malignant transformation of hypoxic melanocytes, to metabolism and immune response and melanin synthesis, and finally to melanoma metastasis. Bedogni et al. in 2005 demonstrated that hypoxia and AKT synergize in transforming melanocytes, thanks to overexpression of HIF-1 alpha that allows anchorage-independent growth under normoxia [51]. Moreover, Akt is

hyperactivated in many melanomas as a consequence of gene amplification and decreased PTEN protein activity. This activation can inhibit the activity of proapoptotic factors such as BAD, caspase 9, forkhead transcription factor, GSK3 and IKKa [52]. Then, Govindarajan et al. in 2007 demonstrated that Akt is associated with malignant transformation melanoma from radial to vertical growth. First, Akt stabilizes cells with heavy mitochondrial DNA mutation, that can lead to ROS. Second, Akt induces the expression of NOX4 enzyme. Akt acts as a molecular switch that increases angiogenesis, through upregulation of VEGF, and the generation of superoxide, promoting more aggressive tumor behavior [53]. Verhaegen et al. demonstrated that mitogen-activated protein kinase can control ROS production by melanoma cells and that it can cooperates with antiapoptotic Bcl-2 family proteins in the maintenance of melanoma cell viability [54]. It is also well known that ROS constitutively activate NF-kB (by H2O2 mainly through the IKK-dependent pathway [55] or by NADPH quinone oxidoreductase [56]) which is involved in melanoma progression [57]. Vartian et al. in 2007 showed that in melanoma ROS are involved in the formation of capillary-like structure [52]. During an inflammatory response, both mast cells and macrophages are recruited and are able to produce ROS as a cytotoxic mediator to kill cells. In transformed cells, as well as melanoma cells, these species can alter permanently their DNA, through point mutation, deletions or rearrangements, which could be followed by a selective pressure of cells with higher resistance to oxidative stress [52]. At low levels of ROS, UVA can increase TXNIP expression, which consequently inhibits Trx activity; this results in ROS levels increase and transendothelial cell migration of melanoma cells [52,58].

1.3 Melanin pigment and skin pigmentation

Generally speaking, melanin is used to describe a group of biological pigments with a variety of aspects (ranging from black and brown to yellow and red), properties (eumelanin, pheomelanin, neuromelanin, allomelanin, and pyomelanin) and functions (from camoflauge and protection to energy harvesting) [59].

Skin pigmentation is mainly determined by the combination of carotenoids, oxy-/deoxy-hemoglobin and different types of melanin, according to their synthesis and deposition. Moreover, skin color variations are also the result of differences in the melanogenic activity and in the number and size of melanosomes and in the type, content and distribution of melanin inside them[60] (Brenner & Hearing, 2008).

1.3.1 Melanosomes biogenesis

Skin, hair and eye pigmentation depend on the production of melanin inside melanosomes, contained in melanocytes, a very specialized population of cells. Melanocytes are derived from precursor cells called melanoblasts during early embryological development. Later, the melanoblasts migrate from the neural crest in the developing organism to the skin, the hair bulb, the eyes and the leptome-nages, where they further differentiate into melanocytes. During weeks 10 to 12 of development, in the skin, melanoblasts differentiate into melanocytes in the dermis. Then, during the next two weeks, melanocytes move to the epidermis, where they represent only 1% of epidermal population cells [60], and locate to the epidermal junction in a particular ordinary dispersed [61]. Indeed, each melanocyte is functionally interfaced, via secreted factors and receptors and via cell-cell contacts, below to fibroblasts in the dermis and above to ketatinocytes in the epidermis [62].

In particular each melanocyte is associated with about 36 keratinocytes and one Langerhans cell to constitute the epidermal melanin unit. In this way, the melanosomes full of mature melanin are secreted from the dendrites of melanocytes and transported to the keratinocytes, where they localize around the nuclei, as supranuclear "caps", acting as a protector shield to DNA from UV rays [60].
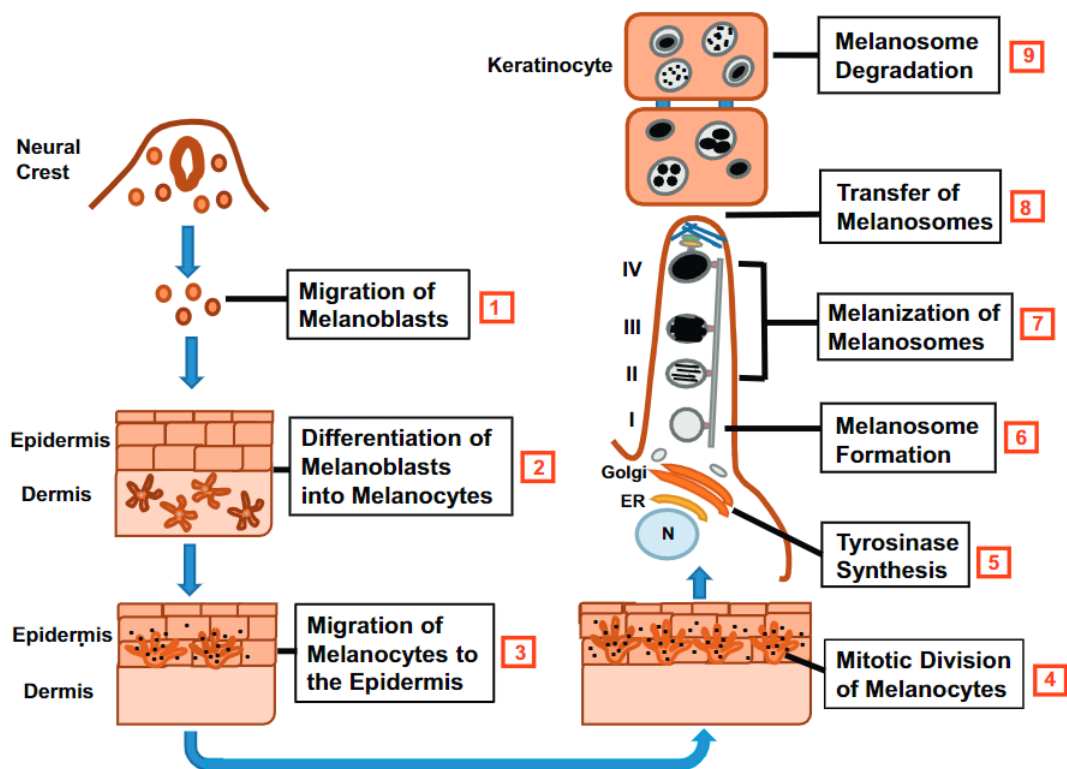
Figure 16. Stages in melanocyte development, melanosome formation and melanization, and melanin transfer to keratinocytes. (Lambert et al. 2019).

Melanization skin level strictly depends from each of these critical processes: migration of melanoblasts from the neural crest to the skin and their differentiation into melanocytes in the dermis. Movement of melanocytes from the dermis to the basal layer of the epidermis. Production of melanosomes and their melanization in the melanocytes. Transport of the melanosomes to the tips of the melanocyte dendrites, their transfer to and degradation within the keratinocytes. Irregularities or defects in any one of these

processes can lead to a number of pigmentary disorders, which can result in increased (hyperpigmentation) or decreased (hypopigmentation) melanin pigmentation in the skin [61]

1.3.1.1 Eumelanosomes and pheomelanosomes

Melanin is located almost exclusively within well-defined specialized organelles derived from early endosomal membranes called melanosomes, whose functions are to synthesize and store melanin. In particular, this spatial separation restricts the entrance of other reagents that could react with melanin and prevents the outflow of highly reactive species originated from pigment synthesis [35]. The size, shape and composition of melanosomes depend on the type of melanin they contain. Eumelanosomes are ellipsoidal and tend to be larger than pheomelanosomes, which are generally more spherical but also more irregularly shaped [63]. The biogenesis of melanosomes is a multistep process: it begins with the synthesis of tyrosinase in the rough endoplasmic reticulum, where it is packaged into vesicles and transported to the Golgi. From here, vesicles containing tyrosinase and enzymes involved in formation of melanin bud off and then further develop into the first stage of melanosomes (round spherical vesicles that contain tyrosinase, tyrosinase-related proteins, and an amorphous matrix). Melanization of the melanosomes takes place. At stage II, melanosomes elongated, getting an ellipsodail shape, and form parallel proteinaceous fibrils of PMEL (pigment cell specific protein), mediated by amyloid-related interactions. At stage III, melanin synthesis starts via the oxidation of L-tyrosine to dopa (3,4-dihydroxyphenylalanine) and dopa to dopaquinone thanks to tyrosinase. From here on eumelanin and pheomelanin biosynthetic pathways diverge. At stage IV, melanin deposition is completed and fills the internal structure of the melanosome. Mature pheomelanin melanosomes has a spherical shape and lack the internal fibrillar

structure. Finally, the mature melanosomes are transported by kinesins along microtubules from the perinuclear area to the tips of the melanocyte dendrites; here, via Rab27a and melanophilin, they interact with myosin-Va, which associates with the peripherial actin network in the melanocyte dendrite. Transfer to keratinocytes takes place [61].
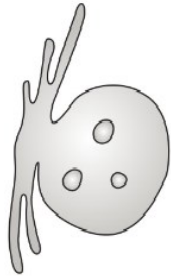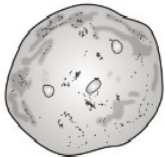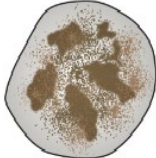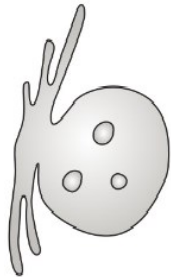
Figure 17. Different stages in the development of melanosomes. (D'Alba et al. 2019).

1.3.2 Role of MITF in melanogenesis cascade

Production of melanogenic enzymes is driven by MITF transcriptor factor, whose activity is regulated by different signalling pathways including: PKC, cAMP, WNT and MEK. In turn, these pathways are activated upstream by receptors such as KIT (ligand: SCF) and MC1R (ligands: α-MSH, ACTH and ASP). The formation of melanin and its transfer to keratinocytes are regulated by paracrine and autocrine factors in response to endogenous and exogenous stimuli, of which the main one is ultraviolet irradiation. In response to genotoxic stress in keratinocytes TP53 is activated, which in turn drives the transcriptional activation of POMC gene. POMC polypeptide is cleaved into α -MSH, beta-endorphins and ACTH. Beta-endorphins induce a state of well-being that support exposure to the sun, which is beneficial because the UV rays allow the photosynthesis of vitamin D3. ACTH reduces the inflammatory effects produced by solar radiation. α-MSH binds MC1R and increases cAMP in melanocytes. PKA is then activated and in turn stimulates CREB transcriptional activity in two ways: (i) phosphorylation of CREB; (ii) inhibition of SIK, a negative regulator of CREB co-activator CRTCs, by phosphorylating SIK. CREB activates the transcription of MITF. In turn, MITF activates the transcription of pigment genes including TYR, TYRP1, DCT, and PMEL [64,65].
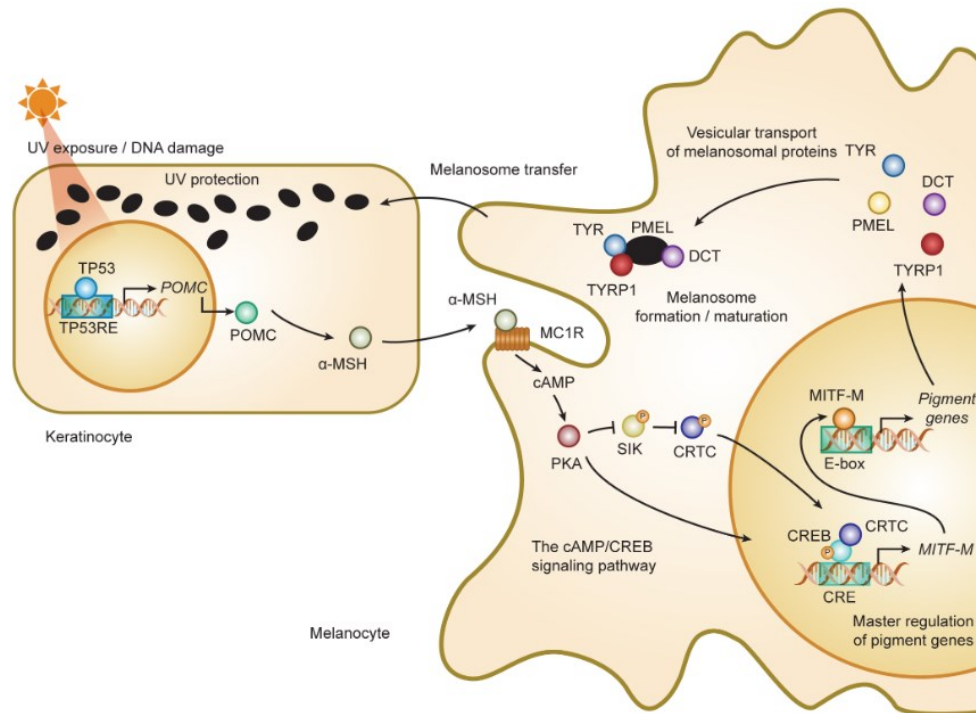
Figure 18. Role of MITF in melanogenesis cascade in human skin. (Hida et al. 2020).

1.3.3 Melanin properties

Melanin has a high refractive index, around 1.8, derived from indirect methods, polarizing interference microscopy and optical modeling. Melanin presents a broad-band absorption spectrum, absorbing light in the UV, visible and near-infra red regions of the electromagnetic spectrum, allowing therefore the protection of tissues by scattering or dissipating light. By controlling the density and distribution of pigments in the integuments of some animals, as cephalopods, chameleons, peacock, it can lead to dynamic colors and affect visual perception and communication. Melanin behaves also as a semiconductor, converting radiation to heat, allowing some organisms the adaption to different thermal environments, a process called thermal melanism. Studies in fungi demonstrated that melanin electrical properties are involved in metabolic processes by

harvesting energy from electromagnetic radiation, referred to as radiosynthesis. Finally, melanin can protect from ionizing radiation by scavenging and or neutralizing the ionized molecules inside the cells, in particular eumelanin, that is rich in carboxyl groups, can reduce and oxidize oxygen radicals [59,63]. The composition of melanin, rich in redox active groups, allows it to participate in redox reactions. The fully reduced melanin building blocks are good electron donors, while the fully oxidized units are responsible for oxidizing properties of the melanin. It is also well known that is an efficient antioxidant that scavenges reactive free radicals [66–68]. In addition, melanin is able to extract metals from the environment and chelate them to coordination sites within the polymer framework. Thanks to its catechol groups, melanin can sequester biorelevant metals such as Na, Ca, Cu, Fe and Zn, together with Hg, Pb, Cr, Mn, more toxic species; in this way, melanin can produce new form of cross-linking networks to improve its mechanical properties and can protect cells from metal toxicity [63].

1.3.3.1 Eumelanin and pheomelanin

Hierarchical organization of melanin, from monomer building blocks to supramolecular assembly in melanosomes, influences its properties. It is accepted that the main subunits of melanin polymerize to relatively small oligomers, that via p−p interaction form proto molecules, and through secondary and tertiary aggregation, form pigment granules(R. M. Slominski et al., 2022). Although eumelanin looks like an anamorphous structure, and due to its insolubility in most solvents and close binding with other cellular tissues, it is very difficult to determine its chemical structure, thanks to X-ray diffraction and high-resolution transmission electron microscopy eumelanin is described as a composition of DHI and DHICA oligomers stacked into lamellae [63]. Less is known about the chemical structure of pheomelanin because it has been study starting from the 60' and usually with

synthetic mimics. It seems to consist of two types of benzothiazine intermediates synthesized in the presence of sufficient cysteine, and specifically, its monomer thought to have a benzothiazine moiety with benzothiazole and isoquinilone moieties [63].

The function of melanogenic enzymes and the availability of substrates influence the production of different types of melanin, in particular the ratio eu-pheo melanin is determined by tyrosinase activity and cysteine availability. The eumelanin is synthesized from the amino acid L-tyrosine via a tyrosinase. As defined as the critical rate-limiting step, tyrosinase converts L-tyrosine into L-3,4-dihydroxyphenylalanine (L-DOPA), and rapidly L-DOPA into dopaquinone. Then, if cysteine is available, it stoichiometrically react with DOPAquinone to produce 3- or 5-cysteinyl DOPAs, which then oxidize and polymerize, bringing to yellow-red soluble melanins, known commonly as pheomelanins (Alba & Shawkey, 2019; Yamaguchi et al., 2007). When intramelanosomal cysteine is depleted, the extra DOPAquinone spontaneously cyclizes to form an orange intermediate known as DOPAchrome. The carboxylic acid of DOPAchrome is naturally lost generating 5,6-dihydroxyindole (DHI), which quickly oxidizes and polymerizes to form dark brown/ black, high molecular weight insoluble polymers, known as DHI-melanin. However, if DOPAchrome tautomerase (DCT) is present, DOPAchrome will tautomerize without missing its carboxylic acid group to form DHI- 2-carboxylicacid (DHICA), which can oxidize and polymerize to create a third type of melanin, known as DHICA-melanin, that is a lighter brown color, moderately soluble and of intermediate size. Human skin usually contains combinations of all three types of melanins, and the ratio of those in part gives rise to visible pigmentation [62].
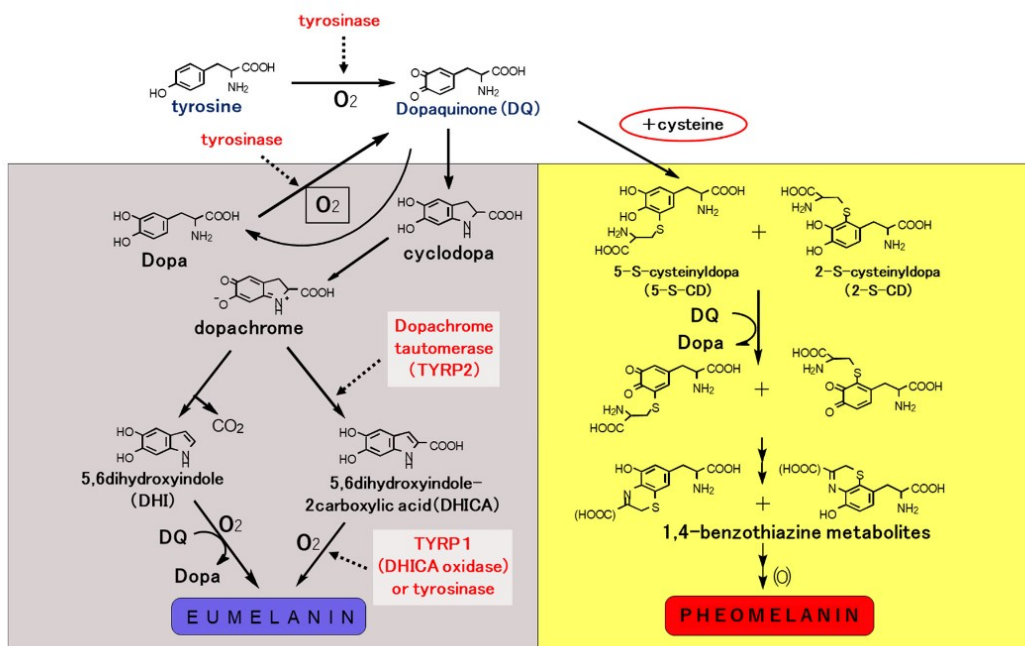
Figure 19. Biosynthetic pathway of eumelanin and pheomelanin. (Hida et al. 2020).

Individuals with light skin are more prone to blistering and burning compared to those with dark skin. Thus, there is a correlation between melanin content in the skin and incidence of skin cancer. Eumelanin strongly absorbs UVR and acts as anti-oxidant, indeed scavenge the UV-generated free radicals and in this way protects deeper layers. Pheomelanin is less able to absorb UVR and becomes pro-oxidant. Moreover, photoprotection is decreased because eumelanin turnover is increased due to a high degradation of its by lysosomal enzymes. Pheomelanin synthesis needs high amounts of antioxidants, that in turn decrease the ROS scavengers as glutathione, making melanocytes more sensitive to ROS-related damage and genetic instability [64,70,71].

1.3.4 Melanogenesis can enhance melanoma progression

Melanin synthesis produces free radicals and highly reactive intermediates with genotoxic and mutagenic properties; pheomelanin in particular, under certain conditions can cause pro-oxidative environment and induce DNA damage. Melanin pigments can also have direct proinflammatory and pro-oxidant effects in keratinocytes, independently from light exposure. Uncontrolled melanogenesis, through reduction of major cell antioxidants and generation of ROS, and the direct action of quinone and semiquinone intermediates on RNA, DNA and regulatory proteins, will generate pro-mutagenic environment contributing to melanomagenesis. Moreover, melanin consumes oxygen, while L-DOPA can induce glycolysis in melanotic melanomas. Melanogenesis and L-DOPA oxidation can also lead to changes in glycoproteins phosphorylation pattern. Finally, melanogenesis in melanoma cells leads to increase HIF-1a accumulation [35].

2 Aim

Targeting metastatic tumors carrying the BRAFV600E mutation with combinations of BRAF and MEK inhibitors has revolutionized melanoma treatment for lots of patients. Unfortunately, MAPK inhibitors still have significant limitations, such as short-lasting efficacy and poor-lived responses, due to early onset of acquired resistance. One of the mechanisms that impair melanoma cells sensitivity to MAPK inhibitors is the increase in pigmentation promoted by the action of miR-211 in a subset of melanoma cell lines. Indeed, in Vitiello et al. 2017, we discovered that miR-211 and miR-204, belonging to the same microRNA family, are the miRNAs most induced by Vemurafenib. However, we demonstrated that they have different characteristics in terms of activation by different transcriptional factors, of induction in different cellular context and of different mechanisms of action. In particular, miR-211 is under the control of *MITF*, and, once induced by Vemurafenib, by targeting EDEM1, it favours Tyrosinase expression and melanin accumulation. In turn, this induction of pigmentation confers more resistance to drug treatment. Since it has been already shown that melanin presence hampers the outcome of other kinds of therapy in melanoma, such as chemotherapy, phototherapy and radiotherapy, we aimed to understand which are the molecular mechanisms by which pigmentation limits targeted therapy. In order to achieve this objective, my three years PhD thesis aimed to:

- Confirm that MAPK pathway inhibition increases pigmentation in melanoma cells, both *in vitro* and *in vivo*, through the study of an extended panel of BRAFV600E cellular lines and through xenograft experiment in nude mice.
- Show that pigmentation levels correlate with resistance to MAPK inhibitors in melanoma cell lines and in metastatic melanoma specimens.

- Prove that pigmentation limits the activity of MAPK inhibitors in xenograft zebrafish experiments.

- Determine whether melanosomes impair vemurafenib activity by staying inside cells or exporting the drug outside.

- Establish whether melanin acts as scavenger of MAPK inhibitors-induced ROS.

- Analyze ROS-induced DNA damage.

- Assess whether melanosomes need to be in physical contact with mitochondria in order to exert their ROS-scavenging activity.

- Test therapy combinations based on MAPK inhibitors with pigmentation inhibitors.

3 Material and Methods

3.1 Materials

3.1.1 Cell lines

Name	Cell Type	Source
501Mel	Metastatic melanoma	From Dr. E. Hernando
A2058	Metastatic melanoma from a lymph node	
A375	Malignant melanoma	ATCC
C32	Melanoma	
Colo800	Metastatic melanoma from hypodermis	commercial
M14	Metastatic melanoma from right buttock; hypodermis.	
MNT1	Metastatic melanoma from a lymph node	
SK-Mel-2	Metastatic melanoma from skin of thigh	ATCC
SK-Mel-5	Metastatic melanoma from axillary lymph node	ATCC
SK-Mel-28	Metastatic melanoma from skin	ATCC
SK-Mel-188	Melanoma	From Dr. A. Brozyna
UACC62	Melanoma	
UACC257	Melanoma	
WM278	Nodular melanoma	Coriell Institute

Table 2: list of melanoma cell lines

3.1.2 Drugs

Product	Cat. No.	Source
Cobimetinib	S8041	Selleckchem
3',4'-dichorobenzamil hydrochloride	D8190	Merck
Dimethyl sulfoxide	472301	Merck
G418 Disulfate salt Geneticin	A1720	Merck
Kifunensine	K1140	Merck
Mn(III)tetrakis(4-benzoic acid)porphyrin chloride	475870	Merck
Oligomycin	75351	Merck
PLX7904	S7964	Selleckchem
PLX8394	S7965	Selleckchem
N-phenylthiourea	P7629	Merck
Puromycin dihydrochloride	P8833	Merck
Sodium Pyruvate	P5280	Merck
Vemurafenib PLX4032	S1267	Selleckchem
Vemurafenib PLX4720	S1152	Selleckchem

Table 3: List of drugs. All drugs were diluted according to the manufacturer's instructions.

3.1.3 Oligos

Primer name	Sequence Fw	Sequence Rv	Source
APE1	TGCTGTGTGGAGACCTCAAT	CTGCAGTAATTCCCCGAAGC	our design
ATPA1	CTCAGATGTGTCCAAGCAAG	GTCAGTGCCCAAGTCAATG	28445987
DCT	CCTTTCTTCCCTCCAGTGAC	AGCCAACAGCACAAAAAGAC	28445987
EXOG	ATGTTGGAAGTGGGTGGTCA	AGGTCAAAGGCCCAGATACC	our design
GAPDH	CGCTCTCTGCTCCTCCTGTT	CCATGGTGTCTGAGCGATGT	28445987
LPL	GGCTGGACGGTAAGGGAGGCTC	GCTCAAGGGCACCAACCAGGT	our design
miR204-family	GGGTACAGCATCTCGGTGTT	TGAATCGAGCACCAGTTACGC	28445987
MITF	TGACCGCATTAAAGAACTAGG	GTGCTCCAGTTTCTTCTGTCG	28445987
MLANA	CTCTTACACCACGGCTGAA	AGACTCCCAGGATCACT	28445987
MLH1	CTCCAAGATGAGGCTGTAGGAA	CCTATGAGATGGAAGGCAAGA	our design
MSH6	CGCCATCCTTGCATTACGAA	ACTTCAGCAGGGACGTAACA	our design
ND1	CAGGCCCCTTCGCCCTATTCTT	GAGTTGGTCGTAGCGGAATCGGG	our design
NOX2	GGGCTGTTCAATGCTTGTGGCT	ACATCTTTCTCCTCATCATGGTGC	29039574
NOX4	GACTTTACAGGTATATCCGGAGCAA	TGCAGATACACTGGGACAATGTAGA	19431059
NOX5	ATCAAGCGGCCCCCTTTTTTTCAC	CTCATTGTCACACTCCTCGACAGC	19779036
NRF2	GAGAGCCCAGTCTTCATTGC	TTGGCTTCTGGACTTGGAAC	26482881
OGG1	TGTTACCCTGGCTCAACTGT	GCGATGTTGTTGTTGGAGGA	our design
PBGD	TCCAAGCGGAGCCATGTCTG	AGAATCTTGTCCCCTGTGGTGGA	28445987
PGC1α	GTCACCACCCAAATCCTTAT	CGGTGTCTGTAGTGGCTTGA	28445987
SDHA	CCACTCGCTATTGCACACC	CACTCCCCATTCTCCATCA	28445987
SNO-44	CCTGGATGATGATAAGC	TGAATCGAGCACCAGTTACGC	28445987
SNO-55	AGCCAACCTTGGAGAGCTGAGC	TGAATCGAGCACCAGTTACGC	28445987
SNO-110	TGATGTCTCCATGTCTCTGAGCAA	TGAATCGAGCACCAGTTACGC	28445987
SOD1	GGAGACTTGGGCAATGTGAC	CACAAGCCAAACGACTTCCA	our design
TRPM1	TGCGAAGGCTGCTGGAAA	CAAGACGATGGACACCACGTTAGG	28445987
TRPM3	GGAGCAGAGGTGAAACTTCG	CCCATCACAGACAACCACTG	28445987
TYR	GATGAGTACATGGGAGGTCAGC	GTACTCCTCCAATCGGCTACAG	28445987
TYRP1	GGACCAGCTTTTCTCACAT	GAATCAAAGTTGCTTCTGGA	28445987
XRCC1	GGGACCGGGTCAAAATTGTT	ACCGTACAAAACTCAAGCCAAAG	15867196
BRAF	AGAAUUGGAUCUGGAUCAUUUUU	AAAUGAUCCAGAUCCAAUUCUUU	28445987
RAB27A-173	ACUCCAGUCUCUAACGUUUUU	AAACGUUAGAGACUGGAGUUU	our design
RAB27A-1658	GGGUCAGGGAACUAGAUUUUU	AAAUCUAGUUCCCUGACCCUU	our design
si-CT	UUCUCCGAACGUGUCACGUUU	ACGUGACACGUUCGGAGAAUU	28445987

Table 4: List of qPCR primers and siRNAs.

3.1.4 Clinical data

NYU Patient Characteristics	Amelanotic (n=40)	Melanotic (n=67)	Total (n=107)
Sex			
Male	27	38	65
Female	13	29	42
Age at Stage IV Diagnosis			
Mean (SD)	55.0 (12.4)	56.7 (13.2)	56.1 (12.9)
Median	57.3	54.7	55.7
Treatment			
Single agent targeted therapy (i.e. vemurafenib)	24	36	60
Dual agent targeted therapy (i.e. dabrafenib + trametinib)	14	25	39
Targeted + Immunotherapy (i.e. dabrafenib + ipilimumab)	2	6	8
Metastasis Location			
Skin/Subcutaneous	5	7	12
Soft Tissue	10	13	23
Nodal	10	27	37
Visceral	11	16	27
Brain	4	4	8

Table 5: NYU patient characteristics

3.2   Methods

3.2.1   Cell culture

Cells were grown at 37°C in a humidified atmosphere with 5% CO_2. A375, SK-Mel-28, M14, 501Mel, SK-Mel-5, UACC257, MNT1 melanoma cell lines were cultured in DMEM High Glucose supplemented with 10% foetal bovine serum, 1% glutamine (Sigma-Aldrich) and 1% penicillin/streptomycin (Euroclone). C32, A2058 were cultured in MEM supplemented 10% foetal bovine serum, 1% glutamine (Sigma-Aldrich) and 1% penicillin/streptomycin (Euroclone). WM278 were cultured in 4/5 MCDB 153 Media (Sigma-Aldrich), 1/5 Leibovitz L-15 Media (Euroclone), 2% Fetal Bovine Serum (Euroclone), 5 μg/uL Insulin (Sigma-Aldrich), 15 μg/uL Bovine Pituitary Extract (Millipore), 1.68 mmol/L $CaCl_2$ (Sigma-Aldrich), 50 μg/mL Epidermal Growth Factor (BD Biosciences). Colo800, UACC62 were cultured in RPMI supplemented with 10% foetal bovine serum, 1% glutamine (Sigma-Aldrich) and 1% penicillin/streptomycin (Euroclone). Human SK-Mel-188 melanoma cell line was a kind gift from Dr Anna Brozyna, Nicolaus Copernicus University, Torun. The cells were cultured in either Ham's F10 or Dulbecco's Modified Eagle's Medium (DMEM) supplemented with 10% foetal bovine serum and 1% glutamine (Sigma-Aldrich) and 1% penicillin/streptomycin (Euroclone).

3.2.2   Growth curve assay with different doses of the drug

Melanoma cells were seeded in 12well plates (2 wells per experimental condition per time point) and 24h later they were treated with different doses of the appropriate drug or with vehicle (DMSO) for a week. Cells were then fixed with 4% PFA and stained with a crystal violet solution (0.1% crystal violet, 20% methanol, in water). After the excess crystal

violet solution was removed and the plates were washed with tap water and dried, cells were de-stained using a 10% acetic acid solution. Absorbance was then read at 590 nm. Each sample was normalized on the vehicle-treated sample and the data were graphed as variation of cell percentage compared to the vehicle-treated sample.

3.2.3   Growth curve assay with different doses of the drug and pigmentation inhibitors pre-treatment

Melanoma cells were seeded in 12well plates (2 wells per experimental condition per point) and 24h later they were treated with pigmentation inhibitor or with vehicle (DMSO) for 72h. Then the cells were treated with BRAFi/MEKi for the next 48h. Cells were then fixed, stained and de-stained as described above.

3.2.4   Transfection of cells with small interference RNA (siRNA)

Cells were seeded in 6well plates in order to reach 80%-90% confluency the day after. 6 μl of 20 μM siRNA stock solution per well were added to 250 μl of DMEM High Glucose (Euroclone), while 10 μl of 1 mg/ml of Lipofectamine 2000 (Thermo Fisher Scientific) were added to additional 250 μl of DMEM High Glucose. These two solutions were then mixed together and the siRNA- Lipofectamine 2000 complexes were allowed to form for 15 min at room temperature. In the meantime, the medium from each well was aspirated and replaced with 1.5 ml of fresh DMEM High Glucose. The mixture was then added to the wells, let stand for 6 h. At the end of the 6h, the medium was changed to complete medium and the cells processed according to the protocol of the different assays.

3.2.5   Cell cycle analysis

Cells were seeded in 100mm plates and the day after were treated with either 2 μM vemurafenib or DMSO. After 48h, cells were harvested with trypsin, then 10^5 cells were

fixed with 95% ethanol and stained with propidium iodide solution (200 μg/ml P.I., 0.1% NaCitrate, 0.5 mg/ml RNAse A, 0.1% Nonidet NP40). For each sample, 10^4 events were analyzed by flowcytometry (CytoFLEX, Beckman Coulter).

3.2.6 Cellular senescence

Cells were seeded in 6well plates in order to do not reach confluency the day after. Seeded cells were treated with 2 μM vem or DMSO for 48 hours. The medium was removed and cell were washed once in 1X PBS and then fixed 7' at room temperature with the fixing solution (0,2% Glutaraldehyde, 2% Formaldehyde and 1X PBS). Then cells were washed twice (5' each) with PBS 1X additioned with 2 mM $MgCl_2$. Next, cells were washed once with 1X Sodium Citrate Phosphate buffer (150mM pH 6) and the staining solution was added (30 mM Sodium Citrate Phosphate Buffer pH 6, 2 mM MgCl2, 150 mM NaCl 5M, 5 mM Potassium Ferrocyanide, 5 mM Potassium Ferricyanide, 1 mg/ml X-Gal and H_2O). The plate was sealed with laboratory tape, cover with aluminum foil and put in an incubator at 37°C. After 24h the staining was checked and left no more than 48h. At the end the staining solution was removed and the plate was washed once with 1X PBS and added 1 ml of new1X PBS to take picture.

3.2.7 Establishment of UACC257-Tyr-Zsgreen stable cell line

Briefly, Tyr-Zsgreen vector (kind gift of Dr. Guideng Li, PMID: 32393797) was cotransfected with 2 plasmids encoding proteins necessary for virus packaging (psPAX2: lentiviral packaging plasmid and pMD2.G: VSV-G envelope expressing plasmid) in $3x10^6$ HEK293T cells with PEI (Polyethylenimine). After 48 hours and 72 hours, media containing lentivirus particles were harvested and viruses were pulled down by using Lenti-X^{TM} Concentrator reagent (Clontech) following the manufacturer's protocol.

8x10^5/p100 UACC257 melanoma cells were then transduced with lentivirus plus 4 μg/ml polybrene. Pools of stably transduced cells were selected by adding 1 μg/ml puromycin to the culture medium.

3.2.8 Generation of 501Mel cells that stably express TYR-mCherry fluorescent protein

The TYR-mCherry (kind gift of Dr. Carmit Levy, Tel Aviv University) plasmid was first linearized with BglII and then was transfected in 501Mel cells using Lipofectamine 2000 (Thermo Fisher Scientific). Transfected cells were then selected using 1 mg/ml Gentamicin. The G418-resistant population, which expresses the plasmid, was later enriched in mCherry positive cells, using fluorescence activated cell sorting (FACSjazz, BD).

3.2.9 Quantification of released melanosomes

TYR-mCherry 501Mel cells were seeded in 100mm plate (1 plate per experimental condition) and 24h later they were treated with 5 μM vem or with DMSO. After 10 days, cells were harvested and counted to normalize the number of released melanosomes. In the meanwhile, the supernatant was harvested and centrifuged at 7197xg for 30 minutes at 4°C to remove debris and cells remained in suspension. Then, to isolate melanosomes, it was subjected to ultracentrifugation at 27000xg for 1h at 4°C. Finally, red melanosomes present in the pellet were quantified using flow cytometry (FACSjazz, BD).

3.2.10 Co-culture assay

Cells were seeded in the insert of a 6-well dish (1 μm pore size, Falcon #353102, upper chamber), and directly in the same 6-well dish (lower chamber). Cell lines seeded in the lower chamber were: Colo800, 501Mel, SK-Mel-5 or MNT1 cells that stably express

EGFP because infected with pGIPZ-tGFP lentiviral vector [42]. Cell lines seeded in the upper chamber were: TYR-mCherry 501Mel cells. The next day, cells were treated with 5 μM vem or DMSO. The percentage of red cells in the lower chamber was evaluated 1 week after drug treatment using flow cytometry (FACSjazz, BD). For each sample, 10^4 events were analyzed.

3.2.11 Clonogenicity assay

2×10^2 cells were seeded in 60 mm plates in triplicate. After 8 days of 2 μM vem or DMSO treatment, cells were fixed and stained with a 0.1% crystal violet, 4% formaldehyde solution. The number of colonies was normalized on the number of colonies obtained in the negative control. The average colony number ± SEM for each group was then used to create a bar graph.

3.2.12 Melanin content evaluation

Melanoma cells were seeded in 60mm plates and 24h later they were treated with either DMSO or drug (vemurafenib or cobimetinib or PTU or DBZ). After 72h, the cells were harvested and counted. Finally, pictures were taken on equal numbers of pelleted cells.

3.2.13 Transmission electron microscope analysis

To evaluate their morphological features, melanoma cells were seeded in 100mm plates. The day after they were treated with either DMSO or 2 μM vemurafenib for 72h. At the end of this period, cells were harvested and pelleted by centrifugation. Pellets were washed three times with phosphate buffered saline (PBS) solution and fixed in 3% glutaraldehyde solution in 0.1M cacodylate buffer, pH 7.2, for 2h at 4°C. Cells were then scraped off and post-fixed in 1% osmium tetroxide in 0.1M cacodylate buffer for 2h at

room temperature. After rapid dehydration in a graded series of ethanol and propylene oxide, cells were embedded in an "Epon-Araldite" mixture. Ultrathin sections, obtained by a diamond knife on an Ultracut Reichert-Jung ultramicrotome, were placed on Formvar-carbon coated nickel grids, stained with uranyl acetate and lead citrate and observed with a Jeol 100 SX transmission electron microscope. The quantification of the number of melanosomes per cell was performed by counting the number of melanosomes per unit of cytoplasmic area.

3.2.14 ROS

3.2.14.1 Total ROS analysis

Cells were plated in 12-well plates and the day after they were treated for 48h or 72h with with 2 µM vem or vehicle (DMSO). Then, total ROS were analyzed using CellROX Deep Red Reagent (C10422, Thermo Fisher Scientific). According to the manufacturer's instructions, cells were incubated for 30 min with CellROX reagent, then washed three times with PBS and collected. For each sample, 10^4 events were analyzed by flow cytometry (C6 Accuri, BD).

3.2.14.2 Mitochondrial ROS analysis

Cells were plated in 12-well plates and the day after they were treated for 48h or 72h with with 2 µM vem or vehicle (DMSO). Then, mitochondrial ROS were analyzed using MitoSOX RED (M36008, Thermo Fisher Scientific). According to the manufacturer's instructions, cells were incubated for 10 min with MitoSOX reagent, then washed three times with PBS and collected. For each sample, 10^4 events were analyzed by flow cytometry (C6 Accuri, BD).

3.2.14.3　　　　Lipidic ROS analysis

Cells were plated in 12-well plates and the day after they were treated for 48h or 72h with with 2 µM vem or vehicle (DMSO). Then, lipidic ROS were analyzed using BODIPY C11 (D3861, Thermo Fisher Scientific). According to the manufacturer's instructions, cells were incubated for 30 min with BODIPY C11 reagent, then washed three times with PBS and collected. For each sample, 10^4 events were analyzed by flow cytometry (C6 Accuri, BD).

3.2.14.4　　　　Mitotracker analysis

Cells were plated in 60 mm plates and the day after were treated for 72h with 2 µM vem or vehicle (DMSO). Then, mitotracker analysis was performed using MitoTracker™ Deep Red FM (M22426, Thermo Fisher Scientific). According to the manufacturer's instructions, cells were incubated for 45 min with MitoTracker reagent, then washed three times with PBS and collected. For each sample, 10^4 events were analyzed by flow cytometry (C6 Accuri, BD).

3.2.15　Synthesis of dopamine melanin nanospheres

Melanin nanoparticles were synthesized starting from an already reported protocol (Zhong G., PMID: 31173033). Briefly, 2 ml of ammonium hydroxide (28–30%) was added to a mixed solution containing 90 ml of DI water and 40 ml of ethanol. The solution was magnetically stirred for 30 minutes at 30°C. 0.5 g of dopamine hydrochloride was dissolved in 10 ml of DI water and was added dropwise to the above solution. Solution turned from pale yellow to dark brown in few minutes. The solution was maintained under stirring overnight at 30°C (20h). The products were collected by centrifugation (15

minutes at 4000 rpm) and purified three times with DI water (3x 3minutes at 13200 rpm). Nanoparticles were maintained at 4 °C and are stable at least for two weeks.

3.2.15.1   Characterization of DM nanospheres

Transmission electron microscopy (TEM) was carried out on a ZEISS Libra 120 PLUS operating at 120 KV and equipped with an In-column Omega filter. The suspensions with the nanoparticles were deposited on a 300-mesh carbon coated copper grid and allowed to dry before image acquisition.

Dynamic Light Scattering (DLS) was used to determine the size distribution profile of the nanospheres. The DLS measurements were performed at 37 °C in a 1 mL quartz cuvette on a Zetasizer nano-ZS90 (Malvern Instruments, Malvern, United Kingdom) following the manufacturer's instructions. The nanomaterials were diluted 1:1000 in 1X PBS and analyzed with a single scattering angle of 90°. For the zeta-potential measurements, the sample was transferred into DTS 1070 standard capillary cells. The values reported are the average of four consecutive measurements.

Zeta-potential. The same sample used for DLS measurements was transferred into DTS 1070 standard capillary cells. The values reported are the average of four consecutive measurements.

Ultra-violet Visible Spectra (UV-Vis Spectra). Absorbance spectra were collected with a double beam spectrophotometer Jasco V-550 UV–vis equipped with quartz cuvettes of 1.5 mm path length. PBS (1X) buffer was employed as solvent and nanoparticles were diluted 1:1000.

3.2.16 2 photon NADH intensity analysis

2 photon imaging was carried out by an Olympus FluoView 1000-ASW-2.0 confocal microscope (Olympus, Japan) coupled with a two-photon Chameleon Ti:Sapphire laser (Coherent, California). A 690 nm beam splitter was used to separate 2 photon excitation and fluorescence emission from unlabeled sample. To excite intracellular NADH 2 photon excitation was tuned at 710 nm and the emission was collected in the $400 - 500$ nm range by using a $60\times$ plan Apo water immersion objective (NA = 1.2). Image analysis was carried out by ImageJ software (NIH, Bethesda): briefly, NADH intensity was measured for each imaged cell treated with DMSO or vemurafenib and then normalized for average intensity of DMSO treated cells.

3.2.17 Oxygen consumption rate measurements

Oxygen consumption rate (OCR) was measured in A375 and 501Mel cells using a Seahorse XFe24 Extracellular Flux Analyzer (Seahorse Bioscience, Agilent, Santa Clara, CA). Cells were counted in an automated cell counter (TC20, Bio-Rad Laboratories Inc.) and seeded in XF24 microplates (Agilent Technologies). The day after cells were treated with 2 µM vem or DMSO for 24, 48 and 72 hours. OCR was measured in XF media (non-buffered DMEM medium, pH 7.4, containing 10 mM glucose, 2 mM L-glutamine and 1 mM sodium pyruvate), under basal conditions and in response to 2 µM oligomycin, 1.5 µM FCCP and 1 µM antimycin A and rotenone (all chemicals from Sigma-Aldrich). Data were normalized for cell number.

3.2.18 RNA extraction and quantification

For general purposes RNA was extracted using QIAzol reagent (Qiagen), following the manufacturer's instructions. For microRNA, RNA was extracted using miRNEasy MINI

Kit (Qiagen), following the manufacturer's instructions. RNA was subsequently quantified using Nanodrop Lite (Thermo Scientific).

3.2.19 DNAse treatment and retrotranscription

When analyzing mRNA expression, 1ug of RNA was retrotranscribed using QuantiTect Reverse Transcription Kit (Qiagen), following the manufacturer's instructions and using a S1000 Thermal Cycler (Bio-Rad). Absence of genomic contamination of RNA was checked by performing a PCR reaction on the cDNA using PCR Master Mix (Thermo Fisher Scientific) and the ATPA1 primers. These primers produce a genomic-derived amplicon of 300bp and a cDNA-derived amplicon of 180bp, allowing for genomic DNA contamination detection. When analyzing miRNA expression, 250ng of RNA were retrotranscribed using miScript II RT Kit (Qiagen), following the manufacturer's instructions and using a S1000 Thermal Cycler (Bio-Rad).

3.2.20 Mitochondrial and nuclear DNA isolation

Cells were seeded in 100 mm plates and were treated with 2 μM vem or DMSO for 72h. Cell pellets were resuspended with lysis buffer (100 mM NaCl, 10 mM EDTA, 0.5% SDS, 20 mM Tris HCl pH 7.4, H_2O) and proteinase K, and the lysate was incubated at 55°C for 3 hours. Then, 100 μg/ml RNAse A was added to degrade RNA present and incubated at 37°C for 30 minutes. Next, 7.5 M ammonium acetate and isopropanol (0.7 v/v) were added and mixed well to obtain "DNA jelly fish". It was centrifuged at 15.000xg for 10 min at 4°C. The supernatant was removed and the pellet was washed with 70% ethanol. Finally, the pellet was dried and resuspended in TE buffer. For qPCR 10 ng DNA/μl was used.

3.2.21 Real-time PCR

1 μl of cDNA (diluited 1:3) was used for quantitative PCR reaction, which was performed using SsoAdvanced Universal Supermix (Bio-Rad) and appropriate primers on a CFX96 Real-Time System (Bio-Rad). The reaction conditions were the following: 98 °C 30 s, (98 °C 3 s, 58 °C 20 s, 72 °C 10 s) × 40 cycles. In order to confirm the specificity of the reaction, a melting curve was performed after each PCR (from 65 °C to 95 °C with an increase of temperature of 0.5 °C/s). All reactions were performed in duplicate. The average of the two Ct values was used to calculate the expression of the different transcripts by the "2-ΔΔCt" method, using the geometrical square mean of three housekeeping genes as a reference (GAPDH, PBGD and SDHA). When analyzing miRNA expression housekeeping genes were sno-44, sno-55 and sno-110. Data were analyzed using CFX Manager Software (Biorad).

3.2.22 Detection of Protein Oxidation

Oxidated proteins were detected using OxyBlot™ Protein Oxidation Detection Kit Catalog No. S7150 (Millipore). Briefly, A375, WM278, 501Mel and SK-Mel-5 cells were seeded in 100 mm plate. 24 hours later they were treated with dmso or 2uM vemurafenib. 48 hours later cells were collected and processed for oxidation detection as follow. Pellets were resuspended in 30 ul of lysis buffer (50 mM Tris HCl, 1% TritonX100, 0.25% of NaDeoxicholate, 1 mM PMSF, 2 mM Orthovanadate, proteinase inhibitors cocktail) added with 50 mM DTT (Dithiothreitol) and were incubated for 30 minutes on ice. Then the suspensions were centrifuged at 14000 rpm for 30 minutes at 4 °C and the collected supernatants were then quantified using Bradford reagent and read at 590 nm. Then the derivatization of the proteins with DNPH (dinitrophenyl hydrazine) solution, SDS-PAGE

polyacrylamide gel electrophoresis, western transfer and immunodetection were performed according to the manufacturer's instructions.

3.2.23 Histone extraction

Cells were seeded in 100 mm plates and were treated with 2 μM vem or DMSO for 48h. Cells were harvested with a scraper and washed twice with ice-cold PBS 1X. Cell pellets were resuspended in Triton Extraction Buffer (TEB: PBS containing 0.5% Triton (v/v), 2 mM phenylmethylsulfonyl fluoride (PMSF), 0.02% (w/v) NaN_3) at a cell density of 10^7 cells per ml. Hence were lysed on ice for 10 minutes with gentle stirring. Then they were centrifuged at 650xg for 10 minutes at 4°C to spin down the nuclei. The supernatant was collected as cytoplasmic fraction. Cell pellets were resuspended in half the volume of TEB and centrifuged as before. Then were resuspended in 0.2 N HCl at a cell density of 4×10^7 cells per ml. The histones were acid extracted over night at 4°C. The day after, samples were centrifuged at 650xg for 10 minutes at 4°C to pellet debris. Supernatants were collected and HCl was neutralized with 2 M NaOH at 1/10 of the volume of the supernatant. Finally, protein content was determined using Bradford reagent and read at 590 nm.

3.2.24 Protein extraction and Western blot analysis

Pellets were resuspended in 30 μl of lysis buffer (Tris HCl 50 mM, 1% TritonX100, 0.25% of NaDeoxicholate, 1 mM PMSF, 2 mM Orthovanadate, proteinase inhibitors cocktail). The mixture was incubated for 30 minutes on ice, then sonicated for 30 minutes and finally centrifuged at 14000 rpm for 30 minutes at 4 °C. The supernatant was then quantified using Bradford reagent and read at 590 nm. The samples were heated at 95 °C for 5 min, separated on 10% SDS-polyacrylamide gels (Mini-PROTEAN Precast gel,

Bio-Rad) and electrotransferred to nitrocellulose membranes (Trans-Blot Turbo Midi 0.2 μm Nitrocellulose Transfer Packs, Biorad) using Trans-Blot Turbo system (Bio-Rad). Membranes were blocked at room temperature for 2 h using 3% BSA in TBST for the detection of DNMT1 or using 3% milk in TBST for the detection of FIBRILLARIN, GAPDH and γH2AX. They were then incubated overnight at 4 °C with the following primary antibodies: anti-DNMT1 (sc-271729, Santa Cruz Biotechnology; mouse monoclonal antibody, dilution 1:100 in 3% BSA in TBST); anti-FIBRILLARIN (#A85370, Novus; mouse monoclonal antibody, dilution 1:250 in 3% milk in TBST); anti-GAPDH (#2118, Cell Signaling; rabbit polyclonal antibody, dilution 1:3000 in 3% milk in TBST); anti- γH2AX (#05-636, Merck; mouse monoclonal antibody, dilution 1:1000 in 3% milk in TBST). According to the manufacturers' indications, all the primary antibodies used have been tested for their ability to recognize the relevant human proteins. The detection of primary antibodies was performed using alkaline phosphatase-conjugated secondary antibodies and enhanced chemiluminescence reagents (BIORAD, Clarity Western ECL Substrate).

3.2.25 DNA damage immunofluorescence staining

Cells were seeded on 12 mm slides and after 48 hours of treatment with 2 μM vem or DMSO, were washed with PBS 1X and fixed with 4% formaldehyde for 10 min at room temperature. Then were washed three times with 1X PBS (5 min each) and were permeabilized with 0.2% triton in PBS for 10 min at room temperature. Cells were washed as above and were blocked with 1% BSA in PBS for 30 min at room temperature. Then they were incubated with anti-8-oxo-dG (#BS-1278R BIOSS, rabbit antibody, dilution 1:200 in blocking) for 1h. Next cells were washed as above and were incubated with anti-rabbit (# A-11037 Thermo Fisher Scientific; dilution 1:500 in PBS) secondary

antibody and with DAPI (DAPI 4',6-Diamidino-2-Phenylindole Dihydrochloride, D1306, Thermo Fisher Scientific) for 30 min at room temperature. Finally, cells were washed and FluoromountTM (K024-xx Diagnostic BioSystems) was used as mounting. Cells were visualized by fluorescence microscopy (Eclipse Ti2 Inverted Research microscope Nikon).

3.2.26 Mitochondria staining in 501Mel-TYR-mCherry cells transfected with siRAB27A

501Mel-TYR-mCherry cells were seeded in 35/10 mm CellView Cell Culture Dish (Greiner Bio-One) and 24 hours later they were transfected with siRAB27A or siCT. After 48 hours of 2 μM vem or DMSO, cells were washed with PBS 1X and fixed with 4% formaldehyde for 10 min at room temperature. Then were washed three times with PBS 1X (5 min each) and were permeabilized with 0.2% triton in PBS for 10 min at room temperature. Cells were washed as above and were blocked with 1% BSA in PBS for 30 min at room temperature. Then they were incubated with anti-TOM20 (#sc-17764 Santa Cruz Biotechnologies, mouse antibody, dilution 1:500 in blocking) for 1h. Next cells were washed as above and were incubated with anti-mouse (# A-28175, Thermo Fisher Scientifc; dilution 1:500 in PBS) secondary antibody and with DAPI (DAPI 4',6-Diamidino-2-Phenylindole Dihydrochloride, D1306, Thermo Fisher Scientific) for 30 min at room temperature. Finally, cells were washed and were visualized by fluorescence microscopy (Eclipse Ti2 Inverted Research microscope Nikon).

3.2.27 Xenograft in zebrafish embryos

501Mel cells were treated with 0.2 μM vem or 3 μM kifunensine or the vehicle DMSO for 48h. Cells were then harvested and used to make a mix of 5×10^5 cells in 2 μl of matrigel (Cultrex Basement Membrane Extract, PathClear). Cell suspension was loaded

into a borosilicate glass capillary and injected (250 cells/nl) into the perivitelline space of 48hpf zebrafish embryos of the Tg(myil7:DsRed) strain (kindly provided by Dr. Didier Stainier, University of California), using a microinjector (Tritech Research). Embryos were previously dechorionated manually or using Pronase (Boehringer Mannheim) and anesthetizes with 0.04 mg tricaine (Sigma-Aldrich). At least 30 embryos were injected per experimental condition and each experiment was repeated three times. Fluorescence imaging was carried out 2 days after the injection, using the Nikon Eclips E600 microscope. Acquisitions were performed using the CoolSnap-CF camera and NIS-Elements software version 2.0. Tumor areas were analyzed using ImageJ software (http://rsb.info.nih.gov).

3.2.28 Xenograft in nude mice

The animal experiments were performed according to the guidelines approved by local ethic authorities (CBS, Centro di Biomedicina Sperimentale, CNR, Pisa) and all experimental protocols were approved by the Italian Ministry of Health (Prot. 317) and were in accordance with the Italian guidelines and regulations. Mice were maintained at the animal facility (CBS) of the CNR of Pisa (Italy). Animals were maintained in a pathogen-free, temperature-controlled, 12 h light and dark cycle environment, and were fed ad libitum. Athymic-nude (Foxn1 nu/nu) female mice, aged 7-8 weeks, were purchased from Harlan Laboratories (Udine, Italy) and were divided into two groups (n= 8 mice per group) as follows: vehicle control and 25 mg/kg vemurafenib treatment. On day 0, 10^6 SK-Mel-5 melanoma cells were resuspended in DMEM/Matrigel (#356234, Corning) 1/1 per 150 ul and were subcutaneously injected with insulin syringe into both lateral flanks of mice. With this conditions and type of cells, tumors started to appear after 10 days. When primary tumors were palpable (50-100 mm^3), blind randomization of mice

in two groups of 8 mice each was performed on the basis of size and presence/absence of palpable tumors on each flank. Mice were treated intraperitoneally twice a day for 19 days with vehicle and 25 mg/kg vemurafenib. Measurements were made with a caliper every three days until surgical resection. Tumor volumes were calculated using the formula: $V = W2 \times L \times 0.5$, where W and L are tumor width and length, respectively. For subsequent studies, the tumor tissues were fixed in 4% paraformaldehyde for IHC analysis.

3.2.29 Immunohistochemistry staining, light microscopy and image processing

Tumor tissues were fixed in 4% paraformaldehyde (PFA) for 24 h at 4°C, dehydrated through a series of graded ethanol baths (70%, 95% and 99%), then immersed in xylene and finally embedded in paraffin. Paraffin-embedded tissues were cut (5 μm thick) using a manual rotary microtome (MEDITE - Manual Rotary Microtome M380). Sections were then rehydrated (xylene, 99%, 95% ethanol and distilled water) and Hematoxylin and Eosin (H&E) staining was carried out using standard methods. Images were acquired with light microscopy (Olympus BX43) at 10× to 40× original magnification and digitized by a video system (Olympus DP20 camera) interfaced to a computer with dedicated software (CellSens Dimension, Olympus) for image acquisition and morphometric and/or color analysis.

3.2.30 Statistical analyses

Unless specified otherwise, data were analyzed with unpaired t test (GraphPad Prism, GraphPad Software Inc.). Values of $p < 0.05$ were considered statistically significant (*p < 0.05, **p < 0.01, *** < 0.001, ****p < 0.0001).

4 Results

4.1   MAPK inhibitors induce pigmentation in melanoma cells

4.1.1   MAPK inhibitors induce pigmentation in a subset of melanoma cell lines *in vitro*

Starting from *in vitro* and *in vivo* data already published, where we showed that the efficacy of MAPK inhibitors is impaired when pigmentation is concomitantly induced [42,72], here our first intention was to further investigate more melanoma cell lines and then to understand the molecular mechanisms that underpin this negative response.

A panel of melanoma cell lines was treated with a BRAFV600E inhibitor, Vemurafenib (2 µM vem), or with a MEK inhibitor, Cobimetinib (0.5 µM cobi) or dmso for 72 hours and according to the color of cell pellet was divided into three groups:

non-pigmentable: A375, C32 and WM278

mild-pigmentable: Colo800, SK-Mel-28 and UACC62

high-pigmentable: M14, A2058, 501Mel, SK-Mel-5, UACC257 and MNT1.

Specifically, after treatment the first group remained white, while the other two got darker, even if the first one in a lighter way (Fig. 20).
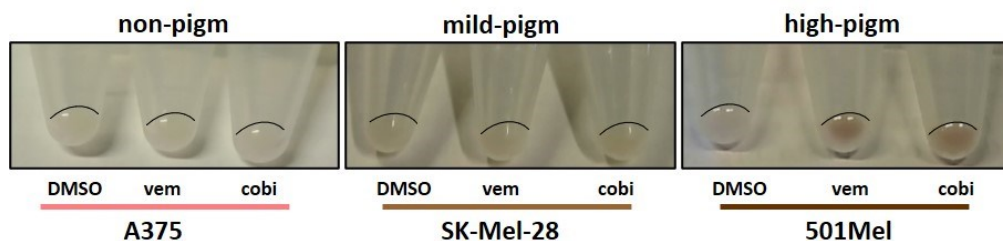

Figure 20. Representative images of cell pellets after 72h of DMSO or 2 µM vem or 0.5 µM cobi in A375 (left), SK-Mel-28 (middle) and 501Mel (right).

Melanin synthesis pathway was checked as well. We found that in all pigmentable cell lines (Colo800, SK-Mel-28, UACC62, M14, A2058, 501Mel, SK-Mel-5, UACC257, MNT1) there is an induction of the genes related to melanin synthesis pathway (*DCT*, *MITF*, *MLANA*, *PGC1alpha*, *TYR*, *TYRP1*) and an induction of *TRPM1*, that is the host gene of miR-211 (it promotes pigmentation) [42]. On the contrary, in all non-pigmentable cell lines (A375, WM278, C32) *TRPM3* is induced, whereas *TRPM1* is not (Fig. 21).
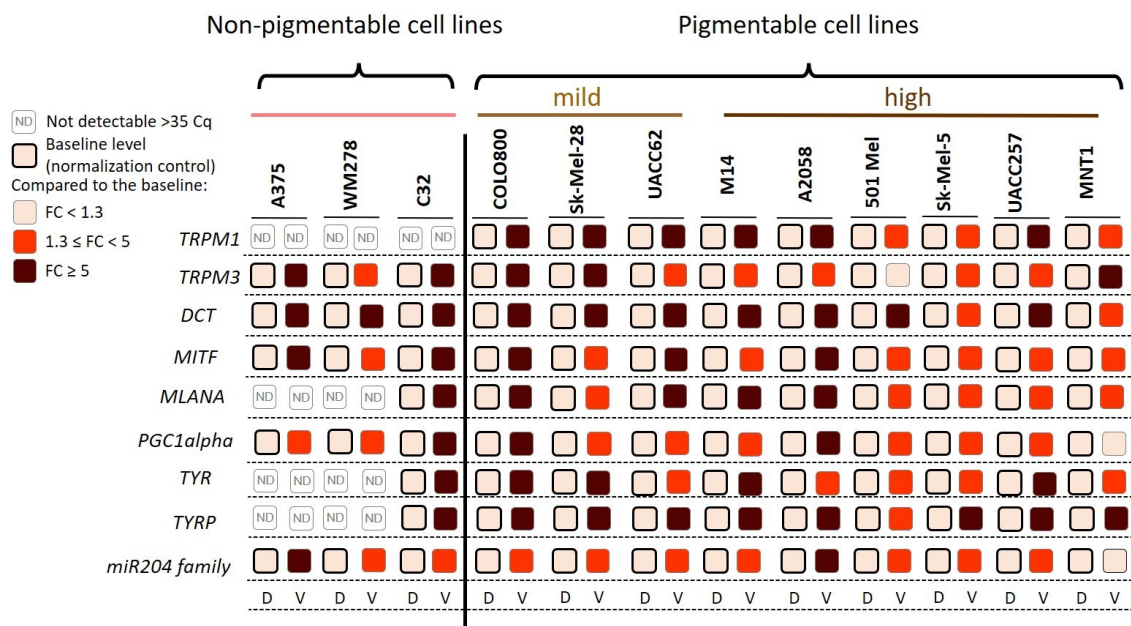

Figure 21. Fold induction of genes related to melanin synthesis upon 48h of treatment of BRAFV600E melanoma cell lines with 2 μM vem. The expression level of DMSO sample is taken as baseline and used as normalization control in each cell line. Fold changes are represented as increases over the baseline (a darker color means a higher fold change). D: DMSO; V: vem.

Then cells treated for 72 hours with vem were analyzed using transmission electron microscope. We found that the change of color is due to general increase of intracellular eumelanosomes, the organelles where melanin is synthesized, in particular those of stage IV that are fully mature (Fig. 22A-B) and with a perinuclear localization (Fig. 22C).
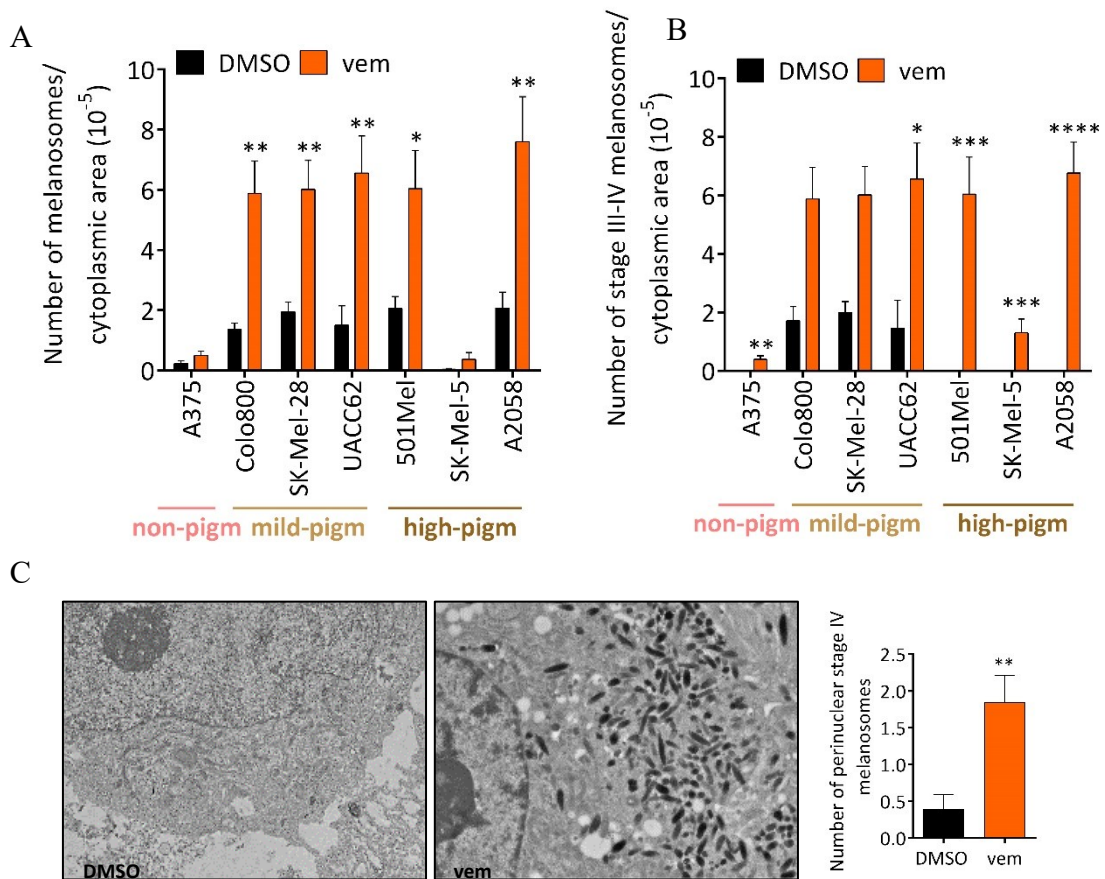

Figure 22. Total (A) and III-IV stage (B) melanosomes detected by TEM in different melanoma cell lines after 72h of treatment with DMSO or 2 μM vem. (C) Pictures of 501 Mel cells taken by transmission electron microscopy. Cells were treated with DMSO and 2 μM vem for 72h (left). Quantification of perinuclear melanosomes in 501Mel (right). The graphs represent the mean±SEM of 3 independent experiments. *p<0.05, **p<0.01, ***p<0.001, ****p<0.0001.

Interestingly, cell lines belonging to the group called mild-pigmentable cells (Colo800, SK-Mel-28, UACC62) did show an induction of *TRPM1* and of the other pigmentation genes, but they got only slightly pigmented after the inhibition of the MAPK pathway, even if their number intracellular eumelanosomes increases in a manner comparable to

that of pigmentable melanoma cell lines. This may depend on the presence of pheomelanosomes and/or on a different level of activity of the enzyme tyrosinase.

According to these data, not all melanoma cell lines exhibit the same level of pigmentation increase, when treated with BRAF and MEK inhibitors.

4.1.2 MAPK inhibitors induce pigmentation *in vivo*

In order to establish whether the induction of pigmentation occurs also in an *in vivo* context, we xenografted SK-Mel-5 cells into nude mice and then treated them with vem or dmso for 19 days. Firstly, we ensured that the experiment worked by looking at the data from tumor volume and weight: mice treated with vemurafenib developed tumors that were smaller compared to those treated with the vehicle (Fig. 23C-D). Then, we checked for melanin presence and found that all the tumors treated with the drug appear black, due to the presence of pigment spots (Fig. 23F). Melanin occurrence was again confirmed with H&E staining (Fig. 23E).
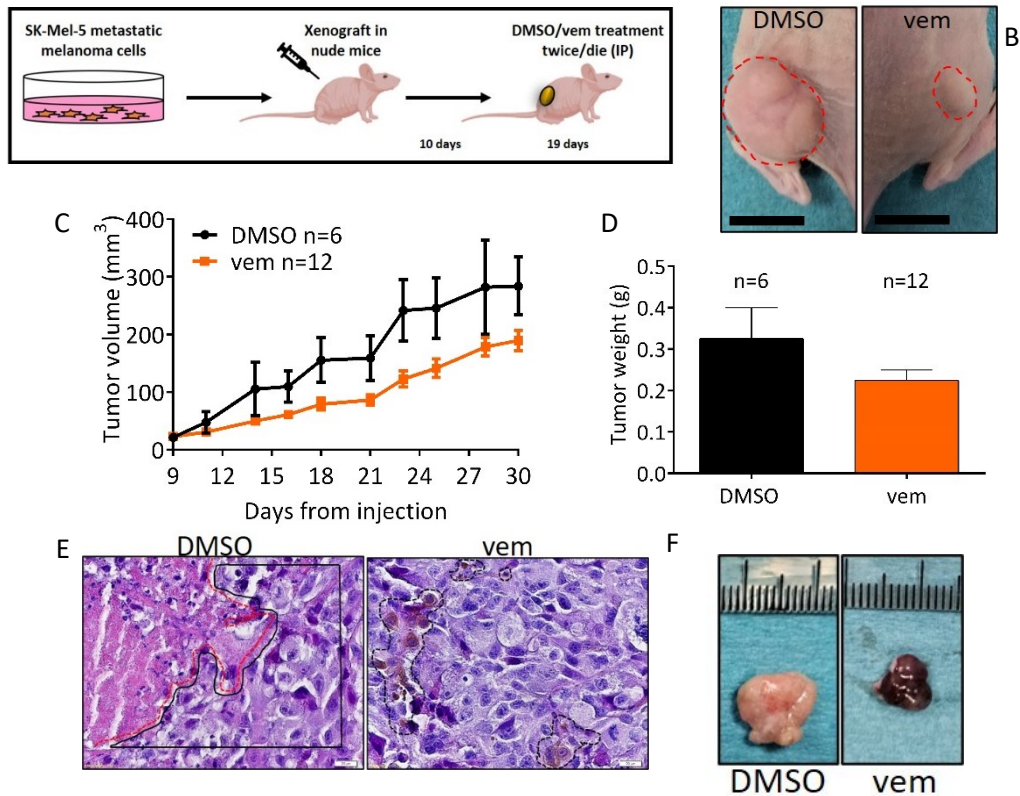
Figure 23. SK-Mel-5 xenografted in nude mice. (A) Cartoon of the experimental design and (B) tumor area in DMSO and vem (scale bar: 1 cm). Mice have been treated with 25mg/kg of vem twice a day. (C) Tumor volume and (D) tumor weight are reported. Melanin presence in vem treated tumors. (E) H&E staining in DMSO and vem samples. (DMSO) Necrotic area is marked with a dashed line. Melanoma cells without melanin are outlined with a box. (vem) Melanin presence is marked with a dashed line (original magnification: 40x; scale bar: 20 µm). (F) Morphology of tumors after DMSO or vem treatment.

To sum up, we demonstrated that the inhibition of MAPK pathway leads to an induction of melanin synthesis with pigmentation increase as readout.

4.2   Differential sensitivity to MAPK inhibitors according to pigmentation levels

4.2.1   Pigmentable melanoma cells are more resistant to MAPK inhibitors

According to results showed in paragraph 1, we expected that the sensitivity to MAPK inhibitors should differ between non-pigmentable and pigmentable cells.

Two non-pigmentable cell lines (A375 and C32) and two high-pigmentable cell lines (501Mel and SK-Mel-5) were treated with 0.1 µM vem or 10 nM of cobi or with their combination for one week. Data display that cell growth inhibition is higher in non pigmentable cells, especially for C32 cell line, compared to pigmentable ones. The difference can be better appreciated when we use the combination of the two drugs, suggesting higher resistance to treatment for pigmentable cells (Fig. 24).
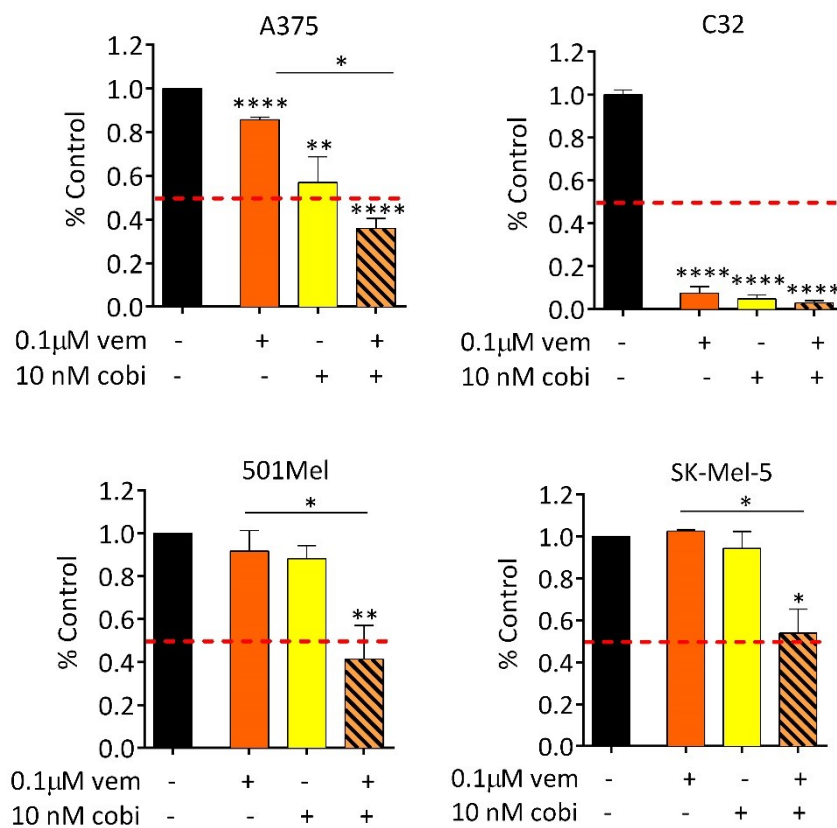

Figure 24. Cell number upon the treatment of A375, C32, 501Mel and SK-Mel-5 cells with 0.1 µM vemurafenib and 10 nM cobimetinib or their combination upon one week. The graphs represent the mean±SEM of 3 independent experiments. *p<0.05, **p<0.01, ***p<0.001, ****p<0.0001.

We then investigated the effects of treatment with MAPKi, looking for a difference in pigmentable and non-pigmentable cells. The two non-pigmentable cell lines (A375 and C32) and two high-pigmentable cell lines (501Mel and SK-Mel-5) were treated with 2 μM vem for 48 hours, fixed and stained with propidium iodide solution for flow cytometry analysis.
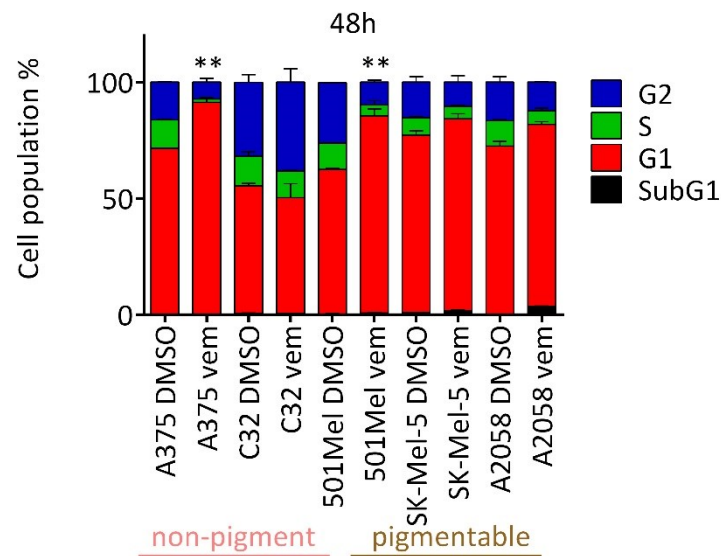

Figure 25. Cell cycle progression phases in A375, C32, 501Mel and SK-Mel-5 cells treated with DMSO or 2 μM vem for 48h. The graphs represent the mean±SEM of 3 independent experiments. *p<0.05, **p<0.01, ***p<0.001, ****p<0.0001.

Consistent with the fact that BRAFV600E inhibition leads to a block of proliferation, data show that in all cell lines S phase decreases upon treatment. Moreover, in A375 and 501Mel cells vem determines an increase in G1 phase, while in C32 cells it provokes an increase in G2 phase, suggesting a different impairment on cell cycle progression, but not strictly related to the degree of pigmentation (Fig. 25).

Since vemurafenib treatment can also induce cellular senescence [73,74], we investigated it in the same melanoma cell lines. Cell lines were treated with dmso or 2 μM vem for 48

hours, then they were fixed and stained for SA-β-galactosidase. Data revealed that A375 and C32 cells went into senescence after vemurafenib treatment, whereas there was high diversity in the pigmentable group: even if A2058 and SK-Mel-5 showed a high basal level of cells in senescence, yet the treatment with the drug did not alter this condition. On the contrary 501Mel cells displayed a high induction of senescence after vemurafenib, comparable to that of A375 cells (Fig. 26). According to these results, it was difficult to draw a conclusion and say that there is a difference among pigmentable and non-pigmentable cells after vemurafenib treatment. Probably, we should perform further experiments, for example we could measure the expression levels of p53, p21 and p16 and other cell cycle regulators, in order to understand which type of senescence is induced, i.e. if senescence is an irreversible G1 arrest or a G2 exit, after the activation of DNA damage response pathways [75,76].

Nevertheless, we confirm our previous observations that MAPK inhibitors are more effective in non-pigmentable cells.
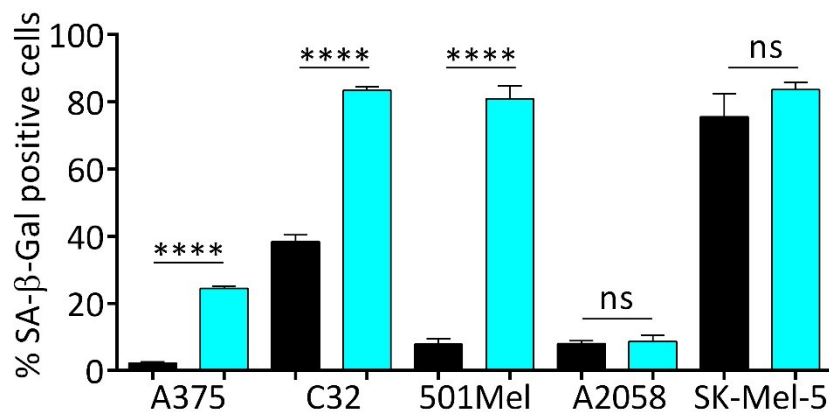

Figure 26. Vemurafenib treatment increased SA-β-Gal positivity in melanoma cells. The graphs represent the mean±SEM of 3 independent experiments. *p<0.05, **p<0.01, ***p<0.001, ****p<0.0001.

4.2.2 Melanotic metastatic tumors respond worse to therapy

Next, we analyzed a cohort of 107 metastatic melanoma patients composed of 67 melanotic tumors and 40 amelanotic tumors, treated with single agent targeted therapy (vemurafenib) or dual agent targeted therapy (dabrafenib + trametinib) or targeted therapy + immunotherapy (dabrafenib + ipilimumab) at New York University (NYU) Langone Medical Center from 2002 to 2021. Patients showing disease progression upon treatment were classified as non-responders, while patients showing stable disease, partial response or complete response upon treatment were classified as responders. We found that patients with metastatic amelanotic tumors appeared to respond better to therapy than patients with melanotic metastatic tumors, confirming again that pigmentation rendered the action of MAPK inhibitors less effective.

	Non-Responders	Responders	Total
Melanotic	48 (72%)	19 (48%)	67
Amelanotic	19 (28%)	21 (52%)	40
Total	67	40	107

Table 6. Response of 67 metastatic melanoma patients with melanotic tumors and 40 metastatic melanoma patients with amelanotic tumors to treatment with single agent targeted therapy or dual agent targeted therapy or targeted and immunotherapy. The Fisher Exact Probability Test indicate that patients with melanotic metastases are significantly more likely to be non-responders to targeted therapy compared to patients with amelanotic metastases (p=0.0145).

4.3 Pigmentation limits the efficacy of MAPK inhibitors

In order to demonstrate that pigmentation limits the efficacy of MAPKi, we decreased/increased pigmentation levels expecting an increase/decrease in sensitivity. We observed the effect of such treatments on the mass of xenografted tumors in zebrafish embryos. We have already shown that when we decrease pigmentation levels by using

Phenylthiourea (PTU), an inhibitor of tyrosinase activity, or by using a specific LNA for the inhibition of endogenous miR-211, we noted an increase in cell proliferation that sustains vem activity [42]. To prove the opposite effect, 501Mel cells were treated with 0.2 μM vem or 3 μM kifunensine (pigmentation inducer) or dmso for 48h. They were then injected into the yolk sac of 48 hours post fertilization zebrafish embryos. After two days from the injection, we measured the mass of the xenografted tumors. We noticed that kifunensine did not alter cell proliferation per se (third column vs first column), but reverted the decrease in proliferation caused by vem (second column vs fourth column) (Fig. 27).
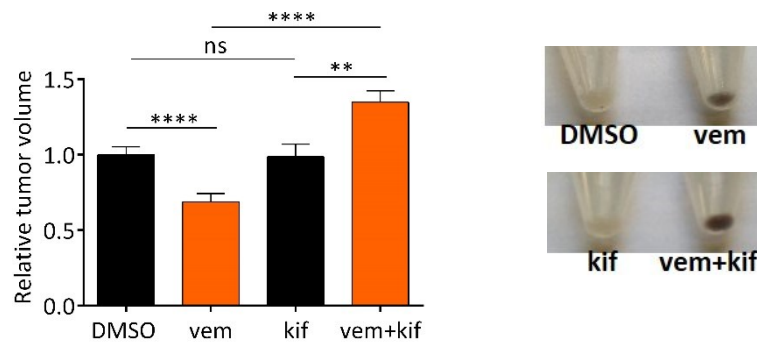

Figure 27. 501Mel cells were treated with 0.2 μM vem or 3 μM kifunensine or the vehicle DMSO for 48h. They were then injected into the yolk sac of 48hfp zebrafish embryos. The masses of the xenografted tumors were measured 48h later (left). Representative images of cell pellets (right). The graphs represent the mean±SEM of 3 independent experiments. *$p<0.05$, **$p<0.01$, ***$p<0.001$, ****$p<0.0001$.

With this xenograft, we confirmed that pigmentation alters the outcome and efficacy of MAPK inhibitors treatment.

Taken together these results indicate that pigmentation makes melanoma cells less responsive and, as a consequence, less vulnerable to MAPK inhibitors treatment both *in vitro* and *in vivo*.

4.4 Intracellular melanosomes limit the efficacy of MAPK inhibitors

4.4.1 An overall melanosome trafficking is induced upon vemurafenib treatment

Since vem treatment causes an increase in the number of intracellular melanosomes, we checked whether the trafficking of melanosomes is induced as well. We use a melanoma cell line, 501Mel-Tyr-mCherry, in which Tyr-mCherry fluorescent protein is stably expressed and its signal reflects the presence of melanosomes (Fig. 28A). Tyr-mCherry 501Mel cells were treated with 5 μM vem or dmso for 10 days. Then, the supernatant was collected and red fluorescent melanosomes released were isolated by ultracentrifugation and counted by flow cytometry. The results show that upon vem treatment there is an increase in the number of melanosomes released from cells (Fig. 28B). In order to detect the opposite phenomenon, the uptake, we performed a co-culture experiment by using again 501Mel-Tyr-mCherry cells as donor cells (upper chamber) and EGFP-expressing pigmentable cells (Colo800, 501Mel, SK-Mel-5 and MNT1) as receiving cells (lower chamber). The cells were treated with 5 μM vem or dmso for one week and then the percentage of red cells present in the lower chamber was measured by flow cytometry. Results show that drug treatment increases the number of uptaked melanosomes as well (Fig. 28C). Data confirm that an overall melanosome trafficking is induced upon vemurafenib treatment.
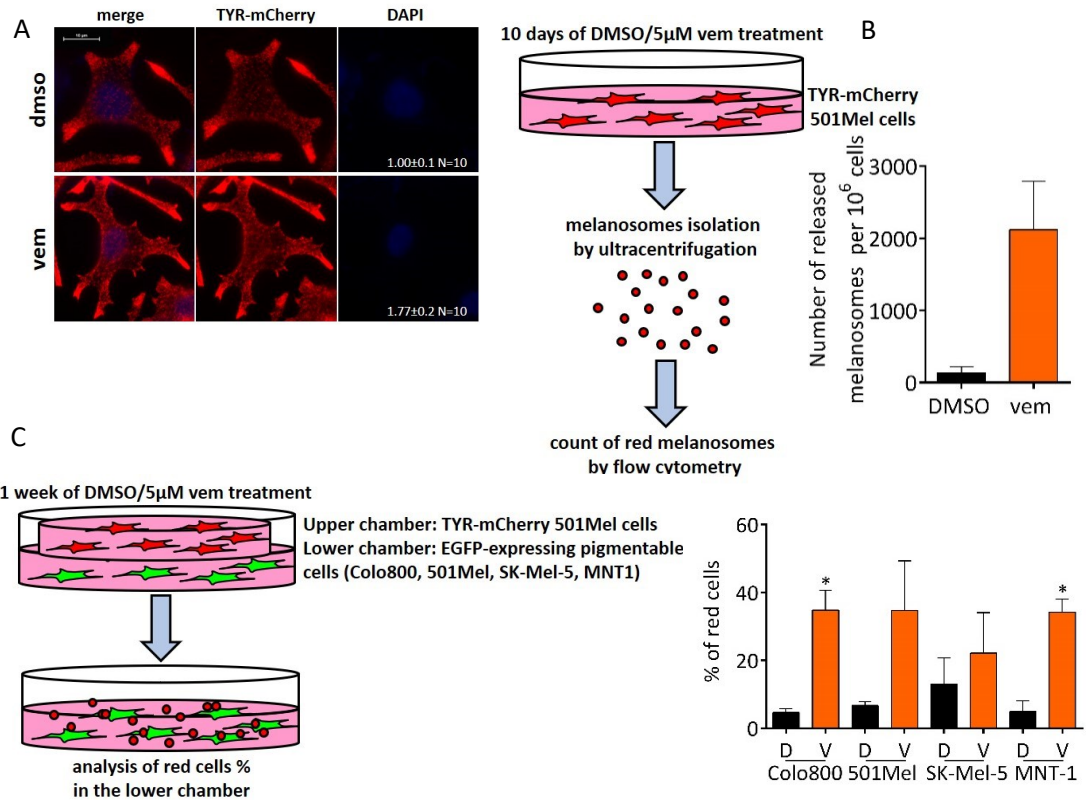
Figure 28. (A) Representative images of TYR-mCherry 501Mel cells, upon 72h of treatment with DMSO vehicle (upper) or 2 μM vem (lower). The increase in melanosomes caused by vem treatment is appreciated as an increase in red fluorescence and can be quantified using ImageJ software (http://rsb.info.nih.gov). Scale bar: 10 μm. (B) Detection of melanosomes released. Cartoon of the experimental design (left) and quantification of melanosome released (right). (C) Detection of melanosomes uptake. Cartoon of the experimental design (left). Quantification (right). The graphs represent the mean±SEM of 3 independent experiments. *p<0.05, **p<0.01, ***p<0.001, ****p<0.0001.

4.4.2 Intracellular melanosomes confer resistant to vemurafenib treatment

Having demonstrated that pigmentation limits the activity of MAPK inhibitors, we wanted to determine whether this happens inside cells, specifically that is due to the presence of melanosomes, rather than the export of the drug, through the release of melanosomes. To achieve this point, we used ultracentrifugation to isolate red melanosomes from the supernatant of 501Mel-Tyr-mCherry cells, then we counted and administered them to naïve 501Mel cells that were subsequently treated with vem. In so doing, we observed that cells receiving extra melanosomes become less sensitive to vem.

This result indicates that actually the increase in the number of intracellular melanosomes

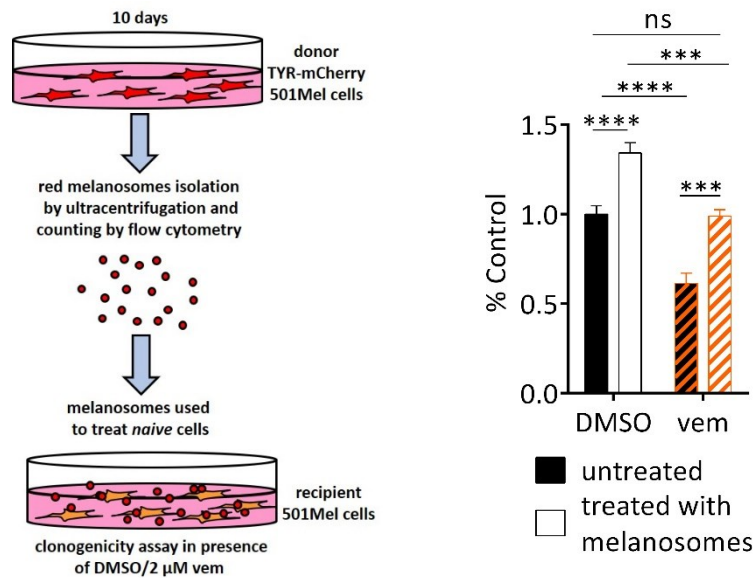confers resistance to vem, by acting inside the cells (Fig. 29)

Figure 29. Clonogenicity assay performed on 501Mel cells treated with isolated melanosomes. Cartoon of the experimental design (left). The number of colonies counted after 10 days of treatment with 2 μM vem or DMSO is reported (right). The graphs represent the mean±SEM of 3 independent experiments. *p<0.05, **p<0.01, ***p<0.001, ****p<0.0001

4.5 Pigmentation acts as scavenger of vem induced-ROS

4.5.1 MAPK pathway inhibition causes an increase in ROS levels

It is reported in the literature that the inhibition of BRAFV600E causes an increase in ROS levels. We obtained similar results by inhibiting the mutated protein in different ways, with drugs and through genetic silencing. A375 cells were treated with dmso or 2 μM vem or paradox breakers 0.5 μM PLX7904 and 2 μM PLX8334 for 48 and 72 hours. Otherwise A375 cells were transfected with a siRNA against BRAF or with a non-targeting control siRNA. Drug treatment causes an increase in both total and mitochondrial ROS. Total ROS levels are higher than control at 48 hours of treatment and increase even further at 72 hours. Mitochondrial ROS levels appear to peak at 48 hours already. Total and mitochondrial ROS levels increase upon siBRAF transfection as well, although to a lesser extent (Fig. 30).
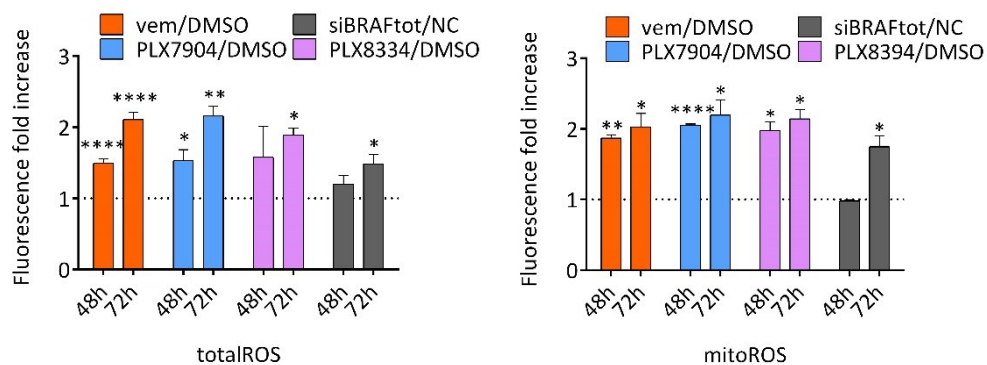

Figure 30. Total (left) and mitochondrial (right) ROS levels measured in A375 cells after 48h or 72h from BRAFV600E inhibition. The graphs represent the mean±SEM of 3 independent experiments. *p<0.05, **p<0.01, ***p<0.001, ****p<0.0001.

4.5.2 Superoxide and hydroil ion are induced by vemurafenib

Moreover, we determined which are the reactive species induced by vemurafenib treatment using known ROS scavengers. A375 were treated for 48 hours with dmso or 2 μM vem or 10 mM sodium pyruvate (SP), a common medium component known to neutralize hydrogen peroxide [77–79], or 100 μM manganese(III)tetrakis(4-benzoic acid)porphyrin (MnTBAP), which acts as superoxide dismutase mimic and hydrogen peroxide scavenger [80,81], or with 20 μl of dmso (DD), notorious for scavenging hydroxyl radical [82]; then total and mitochondrial ROS were detected. We expect that when a ROS scavenger works correctly the levels of reactive species decrease with its presence, and that when it is added to vem treatment, we should notice a decrease in ROS-induced vem as well. Since with MnTBAP and DD the levels of total ROS decrease compare to the control (third and seventh bar vs first) and that their addition to vem, leads to a decrease as well (fourth and eighth bar vs second), we confirm that total ROS detected are superoxide anion and hydroxyl radical. Regarding mitochondrial ROS, only MnTBAP is able to generate a similar effect, proving that the radical species detected is O2- (Fig. 31).
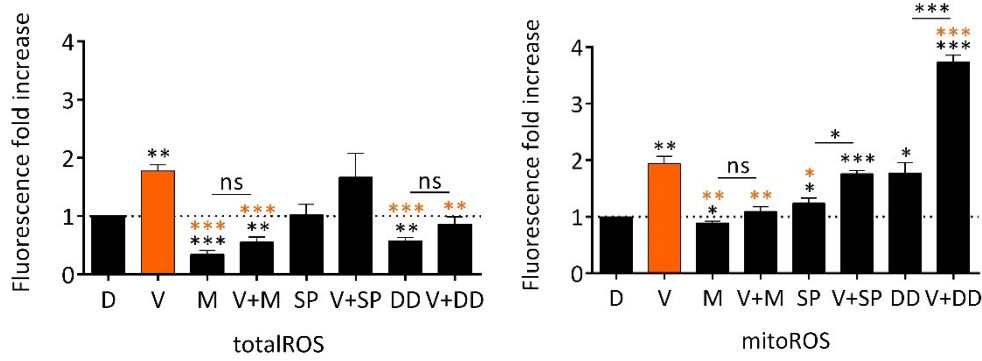
Figure 31. Total (left) and mitochondrial (right) ROS levels measured in A375 after 48h of DMSO or 2 μM vem (V) or 10 mM Sodium Pyruvate (SP) or 100 μM MnTBAP (M) or 20 μl DMSO (DD). The graphs represent the mean±SEM of 3 independent experiments. *p<0.05, **p<0.01, ***p<0.001, ****p<0.0001.

To support these data, we analyzed the expression of pro-oxidant genes such as NAPDH oxidase, which depending on the class they belong, produce different types of ROS. We confirmed, through the induction of NOX2 and NOX5, that upon vem treatment superoxide was produced, while hydrogen peroxide was not, due to low levels of NOX4. Of note, NOX genes were more stimulated in non pigmentable cells compared to pigmentable ones (Fig. 32).
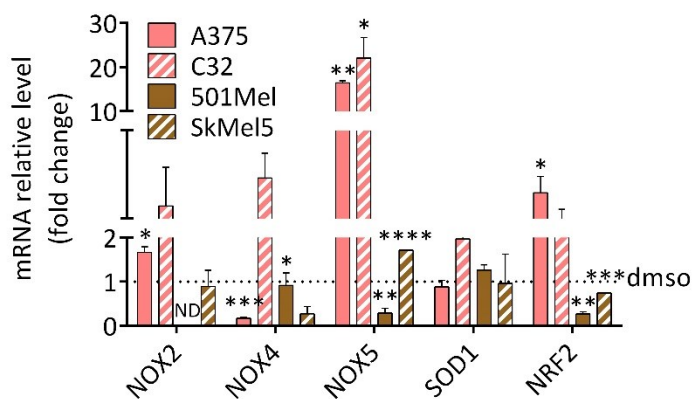

Figure 32. mRNA relative fold change of NOX2, NOX4, NOX5, SOD1 and NRF2 in A375, 501Mel and SK-Mel-5 after 48h of DMSO or 2 μM vem. The graphs represent the mean±SEM of 3 independent experiments. *p<0.05, **p<0.01, ***p<0.001, ****p<0.0001.

4.5.3 Pigmentable cells present lower levels of ROS compared to non-pigmentable cells

Then, we treated our three groups of melanoma cell lines with dmso or 2 µM vem for 48 hours and measured the levels of total and mitochondrial ROS. We observed that the levels of ROS are lower in pigmentable cells compared to non-pigmentable cells, in particular they decrease at the increase in pigmentation level, suggesting an inverse correlation between the presence of melanosomes and sensitivity to ROS (Fig. 33).
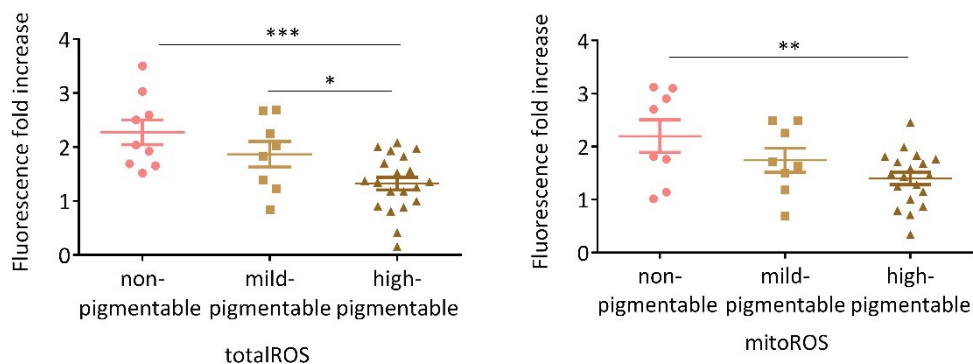

Figure 33. Total (left) and mitochondrial (right) ROS levels measured in non-pigmentable, middle and pigmentable cell lines after 48h of DMSO or 2 µM vem. The graphs represent the mean±SEM of 3 independent experiments. *p<0.05, **p<0.01, ***p<0.001, ****p<0.0001.

4.5.4 ROS levels induced by vem are inversely correlated with pigmentation status

Since melanin is considered a physiological ROS scavenger, acting as a protection agent by quenching toxic oxygen metabolites, we started to speculate that in pigmentable melanoma cells it could act as scavenger of ROS induced by BRAFV600E inhibition. In order to strength these results we took advantage of two *in vitro* model systems. In the first, we used SK-Mel-188, a melanoma cell line whose pigmentation levels can be controlled on the basis of the concentration of L-Tyrosine in the culture medium. Indeed SK-Mel-188 grown in Ham's F10 medium, which is low in melanin precursor L-Tyr, are not pigmented, while SK-Mel-188 grown in DMEM medium, which is rich in L-Tyr, are

pigmented. Since this cell line is wild type for BRAF, it was treated with cobi for 72h and mitochondrial ROS were measured. We noted that the pellet of the cells from Ham's F10 medium remained white and we observed high levels of mitochondrial ROS; on the contrary the pellet of cells from DMEM medium got more pigmented and cells showed a much lower increase in mitochondrial ROS (Fig. 34).
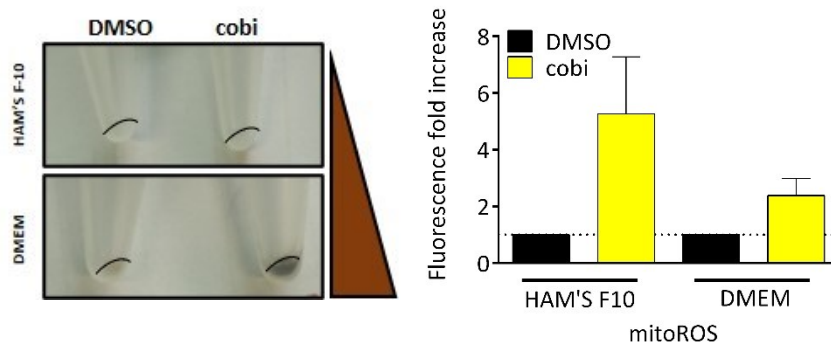

Figure 34. Mitochondrial ROS levels measured in SK-Mel-188 cells grown in Ham's F10 medium or DMEM medium after 72h of DMSO or 10 nM cobi (right). Representative images of cells pellet (left). The graphs represent the mean±SEM of 3 independent experiments. *p<0.05, **p<0.01, ***p<0.001, ****p<0.0001.

For the second model, we stably infected a pigmentable melanoma cell line, UACC257, with TYR-Zsgreen construct, in which Zsgreen reporter is under the control of *TYR* promoter that allowed us to distinguish two populations, HIGH or LOW ZsGreen, according to their level of *MITF* expression and so of TYR. The stable cell line was treated for 72 hours with 2 or 5 μM of vem and ROS were measured. Once distinguished the two populations, HIGH or LOW ZsGreen, we compared the levels of ROS. As supposed, higher levels of mitochondrial ROS are present in LOW ZsGreen population compared to HIGH ZsGreen population. We did not notice any significant difference in the levels of total ROS between the two groups (Fig. 35).
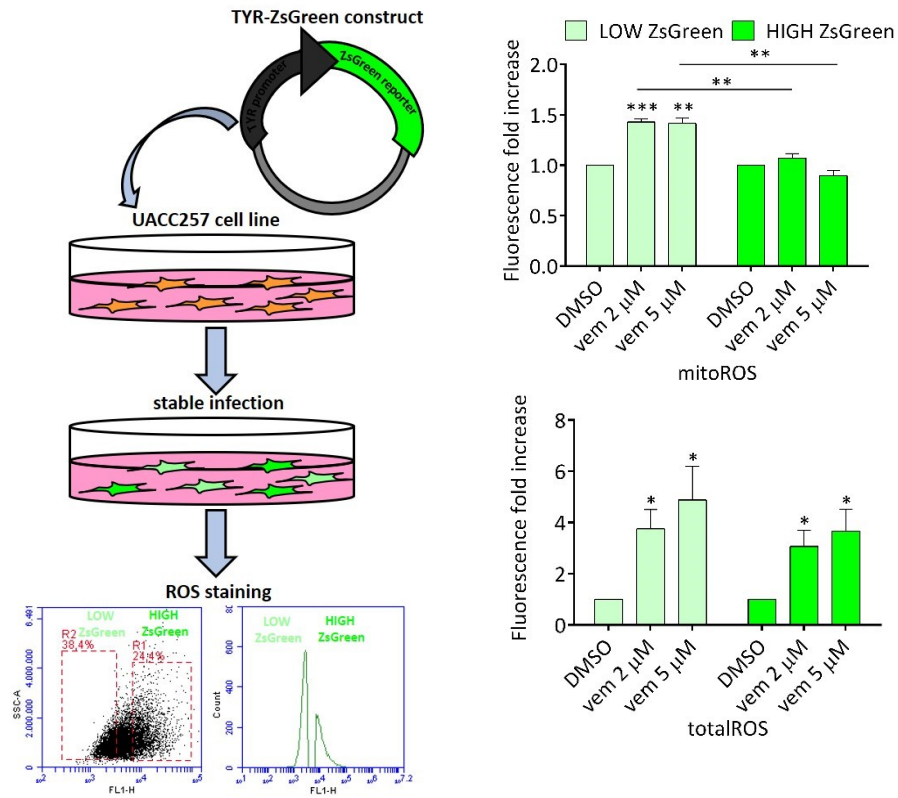
Figure 35. Cartoon of the experimental workflow for UACC257-Tyr-ZsGreen cells (left). Mitochondrial and total ROS levels after 72h of DMSO or 2 μM or 5 μM vem (right). The graphs represent the mean±SEM of 3 independent experiments. *p<0.05, **p<0.01, ***p<0.001, ****p<0.0001.

From these data we proved again that the higher presence of melanin can reduce the levels of ROS induced by MAPK inhibitors treatment, both from an indirect way (the presence of L-Tyrosine that influence the synthesis of melanin) and from a direct way (the transcription of Tyrosine under the control of MITF).

4.5.5 Pigmentation inhibitors rescue the efficacy of vemurafenib

According to the above results, if we diminish pigmentation, by using a pigmentation inhibitor, we should obtain increase in ROS levels. 501Mel and SK-Mel-5 cells were pre-treated with 1 mM of Phenylthiourea (PTU) for 72 hours and then with dmso or 2 μM vem for the next 48 hours, and at the end, color of the pellet, ROS levels and cell growth inhibition were controlled. First, we checked for the loss of pigmentation: when cells are treated with both drugs, the pro-pigmentation effect of vemurafenib failed thanks to PTU action, in both cell lines (Fig. 36A). Then, ROS levels appeared higher in presence of vemurafenib and PTU compared to vemurafenib single treatment (Fig. 36B-C). Finally, we observed a general decrease in cell growth after vemurafenib treatment (compare orange bars versus black bars), although this reduction is more pronounced when we added PTU (compare the second bar with the fourth bar) (Fig. 36D-E). These results suggest that, in absence of melanin, as for non-pigmentable cells, cells were more sensitive to the action of ROS and so to the drugs treatment.

Figure 36. (A) Representative images of cells pellet after 72h of DMSO or 2 μM vem or 0.5 mM PTU or vem-PTU in 501Mel. Total (left) and mitochondrial (right) ROS levels measured in 501Mel (B) and SK-Mel-5 (C) cells after 72h of 1 mM PTU and 48h of DMSO or 2 μM vem. Cell number upon the treatment of 501Mel (D) and SK-Mel-5 (E) cells with 1 mM PTU for 72h and with DMSO or 2 μM vem for 48h. The graphs represent the mean±SEM of 3 independent experiments. *p<0.05, **p<0.01, ***p<0.001, ****p<0.0001.

We repeated these experiments by pre-treating 501Mel and SK-Mel-5 cells with another pigmentation inhibitor, 3′,4′-dichlorobenzamil hydrochloride (DBZ) which impairs melanosomes maturation. We obtained the same effects in term of pigmentation reduction, increase in ROS levels and cell growth inhibition (Fig. 37).
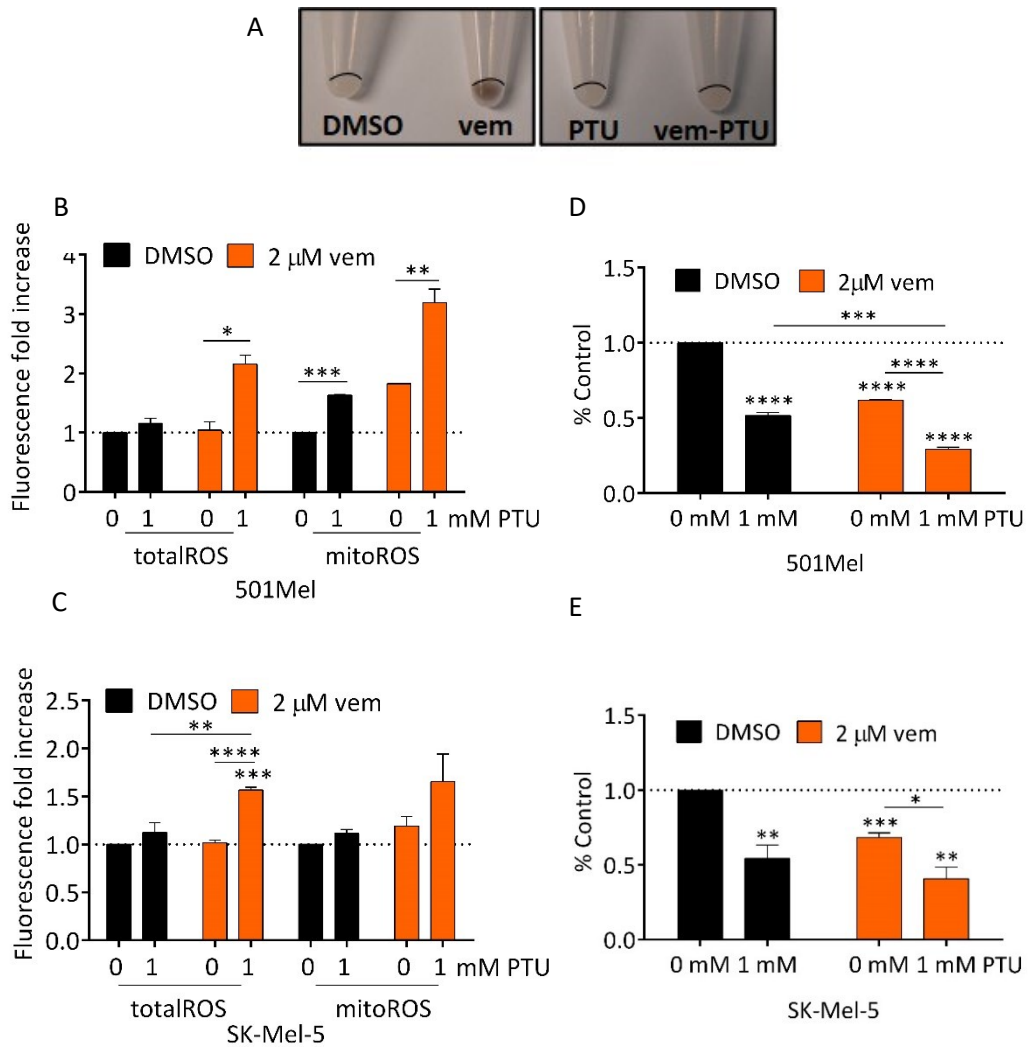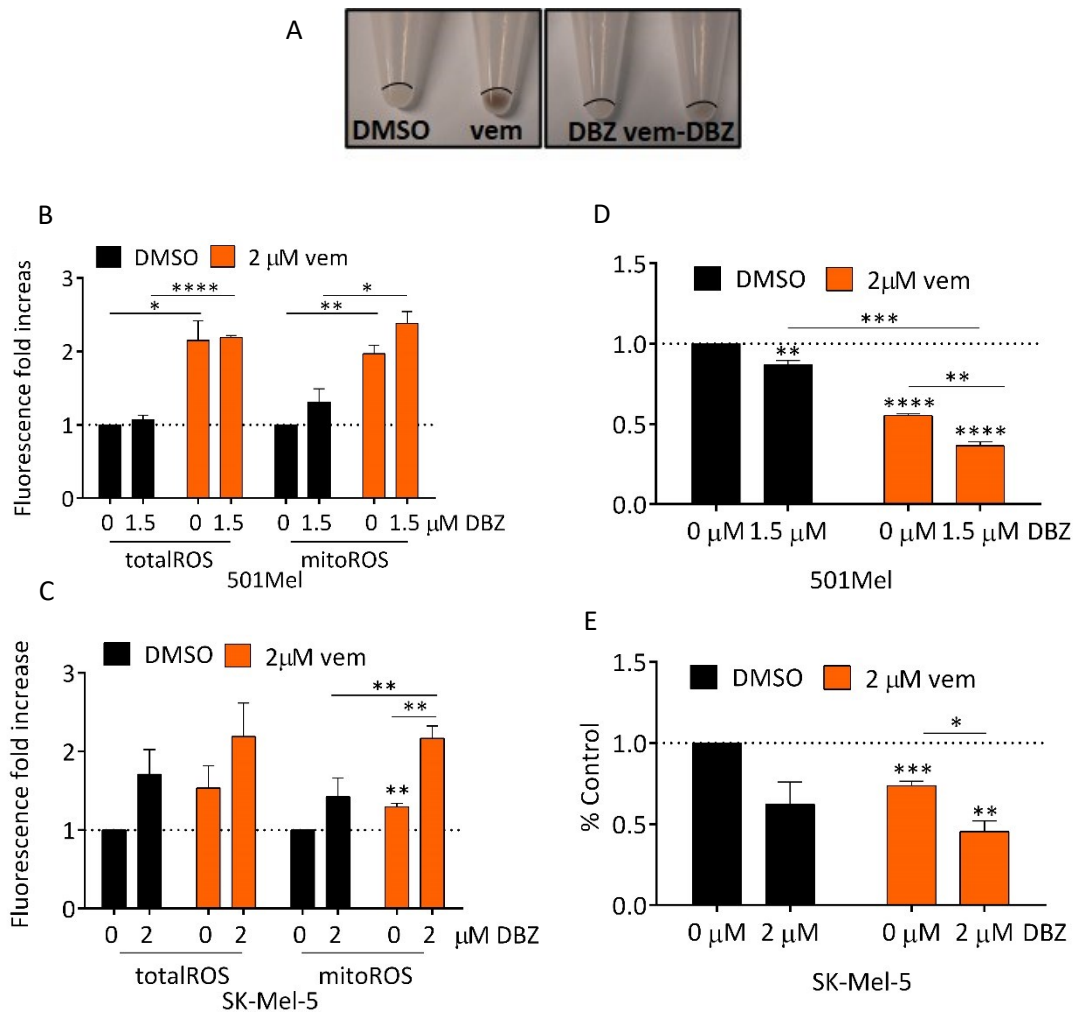

Figure 37. (A) Representative images of cells pellet after 72h of DMSO or 2uM vem or 1.5 uM DBZ or vem-DBZ in 501Mel. Total (left) and mitochondrial (right) ROS levels measured in 501Mel (B) and SK-Mel-5 cells (C) after 72h of 1.5 μM or 2 μM DBZ and 48h of DMSO or 2 μM vem. Cell number upon the treatment of 501Mel (D) and SK-Mel-5 (E) cells with 1.5 μM or 2 μM DBZ for 72h and with DMSO or 2 μM vem for 48h. The graphs represent the mean±SEM of 3 independent experiments. *p<0.05, **p<0.01, ***p<0.001, ****p<0.0001.

4.5.6 Pigmentation inhibitors rescue the efficacy of BRAFi plus MEKi

Then, we then decided to use the dual combination of vemurafenib plus cobimetinib to recreate clinical treatment. 501Mel and SK-Mel-5 cells were pre-treated with a lower concentration of PTU (0.5mM for 72 hours) and then with lower doses of vemurafenib (0.1 μM) and cobimetinib (10 nM) for the next 48 hours. Regarding ROS levels, we detected an increase in their levels starting from the dual treatments (orange, blue and green crossed bars), which reached its peak with the combination of the three drugs. In terms of cell growth inhibition, we obtained significant results starting from the single treatment, better when using the dual combination (compare orange crossed bar and blue crossed bar to red bar, and green crossed bar versus yellow bar), best with the three drugs (purple crossed bar), suggesting a positive interaction between MAPK inhibitor and pigmentation inhibitor (Fig. 38).

Figure 38. Total (left) and mitochondrial (right) ROS levels measured in 501Mel (A) and SK-Mel-5 (B) after 72h of 0.5 mM PTU and 48h of DMSO or 0.1 μM vem or 10 nM cobi. Cell number upon the treatment of 501Mel (C) and SK-Mel-5 (D) cells with 0.5 mM PTU for 72h and with DMSO or 0.1 μM vem or 10 nM cobi for 48h. The graphs represent the mean±SEM of 3 independent experiments. *p<0.05, **p<0.01, ***p<0.001, ****p<0.0001.

Also in this case, we used the second pigmentation inhibitor, DBZ, in both 501Mel and

SK-Mel-5 cells, obtaining similar results (Fig. 39).

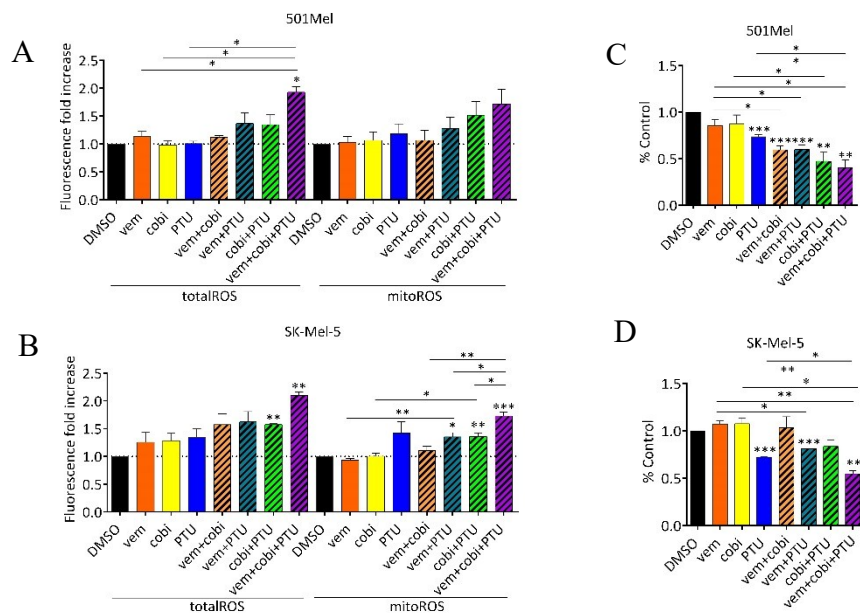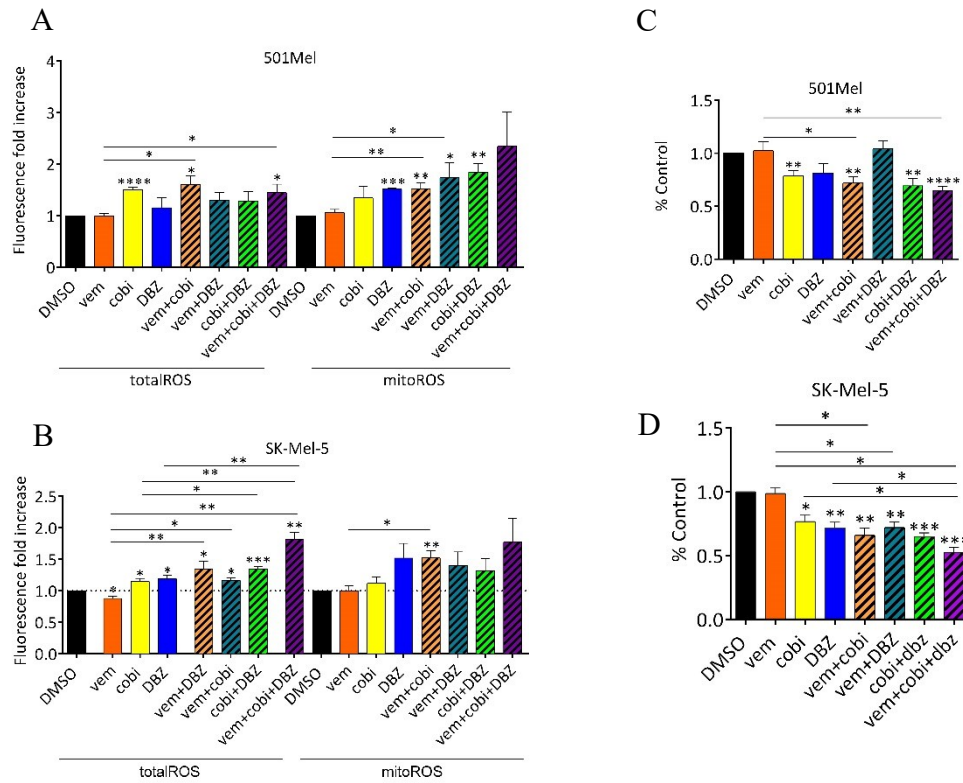

Figure 39. Total (left) and mitochondrial (right) ROS levels measured in 501Mel (A) and SK-Mel-5 (B) after 72h of 1.5 μM DBZ or with 2 μM DBZ and 48h of DMSO or 0.1 μM vem or 10 nM cobi. Cell number upon the treatment of 501Mel (C) with 1.5 μM DBZ and SK-Mel-5 (D) cells with 2 μM DBZ for 72h and with DMSO or 0.1 μM vem or 10 nM cobi for 48h. The graphs represent the mean±SEM of 3 independent experiments. *p<0.05, **p<0.01, ***p<0.001, ****p<0.0001.

4.5.7   Non-pigmentable cells show a decrease in ROS levels when rendered melanotic

Finally, we decided to do the opposite experiment: render non-pigmentable cells

melanotic in order to observe a decrease in ROS levels. A375 cells were treated with

3mg/ml or 9mg/ml of dopamine synthetic nanoparticles for 4 hours and after additional

72 hours of 2 μM vem or dmso treatment total ROS were detected. The results showed

that in the absence of nanoparticles, ROS levels increased as expected, while the addition

of nanoparticles lead to a decrease of ROS, which correlated with the content of melanin

in a dose-dependent manner (Fig. 40). Again, these results were in agreement with the experiments described above.
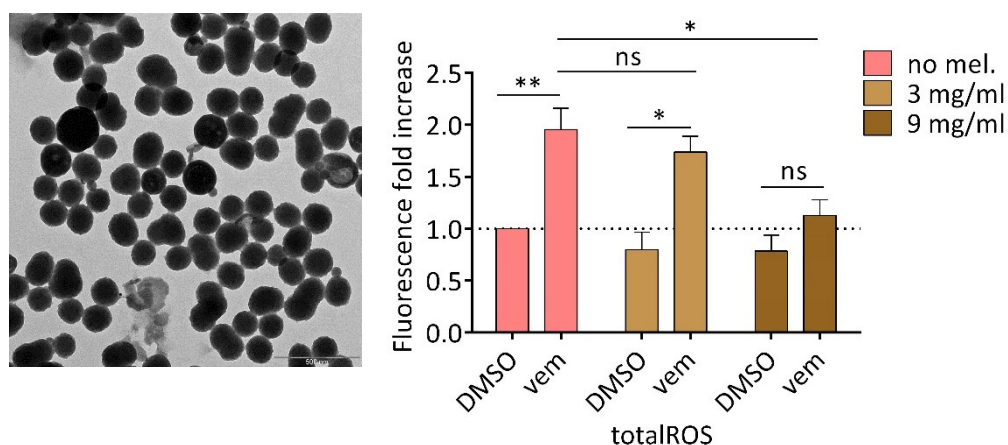
Figure 40. Representative image of synthetic melanin particles detected by TEM (left). Total ROS levels measured in A375 cells after 4h of nanoparticles pre-treatment and 72h of DMSO or 2 μM vem (right). The graphs represent the mean±SEM of 3 independent experiments. *p<0.05, **p<0.01, ***p<0.001, ****p<0.0001.

We concluded that melanin acts as vem induced-ROS scavenger and renders pigmentable melanoma cells less sensitive to the action of MAPK inhibitors therapy.

4.6   ROS induced DNA damage is lower in pigmentable cells

We then analyzed the consequences of increased ROS levels in non-pigmentable and pigmentable cells, presuming that ROS-induced damage is higher in the first group compared to the second. Since ROS have the ability to alter more or less all biological macromolecules, we examined proteins, lipids and DNA, to discover the best context to observe a consistent difference between the two groups of cells.

4.6.1 Protein carbonylation

We started from proteins that are one of the major targets of oxygen free radicals and other reactive species. Oxidative modification of proteins alters the side chains of methionine, histidine, and tyrosine and forms cysteine disulfide bonds. Metal catalyzed oxidation of proteins inserts carbonyl groups (aldehydes and ketones) at lysine, arginine, proline or threonine residues in a site-specific manner. The oxidative modification of proteins can vary biochemical characteristics of proteins such as enzymatic activity, DNA binding activities of transcription factors and the susceptibility to proteolytic degradation. One consequence of oxidative modification is the introduction of carbonyl groups into protein side chains by a site-specific mechanism. We used OxyBlotTM Kit that provides the immunodetection of these carbonyl groups. A375 and WM278 (non-pigmentable cells) and 501Mel and SK-Mel-5 (high-pigmentable cells) were treated for 48 hours with dmso or 2 μM vem, then cells were collected and processed for the analysis. We observed that aside from A375 cells that present a significant increase of oxidation, the other lines show no difference after the treatment, suggesting that protein oxidation probably is not the right way to highlight a distinction between pigmentable and non-pigmentable cells (Fig. 41).
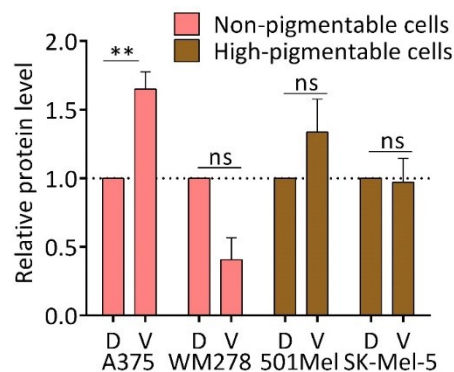
Figure 41. Oxidized protein levels in A375, WM278, 501Mel and SK-Mel-5 cells after 48h of DMSO or 2 μM vem. The graph represents the mean±SEM of 3 independent experiments. *$p<0.05$, **$p<0.01$, ***$p<0.001$, ****$p<0.0001$.

4.6.2 Lipid peroxidation

Another main consequence of ROS is lipid peroxidation, which takes place when membrane phospholipids are put into contact with a ROS oxidising agent. Indeed, cell membranes are susceptible to radical damage due to the presence of polyunsaturated fatty acids. The free radical oxidises an unsaturated lipid chain, leading to the formation of a hydroperoxidised lipid and an alkyl radical. This lipoperoxidation leads to modifications of the membrane structure, impairing its fluidity and damaging its integrity [83].

Our melanoma cell lines were treated with dmso or 2 μM vemurafenib for 24, 48 and 72 hours and then lipidic ROS were measured. Data show that for the greater part of the cells at 48 and 72 hours vemurafenib induces lipid peroxidation, implying that ROS actually hurt cell membranes; however, again, this effect is not sufficient to underscore a difference among the groups (Fig. 42).

Figure 42. Lipidic ROS levels measured in a panel of melanoma cell lines after 24h, 48h or 72h of DMSO or 2 μM vem. The graph represents the mean±SEM of 3 independent experiments. *p<0.05, **p<0.01, ***p<0.001, ****p<0.0001.

4.6.3 DNA base oxidation

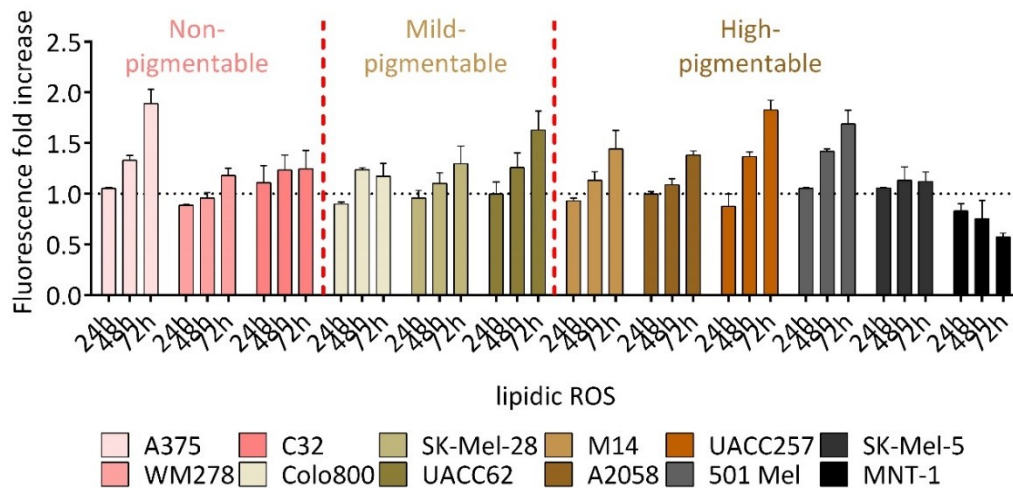In DNA, ROS react with nitrogenous bases and deoxyribose, causing significant oxidative reactions. This oxidation can lead to alterations in DNA bases causing mutagenic alterations or induce DNA break from single to double helix breaks [83]. Among the oxidative DNA damage lesions generated by ROS, 8-Oxo-2'-deoxyguanosine (8-oxo-dG) is an oxidized derivative of deoxyguanosine. It is one of the major products of DNA oxidation. High concentrations of 8-oxo-dG within a cell are a measurement of oxidative stress, with low levels of antioxidant enzymes [50]. One non-pigmentable cell lines, A375, and two pigmentable cell lines, 501Mel and SK-Mel-5, were treated with dmso or 2 μM vemurafenib for 48 hours and then DNA damage was measured by 8-oxo-dG immunofluorescence staining. Images showed that, after drug treatment, the signal of 8-oxo-dG antibody (in red) from being only cytoplasmatic also becomes nuclear, right where the damage is concentrated, in a manner similar to what is observed by [84]. This was mostly visible in A375 cells rather than in 501Mel and SK-Mel-5 cells (Fig. 43).

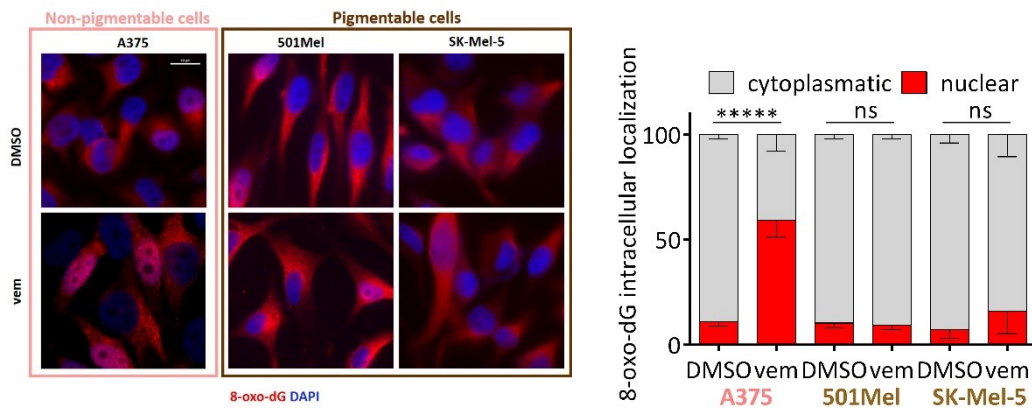Figure 43. 8-oxo-dG immunofluorescence staining of a panel of melanoma cell lines after 48h of dmso or 2 μM vem (left). Quantification plot of 8-oxo-dG staining (right). The graphs represent the mean±SEM of 3 independent experiments. *p<0.05, **p<0.01, ***p<0.001, ****p<0.0001.

8-OHdG inhibits DNA methylation at adjacent cysteine residues leading to DNA hypomethylation [50,85]. It has been shown that DNA methyltransferase 1 (Dnmt1) expression is associated with melanoma progression and it is downregulated during response to B-Raf and mitogen-activated protein kinase kinase (MEK) inhibition, but it is upregulated on drug resistance *in vitro* and *in vivo* [86]. So, we wondered if the higher level of DNA oxidation attested by nuclear 8-OHdG shining was associated with a decrease in DNMT1 levels. A375, C32, 501Mel and SK-Mel-5 cells were treated for 72 hours with dmso or 2 μM vem, then the levels of DNMT1 protein were detected by western blot analysis. Data showed that upon the treatment with the drug all cell lines present a decrease in DNMT1 protein level, but in non-pigmentable cells this decrease is greater (Fig. 44).
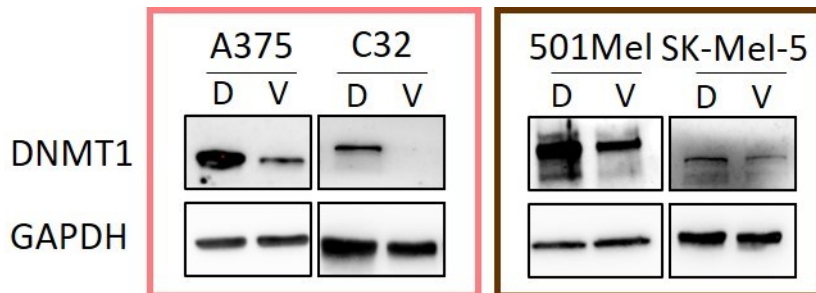
Figure 44. DNMT1 protein levels after 72h of DMSO or 2 μM vem in a panel of melanoma cell lines. Immunoblotting for GAPDH was used as loading control. D: DMSO; V: vem.

Finally, since 8-oxo-dG can be potentially converted to DSBs [87], we examined DNA damage response by assessing the accumulation of γH2AX, a marker for DNA breaks. A375, C32 and 501Mel were treated with dmso or 2 μM vem for 48 hours, while SK-Mel-2 with dmso or 200 nM cobi. Results revealed a very high induction of DNA damage in non-pigmentable cells, while pigmentable cells present intrinsically higher basal level

of γH2AX, in accordance with the fact that they show high basal levels of ROS, but the drug did not alter this level (Fig. 45).
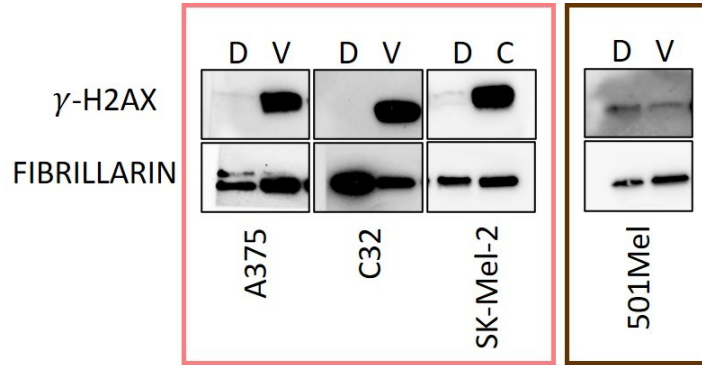
Figure 45. γ-H2AX protein levels after 48h of DMSO or 2 μM vem or 10 nM cobi in a panel of melanoma cell lines. Immunoblotting for Fibrillarin was used as loading control. C: cobi; D: DMSO; V: vem.

Finally, we analyzed the genes involved in DNA repair and surprisingly upon vem treatment neither in pigmentable cells nor in non-pigmentable cells are induced; however, it was consistent with the results obtained by [87,88] (Fig. 46).
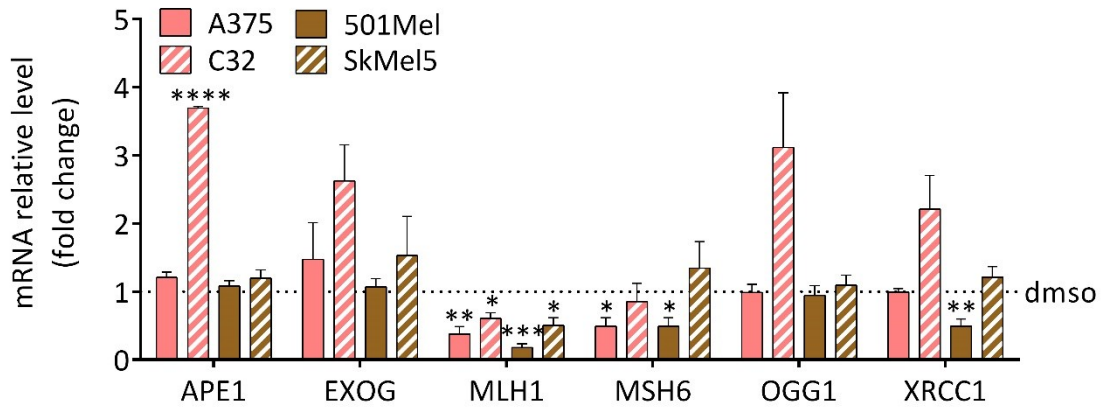
Figure 46. mRNA relative fold change of APE1, EXOG, MLH1, MSH6, OGG1 and XRCC1 in A375, C32, 501Mel and SK-Mel-5 after 48h of DMSO or 2 μM vem. The graphs represent the mean±SEM of 3 independent experiments. *p<0.05, **p<0.01, ***p<0.001, ****p<0.0001.

According to these data we conclude that upon vemurafenib treatment, ROS induced DNA damage striked non-pigmentable cells the most, while pigmentable cells were less affected and the main difference was the presence of melanin (melanosomes).

4.7   Melanosomes-mitochondria physical contacts favor the melanin-mediated scavenging of vem-induced ROS

As reported in paragraph 1.1, upon vem treatment, we found an increase of melanosomes also around the nuclei in 501Mel cells. In this subcellular localization, they come close to mitochondria. Since it has been already demonstrated that mitochondria promote melanosomes maturation through fibrillar bridges composed by a mitochondrial protein, mitofusin2 (MFN2), we wondered whether in turn melanosomes exert their vem induced-ROS-scavenger activity by physical contact with mitochondria. For this purpose, firstly, 501Mel cells were treated with dmso or 2 µM vem or 10 µM PTU for 72 hours and then were analyzed using transmission electron microscope. Data show that vem treatment induces an increase not only in the number of melanosomes (Fig. 47B), but also in the number of physical contacts that they establish with mitochondria (Fig. 47C). On the contrary, the concurrent treatment with PTU decreases the localization and the number of contacts. Interestingly, this happen while no change is observed in the number and in the subcellular localization of mitochondria (Fig. 47A).
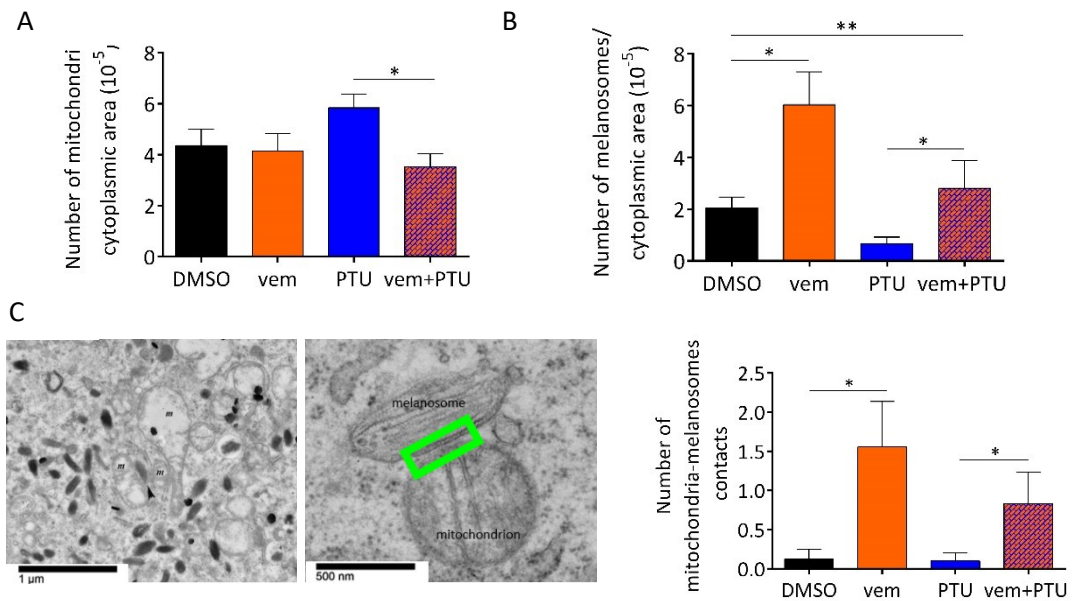
Figure 47. Quantification of mitochondria (A) and melanosomes (B) detected by TEM in 501Mel cells treated with DMSO, 2 μM vem or 10 μM PTU for 72h. Representative image and quantification (C) of the number of contacts between mitochondria and melanosomes detected by TEM in 501Mel cells treated with DMSO, 2 μM vem or 10 μM PTU for 72h. The graphs represent the mean±SEM of 3 independent experiments. *p<0.05, **p<0.01, ***p<0.001, ****p<0.0001.

Starting from the fact that the physical interactor of MFN2, located on the membrane of melanosomes, has not yet been found, we took advantage of the PrePPI database of predicted and experimentally determined protein-protein interactions (PPI) for the human proteome (https://bhapp.c2b2.columbia.edu/PrePPI/). From this analysis RAB27A is the only protein located on melanosomes membrane among the 67 proteins (with score 0.9) predicted as MFN2 interactors. We decided to knock-down RAB27A and observe its effects in terms of melanosomes number and localization, interactions with mitochondria and ROS levels. 501Mel cells were transfected with a siRNA against *RAB27A* or with a control siRNA and the day after were treated with dmso or 2 μM vem for 72 hours. TEM analysis shows that RAB27A silencing does not significantly affect melanosome number

nor stage (Fig. 48A), and notably does not alter the expression levels of protein involved in melanin synthesis pathway (Fig. 48B).
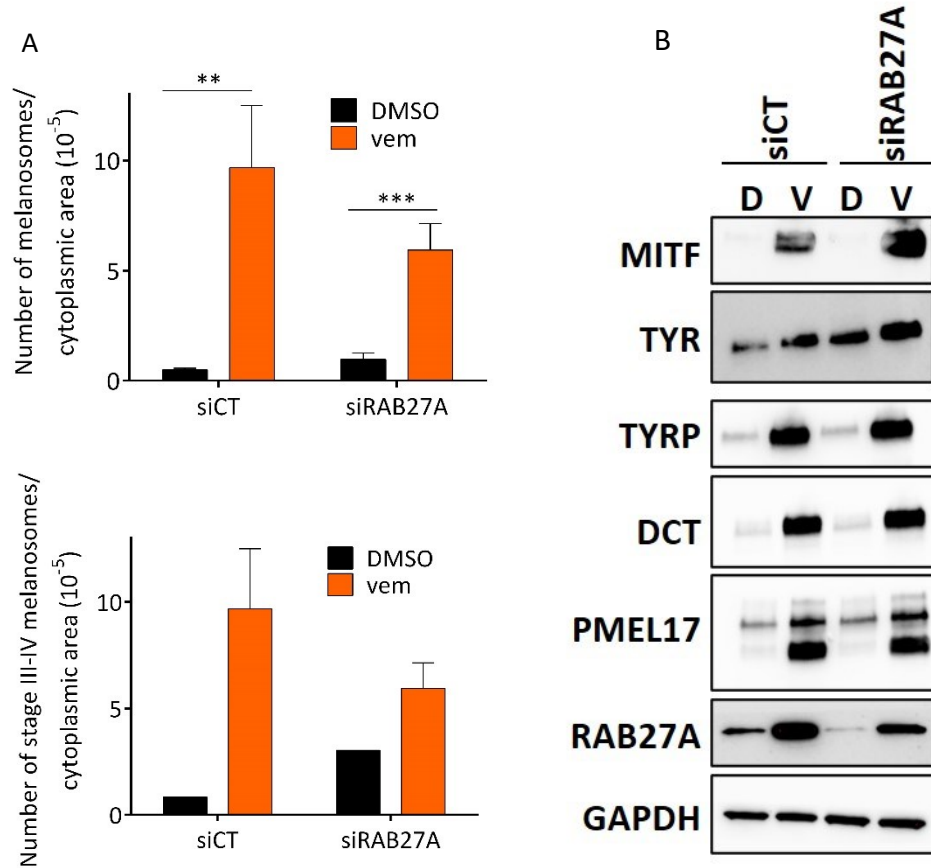
Figure 48. (A) Quantification of all stages (up) and stage III-IV (down) melanosomes detected by TEM in 501Mel cells transfected with siCT or siRAB27A and treated the day after with DMSO or 2 μM vem for 72h. (B) MITF, TYR, TYRP, DCT, PMEL17 and RAB27A protein level in 501Mel cells transfected with siCT or siRAB27A and treated the day after with DMSO (D) or 2 μM vem (V) for 72h. GAPDH is used as loading control. The graphs represent the mean±SEM of 3 independent experiments. *p<0.05, **p<0.01, ***p<0.001, ****p<0.0001.

However, it influences melanosomes localization, that appears less perinuclear (Fig. 49A), and caused a decrease in contacts with mitochondria (Fig. 49B). Crucially, its knock-down induces an increase in total and mitochondrial ROS (Fig. 49C).
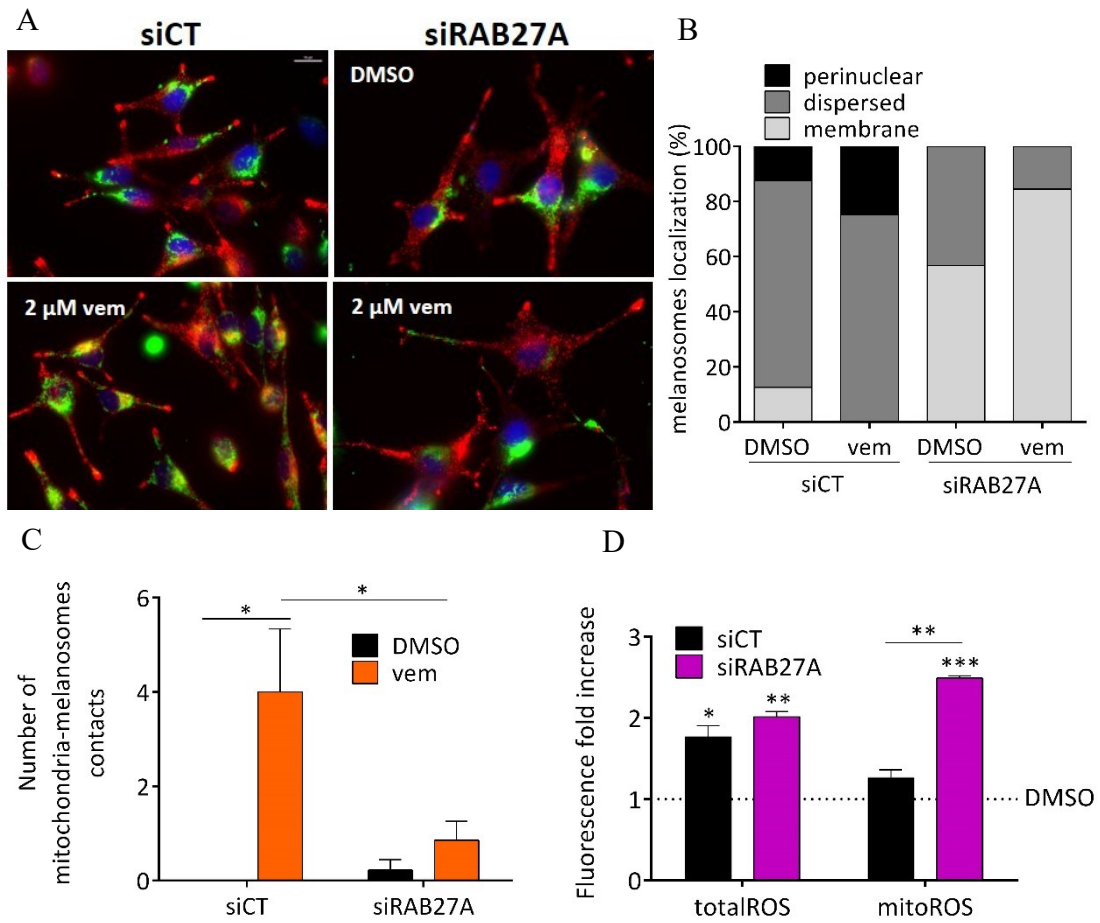
Figure 49. (A) Immunofluorescence staining of melanosomes (red) and mitochondria (green) in cells transfected with siCT or siRab27a and treated the day after with DMSO or 2 μM vem for 48h. For this experiment, 501Mel cells stably expressing TYR-mCherry were used. Blue: DAPI; red: TYR-mCherry; green: TOM20 mitochondrial marker. Scale bar: 10um. (B) Subcellular localization of melanosomes detected by TEM in cells transfected with siCT or siRAB27A and treated the day after with DMSO or 2 μM vem for 72h. (C) Quantification of the number of contacts between mitochondria and melanosomes detected by TEM in cells transfected with siCT or siRab27a and treated the day after with DMSO or 2 μM vem for 72h. (D) Total (left) and mitochondrial (right) ROS levels measured in cells transfected with siCT or siRAB27A and treated the day after with DMSO or 2 μM vem for 72h. The graphs represent the mean±SEM of 3 independent experiments. *$p<0.05$, **$p<0.01$, ***$p<0.001$, ****$p<0.0001$.

These results prompt to further investigate the possible implications of reducing the connections between melanosomes and mitochondria in pigmentable cells as another way to make them more sensitive to the action of MAPK inhibitors.

4.8 The efficacy of MAPKi with pigmentation inhibitors is further enhanced with inhibitors of oxidative phosphorylation

A shift toward oxidative phosphorylation is another adaptive mechanism induced by vemurafenib; thus, we wondered whether such shift is different in pigmentable cells compared to non-pigmentable cells. To this end, we treated A375 and 501Mel cells with dmso or 2 μM for 24, 48 and 72 hours; then, using the Seahorse XFp Cell Mito Stress Test Kit, we found that vem causes a much stronger decrease in ATP production, basal and maximal respiration in A375 compared to 501Mel cells, suggesting that in the first vem treatment induces much higher stress (Fig. 50).
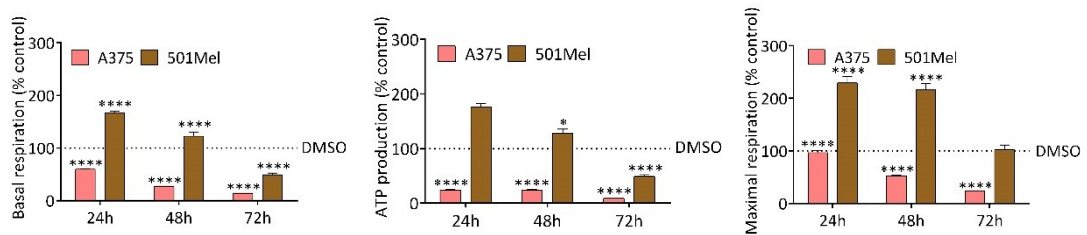
Figure 50. Levels of relative basal respiration (left), ATP production (center) and maximal respiration (right) detected in A375 and 501Mel after 24, 48 and 72h of DMSO or 2 μM vem. The graphs represent the mean±SEM of 3 independent experiments. *p<0.05, **p<0.01, ***p<0.001, ****p<0.0001.

Next, we treated non-pigmentable and pigmentable cells with dmso or 2 μM vem for 72 hours and quantified the number of mitochondria with a qPCR and with mitotracker staining. Consistent with data above, we found that it increases in non-pigmentable cells, as if it was a balancing response to reduced energy production for the cell (Fig. 51).
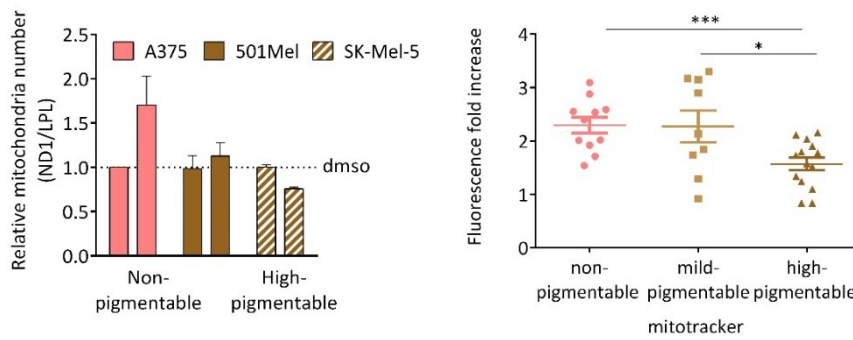
Figure 51. Relative mitochondria number (ND1/LPL) in A375, 501Mel and SK-Mel-5 after 72h of DMSO or 2 μM vem (left). Mitotracker levels measured in non-pigmentable, mild-pigmentable and high-pigmentable cell lines after 72h of DMSO or 2 μM vem (right). The graphs represent the mean±SEM of 3 independent experiments. *$p<0.05$, **$p<0.01$, ***$p<0.001$, ****$p<0.0001$.

Finally, two non-pigmentable cell lines (A375 and WM278) and three high-pigmentable cell lines (501Mel, SK-Mel-5 and A2058) were treated with 2 μM vem for 48 hours and then intracellular total levels of the electron donor NADH were measured by 2-photon Fluorescent Lifetime Imaging. After drug treatment, total NADH increases in the first group and not in the second, suggesting that the levels of the coenzyme increase because its demand decreases, hence its use, confirming the fact that mitochondria are damaged and less functioning (Fig. 52).
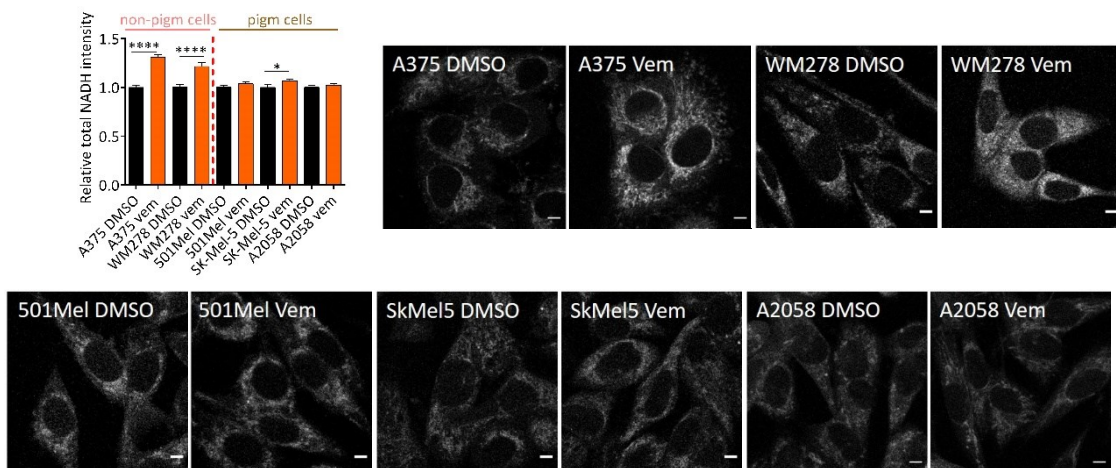
Figure 52. Quantification of relative total NADH intensity detected in a panel of melanoma cell lines after 48h of DMSO or 2 μM vem. The graphs represent the mean±SEM of 3 independent experiments. *$p<0.05$, **$p<0.01$, ***$p<0.001$, ****$p<0.0001$.

According with these data, we expect that the addition of an inhibitor of oxidative phosphorylation could further increase the efficacy of MAPKi plus pigmentation inhibitors. Indeed, we have already published experiments both *in vitro* and *in vivo* showing that the administration of oligomycin plus vemurafenib and PTU can potentiate the activity of the single drug [42]. The data we present here reinforce published results, by showing that vem efficacy on pigmentable melanoma cells can be increased by blocking two of the adaptive responses it induces: increase in pigmentation and shift toward oxidative phosphorylation.

5 Conclusions

This work is based on the evidence that induction of pigmentation is one of the adaptive mechanisms that melanoma cells exploit to react to vem treatment. We set out to investigate the molecular mechanisms that might be behind this process and we found interesting results.

- We demonstrated that MAPK inhibitors induce pigmentation in a subset of melanoma cells, both *in vitro* and *in vivo*.

- We showed that the sensitivity to MAPK inhibitors is inversely correlated with pigmentation levels, both in melanoma cell lines and in metastatic melanoma specimens.

- We formally demonstrated that pigmentation limits the efficacy of MAPK inhibitors.

- We proved that pigmentation limits vem activity due to the presence of intracellular melanosomes.

- We evinced that melanin acts as scavenger of MAPK inhibitors-induced ROS.

- We determined that ROS-induced DNA damage is lower in pigmentable cells.

- We found that melanosomes-mitochondria physical contacts promote the melanin-mediated scavenging of vem-induced ROS.

- We provided evidence that the addition of oxidative phosphorylation inhibitors enhances the efficacy of MAPK inhibitors with pigmentation inhibitors.

6 Discussion and future perspectives

The physical and chemical properties of melanin make melanotic metastatic melanomas less sensitive to therapy in general [89]. Indeed, radiotherapy seems to work better in presence of amelanotic melanomas [23]. Additionally, several mechanisms are involved in melanoma resistance against phototherapy [24]. However, the use of photosensitizers or pigmentation inhibitors activates different responses and increases the susceptibility of pigmented cells [24–27,90]. Furthermore, many are the chemotherapeutic agents that have poor effect on pigmented cells (e.g. cyclophosphoamide, cDDP, carboplatin, DTIC and methotrexate) principally due to melanosomal regulatory genes that influence drug activity and so drug sensitivity [28–33]. As a consequence, different studies reported that patients with melanotic melanomas show worse prognosis [34,39–42,69]. At last, in presence of pigmentation, even targeted therapy fails. As reported by *in vitro* studies this is due to an increase in melanocytic differentiation markers, phenotype switching of cells versus MITF high/differentiated/proliferative state, or elevated TYRP1 levels [36,38,41,42]. Specifically, we reported that miR-211 is upregulated upon vemurafenib treatment, making cells more pigmented and more resistant to the treatment [42–44].

Here, we described extensively that a group of melanoma cell lines get pigmented when treated with MAPK inhibitors. The induction of pigmentation upon vemurafenib treatment was also observed in xenografted nude mice that presented smaller and darker tumors compared to the tumors treated with vehicle. This induction of pigmentation has to be seen as one of the processes that is activated after treatment with the drug, namely one of the mechanisms, together with loss of kinase-dependent negative feedback loop, cell-state transition, metabolic reprogramming and ER stress and autophagy, that cells put

in place to stall and find alternative ways of survival. And it is precisely in this intermediate phase, where cells are in a drug tolerant state, in which we can try to act, before genetic resistance occurs, which most of the times is a point of no return. As a matter of fact, we observed at different levels, *in vitro*, *in vivo*, in patients, that melanin can affect negatively therapy outcome. Pigmentable cells exhibited lower growth inhibition when treated with BRAF and MEK inhibitors; in xenograft experiments in zebrafish embryos, the treatment of kifunensine, as well as the overexpression of miR-211 [42], made vemurafenib less effective, and the tumor volume increased. Contrary, the inhibition of pigmentation, in cells treated with PTU or LNA-211, favors vemurafenib activity, and the tumor volume decreased [42]. Specifically, upon vem treatment we observed a general increase in melanosomes trafficking and we determined that they limit the activity of the drug from the inside of the cells, not secreting the drug outside. Finally, patients with metastatic melanotic tumors appeared to respond worse to therapy than patients with amelanotic metastatic tumors. Thus, pigmentation induced by MAPK inhibitors can be considered as one of the defense mechanisms of cells to escape pharmacological action.

According to our data, not all melanoma cell lines exhibit the same level of pigmentation increase after BRAF and MEK inhibitors treatment. A first classification, based on visual inspection of cell pellet, leads to the distinction of non-pigmentable vs pigmentable cells. At the molecular level, this difference correlates with *TRPM3*/*TRPM1* expression. Specifically, *TRPM3* is the only one expressed and induced by vem treatment in all non-pigmentable cells, while *TRPM3* and *TRPM1* are both expressed in pigmentable cells, but only *TRPM1* is always induced [42]. However, among pigmentable cells we noticed different pigmentation levels, from mild to high, that did not correlate with the degree of

TRPM1 induction, hence prompted us to undertake further investigations with additional assays, including TEM analysis and quantification of Tyrosinase activity by supplying L-DOPA as substrate. In the high-pigmentable cells group, visual observation and more in depth inspection with TEM correlate perfectly with gene expression analysis and Tyrosinase activity. Conversely, the mild-pigmentable cells show some discrepancies: the increase in the number of eumelanosomes and the levels of Tyrosinase activity do not correlate with the darkening of the cell pellet. Interestingly, these cells present pheomelanosomes, although in lower numbers compared to eumelanosomes, and this feature will be further explored to understand if it is responsible for milder darkening. Since they have such mixed characteristics, we have preferred to consider mild-pigmentable cells halfway between non-pigmentable and high-pigmentable cells and we have kept them in a distinct group.

We examined the effects of treatment with MAPKi, looking for a difference in pigmentable and non-pigmentable cells in terms of additional biological features, such as cell cycle progression and induction of cellular senescence. Results showed that in all cell lines there is a block of proliferation, characterized by a decrease of S phase, after vemurafenib treatment, but without being related to the degree of pigmentation; this also applies to cobimetinib treatment, which causes as well a slowdown in cell growth. As for cell cycle analysis, also senescence induction after vemurafenib treatment did not distinguish between pigmentable and non-pigmentable cells. On one hand, we could try to treat the cells for longer time, for example until 96 hours, in order to observe or not a recovery in growth that may discern the two groups of cells; on the other hand, we could reinforce the data using additional markers besides beta-galactosidase, for example p16 tumor suppressor protein. Another consideration is that pH stability is very important for

the detection of beta-galactosidase activity, thus we could improve our protocol in order to observe any other difference.

Another intriguing aspect is that, when signalling through MAPK pathway is modulated, alterations in mitochondrial oxidative metabolism occur. Indeed, in melanoma cells vemurafenib treatment causes an increase in oxidative metabolism, through mitochondria biogenesis and mitochondria respiration, and, as a consequence, a switch away from glucose metabolism occurs [91,92], and provoking rise in ROS levels [93–95].

In our melanoma cell lines we confirmed the increase in total and mitochondrial ROS upon vemurafenib treatment, but with a peculiar characteristic: according to the quantity of melanin presence in the cells, the amount of ROS is different, specifically more melanin less ROS, less melanin more ROS. In this work, we tried to understand whether the lower levels of ROS could provide an explanation for the reduced sensitivity of pigmented melanoma cells to the MAPK inhibitor treatment. Our hypothesis was that melanin, thanks to its properties, could quench ROS induced by vemurafenib treatment. We were able to prove our hypothesis, also through the support of two *in vitro* model systems: SK-Mel-188 melanoma cells "switch medium" and UACC257-Tyr-ZsGreen cell line. Crucially, when we made rescue experiments in 501Mel and SK-Mel-5 pigmentable cells, by decreasing melanin with PTU or DBZ, we obtained a strong increase in ROS level and cell sensitivity as observed in non pigmentable cells. On the contrary, by making A375 cells pigmentable, ROS levels and the sensitivity to the drug decreased. From the results obtained we conclude that melanosomes act as scavengers of ROS induced by vemurafenib. We propose a new mechanism of cell evasion to vemurafenib treatment, through this activity of melanosomes, which should be added to those already observed [31,96–98]. Remarkably, the use of PTU on non pigmentable cells

results ineffective *per se* both in terms of growth inhibition [42] and of ROS levels, and does not alter the activity of MAPK inhibitors, highlighting the treatment of metastatic melanotic melanomas with the addition of pigmentation inhibitor as a very 'on target' approach.

Another way to further improve the efficacy of MAPK inhibitors plus pigmentation inhibitors is the repression of oxidative phosphorylation, which is another adaptive mechanism induced by vem itself. We have already published experiments both *in vitro* and *in vivo* showing that the administration of oligomycin can further increase the efficacy of vemurafenib and PTU [42]. Significantly, here we established how pigmentable cells and non-pigmentable cells differ in terms of ATP production, number of mitochondria and total NADH level upon vemurafenib treatment: non pigmentable A375 cells show a stronger impairment in oxidative phosphorylation compared to pigmentable 501Mel cells; however, by treating 501Mel with vem, PTU and oligomycin, preliminary data display that proteins of electron chain transport are affected. These data can be explained by the fact that, on one hand, BRAF inhibition leads to the overexpression of *MITF* and so to the induction of oxidative metabolism gene signature [93], and, on the other hand, *MITF* induction in pigmentable cells drives miR-211 expression, thus causing the chain of events which leads to the induction of pigmentation. Thus, although experiments should be extended to more pigmentable cell lines, an inhibitor of oxidative phosphorylation may block ATP production in pigmentable cells, like an inhibitor of pigmentation causes an increase in ROS levels, ultimately contributing to potentiate vem efficacy.

We also analyzed the ROS-induced damage. Since pigmentable cells present melanin, which acts as a ROS-protector agent, they are less subjected to the negative action of ROS

compared to non-pigmentable cells. In particular, results showed that ROS-induced vemurafenib principally affect DNA, consistent with [99–102], by increasing the amount of 8-oxo-dG and γ-H2AX. Now we are proceeding with rescue experiment in pigmentable cells by adding PTU or DBZ, in order to detect an increase in DNA damage, similar to that observed by [103]. Obtaining a positive result would be the confirmation that melanosomes act as a protective cap of ROS induced by vemurafenib. We also observed that upon vemurafenib treatment, in 501Mel cells melanosomes are found in higher number around nuclei, a bit like when melanosomes form the nuclear cap around the keratinocytes, in order to protect them from UV radiation damage. Here, it could be that melanosomes get around the nucleus and protect it from ROS induced by vemurafenib. In particular, in this localization they enter in contact with the mitochondria, that are one of the main sources of ROS inside a cell. It might be that melanosomes need to be in physical contact with mitochondria in order to exert their vem induced-ROS-scavenger activity. It has been already demonstrated that mitochondria promote melanosomes maturation through fibrillar bridges composed by mitofusin2 protein (MFN2) [104]. Interestingly, in 501Mel cells, we noted that vem treatment causes an increase also in the number of physical contacts between these two organelles. On the contrary, the simultaneous treatment with PTU decreased both, the localization and the number of contacts. Markedly, we did not observe any changes in the number and in the subcellular localization of mitochondria. Later we determined RAB27A as a possible candidate as a mediator of physical contact with mitochondria upon vem treatment. Indeed, this protein belongs to the RAB family of small GTPases, is present in melanosomes and acts to promote peripheral release of melanosomes via recruitment of myosin Va through its effector melanophilin (Mlph). In melanoma, RAB27A is reported

to be oncogenic: amplified and/or overexpressed, it promotes proliferation, and motility/metastatization [105]. Moreover, according to our RNAseq analysis, *RAB27A* results upregulated in vem-treated 501Mel and SK-Mel-5 pigmentable melanoma cell lines (log2FoldChange=1.1, ****padj) and together with other 4 mRNAs is accountable for their higher resistance to vem compared to A375 non-pigmentable melanoma cells [106]. Our data showed that, upon 72h vem treatment in 501Mel cells, RAB27A knock-down did not significantly impact melanosome number nor stage. However, it affects melanosomes localization, that appeared less perinuclear, and caused a decrease in contacts with mitochondria. Furthermore, RAB27A silencing provokes an increase in both total and mitochondrial ROS levels. Hence the simultaneous knock down of MFN2 and RAB27A could impede and remove the formation of physical contact between mitochondria and melanosomes, thus expecting a further increase in ROS levels and making pigmentable cells more susceptible to the action of MAPK inhibitors. In the near future we also plan to use the genetic or chemical inhibition of the interaction between RAB27A and MLPH, through siRNA against MLPH in the first case and drugs, such as hesperidin and wogonin, in the second case, expecting a decrease in the release of melanosomes, hence, their intracellular accumulation, followed by a decrease in ROS levels.

Finally, another crucial topic is drug delivery that often determines the outcome of therapy. As long as it is cutaneous melanoma we can act with topical agents, but everything is complicated when the tumor reaches advanced stages with the presence of metastasis that are difficult to get access. In these terms, the approach we are pursuing is based on Listeria monocytogenes (Lm[at]) as a drug carrier for the selective delivery of BRAF and pigmentation inhibitors, as well as anti-melanoma vaccine. Indeed, we have

already demonstrated that it causes a strong decrease in the size and volume of primary melanoma tumors, as well as a reduction of the metastatic burden, and also potentiates the immune response of the organism against the infected tumor in a mouse melanoma model [107]. In this way we expect to minimize the side effects of both MAPK inhibitors and pigmentation inhibitors, when not administered topically.

In conclusion we propose a new molecular mechanism by which pigmentation mitigates the efficacy of MAPK inhibitor in melanoma cells through scavenging of vem induced ROS. We also propose the combination of MAPKi, pigmentation inhibitors and drugs decreasing mitochondria activity as a way to tame the resistance of pigmentable melanoma cells. Lastly, we suggest that an analysis of pigmentation status could be introduced in the step of diagnosis, and more generally in the classification of subtype, to have a more complete view of the tumor. Indeed, to date, with the latest WHO classification of skin tumors (4th edition, 2018), melanoma is classified according to sun exposure and genomic features. Classification has evolved over the years, from a purely histological classification to the current genomic classification (BRAF, NRAS, NF1 and Triple wild-type subtype) that takes into account genetic alterations identified in the last decades. Thus, we highlight the necessity to stratify melanoma tumors according to their pigmentation status as well in order to tailor the best treatment option.

7 References

1. Cives M, Mannavola F, Lospalluti L, Sergi MC, Cazzato G, Filoni E, et al. Non-melanoma skin cancers: Biological and clinical features. Int J Mol Sci. MDPI AG; 2020. p. 1–24.

2. Khan NH, Mir M, Qian L, Baloch M, Ali Khan MF, Rehman A ur, et al. Skin cancer biology and barriers to treatment: Recent applications of polymeric micro/nanostructures. J Adv Res. Elsevier B.V.; 2022. p. 223–47.

3. Arnold M, Singh D, Laversanne M, Vignat J, Vaccarella S, Meheus F, et al. Global Burden of Cutaneous Melanoma in 2020 and Projections to 2040. JAMA Dermatol. 2022;158:495.

4. Davis LE, Shalin SC, Tackett AJ. Current state of melanoma diagnosis and treatment. Cancer Biol Ther. Taylor and Francis Inc.; 2019. p. 1366–79.

5. Bobos M. Histopathologic classification and prognostic factors of melanoma: A 2021 update. Italian Journal of Dermatology and Venereology. Edizioni Minerva Medica; 2021. p. 300–21.

6. Teixido C, Castillo P, Martinez-Vila C, Arance A, Alos L. Molecular markers and targets in melanoma. Cells. MDPI; 2021.

7. Akbani R, Akdemir KC, Aksoy BA, Albert M, Ally A, Amin SB, et al. Genomic Classification of Cutaneous Melanoma. Cell. Cell Press; 2015;161:1681–96.

8. Plotnikov A, Zehorai E, Procaccia S, Seger R. The MAPK cascades: Signaling components, nuclear roles and mechanisms of nuclear translocation. Biochim Biophys Acta Mol Cell Res. 2011. p. 1619–33.

9. Guo Y, Pan W, Liu S, Shen Z, Xu Y, Hu L. ERK/MAPK signalling pathway and tumorigenesis (Review). Exp Ther Med. Spandidos Publications; 2020;

10. Czarnecka AM, Bartnik E, Fiedorowicz M, Rutkowski P. Targeted therapy in melanoma and mechanisms of resistance. Int J Mol Sci. MDPI AG; 2020. p. 1–21.

11. Saei A, Eichhorn PJA. Adaptive responses as mechanisms of resistance to braf inhibitors in melanoma. Cancers (Basel). MDPI AG; 2019.

12. Khaliq M, Fallahi-Sichani M. Epigenetic mechanisms of escape from BRAF oncogene dependency. Cancers (Basel). MDPI AG; 2019.

13. Subbiah V, Baik C, Kirkwood JM. Clinical Development of BRAF plus MEK Inhibitor Combinations. Trends Cancer. Cell Press; 2020. p. 797–810.

14. Nguyen K, Hignett E, Khachemoune A. Current and emerging treatment options for metastatic melanoma: A focused review. Dermatol Online J. Dermatology Online Journal; 2020.

15. Patton EE, Mueller KL, Adams DJ, Anandasabapathy N, Aplin AE, Bertolotto C, et al. Melanoma models for the next generation of therapies. Cancer Cell. Cell Press; 2021. p. 610–31.

16. Tangella LP, Clark ME, Gray ES. Resistance mechanisms to targeted therapy in BRAF-mutant melanoma - A mini review. Biochim Biophys Acta Gen Subj. Elsevier B.V.; 2021.

17. Manzano JL, Layos L, Bugés C, De los Llanos Gil M, Vila L, Martínez-Balibrea E, et al. Resistant mechanisms to BRAF inhibitors in melanoma. Ann Transl Med. AME Publishing Company; 2016;4:1–9.

18. Rambow F, Rogiers A, Marin-Bejar O, Aibar S, Femel J, Dewaele M, et al. Toward Minimal Residual Disease-Directed Therapy in Melanoma. Cell. 2018;174:843-855.e19.

19. Basile KJ, Abel E v, Aplin AE. Adaptive upregulation of FOXD3 and resistance to PLX4032/4720-induced cell death in mutant B-RAF melanoma cells. Oncogene. 2012;31:2471–9.

20. Tsoi J, Robert L, Paraiso K, Galvan C, Sheu KM, Lay J, et al. Multi-stage Differentiation Defines Melanoma Subtypes with Differential Vulnerability to Drug-Induced Iron-Dependent Oxidative Stress. Cancer Cell. 2018;33:890-904.e5.

21. Marin-Bejar O, Rogiers A, Dewaele M, Femel J, Karras P, Pozniak J, et al. Evolutionary predictability of genetic versus nongenetic resistance to anticancer drugs in melanoma. Cancer Cell. 2021;39:1135-1149.e8.

22. Hopkins ZH. Risk Factors and Predictors of Survival Among Patients with Amelanotic Melanoma Compared to Melanotic Melanoma in the National Cancer Database. 2021;

23. Brożyna AA, Jóźwicki W, Roszkowski K, Filipiak J, Slominski AT. Melanin content in melanoma metastases affects the outcome of radiotherapy [Internet]. Oncotarget. 2016. Available from: www.impactjournals.com/oncotarget/

24. Baldea I, Giurgiu L, Teacoe ID, Olteanu DE, Olteanu FC, Clichici S, et al. Photodynamic Therapy in Melanoma - Where do we Stand? Curr Med Chem. Bentham Science Publishers Ltd.; 2017;25:5540–63.

25. Sharma K V., Davids LM. Depigmentation in melanomas increases the efficacy of hypericin-mediated photodynamic-induced cell death. Photodiagnosis Photodyn Ther. 2012;9:156–63.

26. de Souza Contatori CG, Silva CR, de Toledo Pereira S, Rodrigues MFSD, de Lima Luna AC, Marques MM, et al. Responses of melanoma cells to photobiomodulation depend on cell pigmentation and light parameters. J Photochem Photobiol B. 2022;235:112567.

27. Hamblin MR, Huang YY, Vecchio D, Avci P, Yin R, Garcia-Diaz M. Melanoma resistance to photodynamic therapy: New insights. Biol Chem. Walter de Gruyter GmbH; 2013. p. 239–50.

28. Slominski A, Zbytek B, Slominski R. Inhibitors of melanogenesis increase toxicity of cyclophosphamide and lymphocytes against melanoma cells. Int J Cancer. 2009;124:1470–7.

29. Pawlikowska M, Piotrowski J, Jędrzejewski T, Kozak W, Slominski AT, Brożyna AA. Coriolus versicolor-derived protein-bound polysaccharides trigger the caspase-independent cell death pathway in amelanotic but not melanotic melanoma cells. Phytotherapy Research. John Wiley and Sons Ltd; 2020;34:173–83.

30. Huang ZM, Chinen M, Chang PJ, Xie T, Zhong L, Demetriou S, et al. Targeting protein-trafficking pathways alters melanoma treatment sensitivity. Proc Natl Acad Sci U S A. 2012;109:553–8.

31. Xie T, Nguyen T, Hupe M, Wei ML. Multidrug resistance decreases with mutations of melanosomal regulatory genes. Cancer Res. 2009;69:992–9.

32. Chen KG, Valencia JC, Lai B, Zhang G, Paterson JK, Rouzaud F, et al. Melanosomal sequestration of cytotoxic drugs contributes to the intractability of malignant melanomas [Internet]. 2006. Available from: www.pnas.orgcgidoi10.1073pnas.0600213103

33. Sánchez-Del-Campo L, Montenegro MF, Cabezas-Herrera J, Rodríguez-López JN. The critical role of alpha-folate receptor in the resistance of melanoma to methotrexate. Pigment Cell Melanoma Res. 2009;22:588–600.

34. Brozyna AA, Jóźwicki W, Carlson JA, Slominski AT. Melanogenesis affects overall and disease-free survival in patients with stage III and IV melanoma. Hum Pathol. 2013;44:2071–4.

35. Slominski RM, Sarna T, Płonka PM, Raman C, Brożyna AA, Slominski AT. Melanoma, Melanin, and Melanogenesis: The Yin and Yang Relationship. Front Oncol. Frontiers Media S.A.; 2022.

36. Damsky WE, Curley DP, Santhanakrishnan M, Rosenbaum LE, Platt JT, Gould Rothberg BE, et al. β-Catenin Signaling Controls Metastasis in Braf-Activated Pten-Deficient Melanomas. Cancer Cell. Cell Press; 2011;20:741–54.

37. Kim IS, Heilmann S, Kansler ER, Zhang Y, Zimmer M, Ratnakumar K, et al. Microenvironment-derived factors driving metastatic plasticity in melanoma. Nat Commun. Nature Publishing Group; 2017;8.

38. Gilot D, Migault M, Bachelot L, Journé F, Rogiers A, Donnou-Fournet E, et al. A non-coding function of TYRP1 mRNA promotes melanoma growth. Nat Cell Biol. Nature Publishing Group; 2017;19:1348–57.

39. Jönsson G, Busch C, Knappskog S, Geisler J, Miletic H, Ringnér M, et al. Gene expression profiling-based identification of molecular subtypes in stage IV melanomas with different clinical outcome. Clinical Cancer Research. 2010;16:3356–67.

40. Cirenajwis H, Ekedahl H, Lauss M, Harbst K, Carneiro A, Enoksson J, et al. Molecular stratification of metastatic melanoma using gene expression profiling : Prediction of survival outcome and benefit from molecular targeted therapy [Internet]. Oncotarget. 2015. Available from: www.impactjournals.com/oncotarget/

41. Journe F, Boufker HI, van Kempen L, Galibert MD, Wiedig M, Salès F, et al. TYRP1 mRNA expression in melanoma metastases correlates with clinical outcome. Br J Cancer. 2011;105:1726–32.

42. Vitiello M, Tuccoli A, D'aurizio R, Sarti S, Giannecchini L, Lubrano S, et al. Context-dependent miR-204 and miR-211 affect the biological properties of amelanotic and melanotic melanoma cells [Internet]. 2017. Available from: www.impactjournals.com/oncotarget

43. Sahoo A, Sahoo SK, Joshi P, Lee B, Perera RJ. MicroRNA-211 Loss Promotes Metabolic Vulnerability and BRAF Inhibitor Sensitivity in Melanoma. Journal of Investigative Dermatology. Elsevier B.V.; 2019;139:167–76.

44. Lee B, Sahoo A, Sawada J, Marchica J, Sahoo S, Layng FIAL, et al. MicroRNA-211 Modulates the DUSP6-ERK5 Signaling Axis to Promote BRAFV600E-Driven Melanoma Growth In Vivo and BRAF/MEK Inhibitor Resistance. Journal of Investigative Dermatology. Elsevier B.V.; 2021;141:385–94.

45. Mittler R. ROS Are Good. Trends Plant Sci. Elsevier Ltd; 2017. p. 11–9.

46. Mishra R, Patel H, Yuan L, Garrett J. Role of Reactive Oxygen Species and Targeted Therapy in Metastatic Melanoma. Cancer Res Front [Internet]. 2018;4:101–30. Available from: http://cancer-research-frontiers.org/2018-4-101/

47. Davalli P, Marverti G, Lauriola A, D'Arca D. Targeting oxidatively induced DNA damage response in cancer: Opportunities for novel cancer therapies. Oxid Med Cell Longev. Hindawi Limited; 2018.

48. Moloney JN, Cotter TG. ROS signalling in the biology of cancer. Semin Cell Dev Biol. Elsevier Ltd; 2018. p. 50–64.

49. Su LJ, Zhang JH, Gomez H, Murugan R, Hong X, Xu D, et al. Reactive Oxygen Species-Induced Lipid Peroxidation in Apoptosis, Autophagy, and Ferroptosis. Oxid Med Cell Longev. Hindawi Limited; 2019.

50. Bhat A v., Hora S, Pal A, Jha S, Taneja R. Stressing the (Epi)Genome: Dealing with Reactive Oxygen Species in Cancer. Antioxid Redox Signal. Mary Ann Liebert Inc.; 2018. p. 1273–92.

51. Bedogni B, Welford SM, Cassarino DS, Nickoloff BJ, Giaccia AJ, Powell MB. The hypoxic microenvironment of the skin contributes to Akt-mediated melanocyte transformation. Cancer Cell. Cell Press; 2005;8:443–54.

52. Wittgen HGM, On L, van Kempen CLT. Reactive oxygen species in melanoma and its therapeutic implications Reactive oxygen species. Melanoma Res. Wolters Kluwer Health | Lippincott Williams & Wilkins; 2007.

53. Govindarajan B, Sligh JE, Vincent BJ, Li M, Canter JA, Nickoloff BJ, et al. Overexpression of Akt converts radial growth melanoma to vertical growth melanoma. Journal of Clinical Investigation. 2007;117:719–29.

54. Verhaegen M, Bauer JA, de La Vega CM, Wang G, Wolter KG, Brenner JC, et al. A novel BH3 mimetic reveals a mitogen-activated protein kinase-dependent mechanism of melanoma cell death controlled by p53 and reactive oxygen species. Cancer Res. 2006;66:11348–59.

55. Gloire G, Legrand-Poels S, Piette J. NF-κB activation by reactive oxygen species: Fifteen years later. Biochem Pharmacol. 2006;72:1493–505.

56. Brar SS, Kennedy TP, Richard Whorton A, Sturrock AB, Huecksteadt TP, Ghio AJ, et al. Reactive oxygen species from NAD(P)H:quinone oxidoreductase constitutively activate NF-κB in malignant melanoma cells [Internet]. Am J Physiol Cell Physiol. 2001. Available from: http://www.ajpcell.org

57. Ueda Y, Richmond A. NF-κB activation in melanoma. Pigment Cell Res. 2006. p. 112–24.

58. Sagwal SK, Bekeschus S. ROS Pleiotropy in Melanoma and Local Therapy with Physical Modalities. Oxid Med Cell Longev. Hindawi Limited; 2021.

59. Cordero RJB, Casadevall A. Melanin. Current Biology. Cell Press; 2020;30:R142–3.

60. Brenner M, Hearing VJ. The protective role of melanin against UV damage in human skin. Photochem Photobiol. 2008. p. 539–49.

61. Lambert MW, Maddukuri S, Karanfilian KM, Elias ML, Lambert WC. The physiology of melanin deposition in health and disease. Clin Dermatol. Elsevier Inc.; 2019;37:402–17.

62. Yamaguchi Y, Brenner M, Hearing VJ. The regulation of skin pigmentation. Journal of Biological Chemistry. 2007. p. 27557–61.

63. Alba LD', Shawkey MD. MELANOSOMES: BIOGENESIS, PROPERTIES, AND EVOLUTION OF AN ANCIENT ORGANELLE. Ancient Organelle Physiol Rev [Internet]. 2019;99:1–19. Available from: www.prv.org

64. D'Mello SAN, Finlay GJ, Baguley BC, Askarian-Amiri ME. Signaling pathways in melanogenesis. Int J Mol Sci. MDPI AG; 2016.

65. Hida T, Kamiya T, Kawakami A, Ogino J, Sohma H, Uhara H, et al. Elucidation of melanogenesis cascade for identifying pathophysiology and therapeutic approach of pigmentary disorders and melanoma. Int J Mol Sci. MDPI AG; 2020. p. 1–23.

66. Sarna T, Pilas B, Land EJ, Truscott TG. Interaction of radicals from water radiolysis with melanin. 1986.

67. R´o˙ M, Zanowska R, Sarna T, Land EJ, George Truscott T. Original Contribution FREE RADICAL SCAVENGING PROPERTIES OF MELANIN INTERACTION OF EU-AND PHEO-MELANIN MODELS WITH REDUCING AND OXIDISING RADICALS. 1999.

68. Bustamante,' Luis Bredeston,' J, Malanga G, Mordoh2 J. Original Articles Role of Melanin as a Scavenger of Active Oxygen Species. Pigment Cell Re8. 1998;6:348458.

69. Slominski RM, Sarna T, Płonka PM, Raman C, Brożyna AA, Slominski AT. Melanoma, Melanin, and Melanogenesis: The Yin and Yang Relationship. Front Oncol. Frontiers Media S.A.; 2022.

70. Nasti TH, Timares L. MC1R, eumelanin and pheomelanin: Their role in determining the susceptibility to skin cancer. Photochem Photobiol. Blackwell Publishing Inc.; 2015;91:188–200.

71. Liu-Smith F, Poe C, Farmer PJ, Meyskens FL. Amyloids, melanins and oxidative stress in melanomagenesis. Exp Dermatol. 2015;24:171–4.

72. Sarti S, de Paolo R, Ippolito C, Pucci A, Pitto L, Poliseno L. Inducible modulation of miR-204 levels in a zebrafish melanoma model. Biol Open. Company of Biologists Ltd; 2020;9.

73. Krayem M, Najem A, Journe F, Morandini R, Sales F, Awada A, et al. Acquired resistance to BRAFi reverses senescence-like phenotype in mutant BRAF melanoma [Internet]. Oncotarget. 2018. Available from: www.oncotarget.com

74. Haferkamp S, Borst A, Adam C, Becker TM, Motschenbacher S, Windhövel S, et al. Vemurafenib induces senescence features in melanoma cells. Journal of Investigative Dermatology. Nature Publishing Group; 2013;133:1601–9.

75. Kumari R, Jat P. Mechanisms of Cellular Senescence: Cell Cycle Arrest and Senescence Associated Secretory Phenotype. Front Cell Dev Biol. 2021;9.

76. Gire V, Dulic V. Senescence from G2 arrest, revisited. Cell Cycle. 2015;14:297–304.

77. Wang G, Wei C, Hong X, Fu Z, Huang W. Sodium pyruvate as a peroxide scavenger in aerobic oxidation under carbene catalysis. Green Chemistry. Royal Society of Chemistry; 2020;22:6819–26.

78. Wang X, Perez E, Liu R, Yan L-J, Mallet RT, Yang S-H. Pyruvate Protects Mitochondria from Oxidative Stress in Human Neuroblastoma SK-N-SH Cells. 2007.

79. Giandomenico AR, Cerniglia GE, Biaglow JE, Stevens CW, Koch CJ. Original Contribution THE IMPORTANCE OF SODIUM PYRUVATE IN ASSESSING DAMAGE PRODUCED BY HYDROGEN PEROXIDE. Free Radic Biol Med. 1997.

80. Vergun O. Exploration of the role of reactive oxygen species in glutamate neurotoxicity in rat hippocampal neurones in culture. 2000.

81. Liu D, Shan Y, Valluru L, Bao F. Mn (III) tetrakis (4-benzoic acid) porphyrin scavenges reactive species, reduces oxidative stress, and improves functional recovery after experimental spinal cord injury in rats: Comparison with methylprednisolone. BMC Neurosci. 2013;14.

82. Sanmartín-Suárez C, Soto-Otero R, Sánchez-Sellero I, Méndez-Álvarez E. Antioxidant properties of dimethyl sulfoxide and its viability as a solvent in the evaluation of neuroprotective antioxidants. J Pharmacol Toxicol Methods. 2011;63:209–15.

83. Andrés Juan C, Manuel Pérez de la Lastra J, Plou FJ, Pérez-Lebeña E, Reinbothe S. Molecular Sciences The Chemistry of Reactive Oxygen Species (ROS) Revisited: Outlining Their Role in Biological Macromolecules (DNA, Lipids and Proteins) and Induced Pathologies. Int J Mol Sci [Internet]. 2021;22:4642. Available from: https://doi.org/10.3390/ijms

84. Sirigu. Nuclear 8-hydroxy-2'-deoxyguanosine as survival biomarker in patients with cutaneous melanoma. Oncol Rep. Spandidos Publications; 2009;23.

85. Wu Q, Ni X. ROS-Mediated DNA Methylation Pattern Alterations in Carcinogenesis. Curr Drug Targets. 2015;16:13–9.

86. Gassenmaier M, Rentschler M, Fehrenbacher B, Eigentler TK, Ikenberg K, Kosnopfel C, et al. Expression of DNA Methyltransferase 1 Is a Hallmark of Melanoma, Correlating with Proliferation and Response to B-Raf and Mitogen-Activated Protein Kinase Inhibition in Melanocytic Tumors. American Journal of Pathology. Elsevier Inc.; 2020;190:2155–64.

87. Srinivas US, Tan BWQ, Vellayappan BA, Jeyasekharan AD. ROS and the DNA damage response in cancer. Redox Biol. Elsevier B.V.; 2019.

88. Maertens O, Kuzmickas R, Manchester HE, Emerson CE, Gavin AG, Guild CJ, et al. MAPK pathway suppression unmasks latent dna repair defects and confers a chemical synthetic vulnerability in BRAF-, NRAS-, and NF1 -mutant melanomas. Cancer Discov. American Association for Cancer Research Inc.; 2019;9:526–45.

89. Slominski A, Wortsman J, Nickoloff B, McClatchey K, Mihm MC, Ross JS. Molecular pathology of malignant melanoma. Am J Clin Pathol. 1998;110:788–94.

90. Ma L-W, Nielsen KP, Iani V, Moan J. A new method for photodynamic therapy of melanotic melanoma -- effects of depigmentation with violet light photodynamic therapy. J Environ Pathol Toxicol Oncol. 2007;26:165–72.

91. Baenke F, Chaneton B, Smith M, van den Broek N, Hogan K, Tang H, et al. Resistance to BRAF inhibitors induces glutamine dependency in melanoma cells. Mol Oncol. Elsevier B.V.; 2016;10:73–84.

92. Hernandez-Davies JE, Tran TQ, Reid MA, Rosales KR, Lowman XH, Pan M, et al. Vemurafenib resistance reprograms melanoma cells towards glutamine dependence. J Transl Med. BioMed Central Ltd.; 2015;13.

93. Haq R, Shoag J, Andreu-Perez P, Yokoyama S, Edelman H, Rowe GC, et al. Oncogenic BRAF regulates oxidative metabolism via PGC1α and MITF. Cancer Cell. Cell Press; 2013;23:302–15.

94. Corazao-Rozas P, Guerreschi P, Jendoubi M, André F, Jonneaux A, Scalbert C, et al. Mitochondrial oxidative stress is the achille's heel of melanoma cells resistant to Braf-mutant inhibitor [Internet]. Oncotarget. 2013. Available from: www.impactjournals.com/oncotarget

95. Wang L, Leite de Oliveira R, Huijberts S, Bosdriesz E, Pencheva N, Brunen D, et al. An Acquired Vulnerability of Drug-Resistant Melanoma with Therapeutic Potential. Cell. Cell Press; 2018;173:1413-1425.e14.

96. Bahrpeyma S, Reinisalo M, Hellinen L, Auriola S, del Amo EM, Urtti A. Mechanisms of cellular retention of melanin bound drugs: Experiments and computational modeling. Journal of Controlled Release. Elsevier B.V.; 2022;348:760–70.

97. Chen KG, Leapman RD, Zhang G, Lai B, Valencia JC, Cardarelli CO, et al. Influence of melanosome dynamics on melanoma drug sensitivity. J Natl Cancer Inst. 2009;101:1256–71.

98. Sun M-C, Xu X-L, Du Y, Lou X-F, Wang W, You Y-C, et al. Biomimetic Melanosomes Promote Orientation-Selective Delivery and Melanocyte Pigmentation in the H2O2-Induced Vitiligo Mouse Model. ACS Nano. 2021;15:17361–74.

99. Das I, Gad H, Bräutigam L, Pudelko L, Tuominen R, Höiom V, et al. AXL and CAV-1 play a role for MTH1 inhibitor TH1579 sensitivity in cutaneous malignant melanoma. Cell Death Differ. Springer Nature; 2020;27:2081–98.

100. Li J, Long J, Zhang J, Liu N, Yan B, Tang L, et al. Novel chloroquine derivative suppresses melanoma cell growth by DNA damage through increasing ROS levels. J Cell Mol Med. John Wiley and Sons Inc; 2022;26:2579–93.

101. Bauer D, Werth F, Nguyen HA, Kiecker F, Eberle J. Critical role of reactive oxygen species (ROS) for synergistic enhancement of apoptosis by vemurafenib and the potassium channel inhibitor TRAM-34 in melanoma cells. Cell Death Dis. Nature Publishing Group; 2017;8.

102. Yuan L, Mishra R, Patel H, Abdulsalam S, Greis KD, Kadekaro AL, et al. Utilization of reactive oxygen species targeted therapy to prolong the efficacy of braf inhibitors in melanoma. J Cancer. Ivyspring International Publisher; 2018;9:4665–76.

103. Poma A, Bianchini S, Miranda M. Inhibition of L-tyrosine-induced micronuclei production by phenylthiourea in human melanoma cells [Internet]. Mutat Res. 1999. Available from: www.elsevier.comrlocatergentoxCommunityaddress:www.elsevier.comrlocatermutres

104. Daniele T, Hurbain I, Vago R, Casari G, Raposo G, Tacchetti C, et al. Mitochondria and melanosomes establish physical contacts modulated by Mfn2 and involved in organelle biogenesis. Current Biology. 2014;24:393–403.

105. Li Z, Fang R, Fang J, He S, Liu T. Functional implications of Rab27 GTPases in Cancer. Cell Communication and Signaling. 2018;16:44.

106. Vitiello M, Mercatanti A, Podda MS, Baldanzi C, Prantera A, Sarti S, et al. A Network of MicroRNAs and mRNAs Involved in Melanosome Maturation and Trafficking Defines the Lower Response of Pigmentable Melanoma Cells to Targeted Therapy. Cancers (Basel). 2023;15.

107. Vitiello M, Evangelista M, di Lascio N, Kusmic C, Massa A, Orso F, et al. Antitumoral effects of attenuated Listeria monocytogenes in a genetically engineered mouse model of melanoma. Oncogene. Nature Publishing Group; 2019;38:3756–62.